

# **AN INVESTIGATION OF THE STRUCTURALLY INDUCED ACOUSTIC FIELD IN A CAR PASSENGER COMPARTMENT**

**F.R. WHEAR**

**A thesis submitted in partial fulfilment of the requirements of  
Oxford Brookes University for the degree of Doctor of Philosophy**

**MAY 1994**

**In Collaboration With Rover Group**

## **IMAGING SERVICES NORTH**

Boston Spa, Wetherby

West Yorkshire, LS23 7BQ

[www.bl.uk](http://www.bl.uk)

**PAGE NUMBERS CLOSE TO  
THE EDGE OF THE PAGE.  
SOME ARE CUT OFF**

## **Abstract.**

The causes and characteristics of structurally induced interior noise in cars in relation to the boom problem is discussed and the relevant theory developed. The work is concerned with structural excitation of the air within the passenger compartment associated with the second order component of the engine crankshaft out of balance forces. This limits the frequency range of interest to below 200 Hz. Firstly, the acoustic modes of a Rover Metro passenger compartment are predicted using the finite element method.

A new method for the experimental acoustic modal analysis of cavities is introduced and verified for a rectangular rigid walled room. The method is then applied to the untrimmed passenger compartment of a Rover Metro to determine its acoustic modes and to study the interaction of the structural modes of the vehicle body and acoustic response of the cavity.

The acoustics of a Rover Metro passenger compartment are modelled using the finite element method with experimental structural FRF data from the car body as a forcing function. This model is used to predict the noise spectra associated with the second order component of engine excitation experienced by occupants for the bare body. The acoustic effects of various items of trim are added to the model as acoustic absorption coefficients to show the significance of trim in reducing low frequency boom in car passenger compartments. The necessary absorption coefficients were measured with an impedance tube.

## **Contents.**

	<b>Page.</b>
a. Title.	1
b. Abstract.	2
c. Contents.	3
d. List of Figures.	6
e. List of Plates	9
f. List of Tables.	9
g. Acknowledgements.	10
h. Nomenclature.	11
1. Introduction.	13
1.1 The Development and Manufacture of new Motor Cars	13
1.2 Available modelling and test techniques	14
1.3 Programme of work undertaken	15
2. Review of Previous Work.	16
2.1 Noise in Cars.	16
2.2 The Use of Finite Elements for Studying Car Interior Acoustics.	18
2.3 Experimental Analysis of Acoustic Modes.	20
2.4 Measurement of the Absorption Coefficient of Trim Materials.	21
2.5 Noise Control Methods.	22
3. Theory.	23
3.1 Modelling System Dynamics.	23
3.2 Structural Modal Theory.	23
3.2.1 Single Degree of Freedom System.	23
3.2.2 Multi Degree of Freedom System.	24
3.2.3 Damping.	25
3.3 Modal Normalization.	25
3.4 Experimental Modal Analysis.	26
3.4.1 Peak Amplitude Method.	27
3.4.2 Circle Fit Method.	27
3.5 Acoustic Modal Theory.	29
3.5.1 Travelling and Standing Waves.	29
3.5.2 Normal Modes of Rectangular Cavities.	31



3.6	Sound Absorption.	34
3.7	Finite Element Method.	34
3.7.1	Analysis types.	35
3.7.2	Discretization of Acoustic Systems.	35
4.	Modelling Car Cavity Acoustic Modes.	38
4.1	ANSYS Acoustic Elements.	38
4.2	Finite Element Modal Extraction and Expansion.	38
4.3	Construction of the Model.	39
4.4	Metro-R6 Acoustic Modes Predicted by FEA.	39
5.	Experimental Method of Acoustic Modal Analysis.	44
5.1	Theory.	44
5.2	Method.	45
5.3	Verification.	47
5.4	Results.	49
5.5	Discussion.	58
6.	Acoustic Modal Analysis of a Rover Metro Passenger Compartment.	59
6.1	Measurement of Acoustic Modes.	59
6.1.1	Excitation.	59
6.1.2	Method.	60
6.1.3	Results.	63
6.1.4	Discussion.	67
6.2	Investigation of Structural-Acoustic Interaction.	68
6.2.1	Method.	69
6.2.2	Results.	70
6.2.3	Discussion.	82
6.2.4	Conclusion.	83
7.	Measurement of Acoustic Absorption Coefficient of Trim Materials.	84
7.1	Method.	84
7.2	Results.	87
7.3	Discussion.	90
8.	Modelling Car Cavity Acoustic Response to Structural Excitation.	91
8.1	Assumptions and Restrictions.	91
8.2	Construction of the Model.	92
8.2.1	Modelling the Untrimmed Body.	93
8.2.2	Modelling the Trimmed Body.	95
8.2.3	Application of the Boundary Element Method.	96
8.3	Results.	97

8.4	Discussion.	111
8.5	Conclusion.	112
9.	Discussion.	113
9.1	Errors and Experimental Accuracy	114a
10.	Conclusion.	115
11.	References.	116
12.	Bibliography.	123
Appendix 1: ANSYS Batch File For Extracting the Acoustic Modes of a Rover Metro.		124
Appendix 2 Analogue Difference Circuit.		125
Appendix 3: ANSYS Batch File For a Harmonic Analysis of a Rover Metro Acoustics.		126
Appendix 4: Accepted Papers.		129

## List of Figures.

		Page.
1.1a	Structural measurement mesh for the Rover Metro body.	13
1.1b	Acoustic mesh for the Rover Metro passenger compartment.	13
3.1	Modal, Spatial and Response Models.	23
3.2	SDOF System.	24
3.3	SDOF Resonance.	27
3.4	Nyquist Plot.	28
3.5	Rectangular Cavity.	31
3.6	Reflection of Normally Incident Sound at a Surface.	34
3.7	Defined Continuum.	35
4.1	Metro-R6 First Acoustic Mode.	40
4.2	Metro-R6 Second Acoustic Mode.	41
4.3	Metro-R6 Third Acoustic Mode.	41
4.4	Metro-R6 Fourth Acoustic Mode.	42
4.5	Metro-R6 Fifth Acoustic Mode.	42
4.6	Metro-R6 Sixth Acoustic Mode.	43
4.7	Metro-R6 Seventh Acoustic Mode.	43
5.1	Finite Difference Calculation.	45
5.2	Experimental Setup.	46
5.3	Modal Mesh.	48
5.4	Sample Office Acoustic FRFs (Directional).	50
5.5	Single Microphone Pressure Transfer Function.	50
5.6	Circle Fit Results.	51
5.7	First Office Acoustic Mode (1 0 0).	52
5.8	Second Office Acoustic Mode (0 1 0).	53
5.9	Third Office Acoustic Mode (0 0 1).	54
5.10	Fourth Office Acoustic Mode (1 1 0).	55
5.11	Fifth Office Acoustic Mode (1 0 1).	56
5.12	Sixth Office Acoustic Mode (0 1 1).	57
6.1	Cavity Response at Driver's Head to Excitation by a Loud Speaker.	59
6.2	Cavity Response to Structural Excitation with an Electromagnetic Shaker.	60
6.3	Modal Mesh.	62
6.4	First Metro-R6 Acoustic Mode (1 0 0).	63
6.5	Second Metro-R6 Acoustic Mode (0 1 0).	64
6.6	Third Metro-R6 Acoustic Mode (2 0 0).	64
6.7	Fourth Metro-R6 Acoustic Mode (1 1 0).	65
6.8	Fifth Metro-R6 Acoustic Mode (0 0 1).	65

6.9	Sixth Metro-R6 Acoustic Mode (1 0 1).	66
6.10	Seventh Metro-R6 Acoustic Mode (2 1 0).	66
6.11	Cavity Response to Structural Excitation with an Electromagnetic Shaker.	68
6.12	Structural Modal Analysis Equipment.	69
6.13	30 And 210 Node Modal Meshes.	70
6.14	Sample Peaks Not Associated with Acoustic Modes.	71
6.15	Circle Fits for Peaks Shown in Figure 6.14.	72
6.16	Structural Mode associated with Peak A.	73
6.17	Structural Mode associated with Peak B.	74
6.18	Modes Associated with Peak C.	75
6.19	Modes Associated with Peak D.	76
6.20	Modes Associated with Peak E.	77
6.21	Modes Associated with Peak F.	78
6.22	Modes Associated with Peak G.	79
6.23	Modes Associated with Peak H.	80
6.24	Comparison of Structural FRF Data for a Body Panel and a Structural Member.	81
7.1	Absorption Coefficient Measurement Equipment.	84
7.2	Absorption Coefficient for the Bare Tube.	87
7.3	Absorption Coefficient for Seat Foam.	88
7.4	Absorption Coefficient for Carpet with Foam Underlay.	88
7.5	Absorption Coefficient for Carpet with Felt Underlay.	89
7.6	Absorption Coefficient for Rear Seat Back Covering.	89
8.1	Structural Modal Damping.	94
8.2	Equivalent Structural Modal Damping.	94
8.3	Trimmed Cavity Acoustic Model.	96
8.4	Structurally Induced Acoustic Field at 33 Hz.	97
8.5	Structurally Induced Acoustic Field at 48 Hz.	98
8.6	Structurally Induced Acoustic Field at 73.5 Hz.	98
8.7	Structurally Induced Acoustic Field at 84 Hz.	99
8.8	Structurally Induced Acoustic Field at 138 Hz.	99
8.9	Structurally Induced Acoustic Field at 141 Hz.	100
8.10	Structurally Induced Acoustic Field at 162 Hz.	100
8.11	Structurally Induced Acoustic Field at 166.5 Hz.	101
8.12	Structurally Induced Acoustic Field at 175.5 Hz.	101
8.13	Structurally Induced Acoustic Field at 189 Hz.	102
8.14	Structurally Induced Acoustic Field at 196.5 Hz.	102
8.15	Acoustic Response at the Drivers Head Location, Untrimmed - FEA.	103
8.16	Acoustic Response at the Drivers Head Location with Carpets - FEA.	103
8.17	Acoustic Response at the Drivers Head Location with Seats -FEA.	104
8.18	Acoustic Response at the Drivers Head Location with Carpets and Seats - FEA.	104

8.19	Panel Contributions at 33 Hz at Drivers Head Location.	105
8.20	Panel Contributions at 48 Hz at Drivers Head Location.	106
8.21	Panel Contributions at 73.5 Hz at Drivers Head Location.	106
8.22	Panel Contributions at 84 Hz at Drivers Head Location.	107
8.23	Panel Contributions at 138 Hz at Drivers Head Location.	107
8.24	Panel Contributions at 141 Hz at Drivers Head Location.	108
8.25	Panel Contributions at 162 Hz at Drivers Head Location.	108
8.26	Panel Contributions at 166.5 Hz at Drivers Head Location.	109
8.27	Panel Contributions at 175.5 Hz at Drivers Head Location.	109
8.28	Panel Contributions at 189 Hz at Drivers Head Location.	110
8.29	Panel Contributions at 196.5 Hz at Drivers Head Location.	110
9.1	Acoustic Response for the Unmodified and Modified Structure.	114

**List of Plates.**

	Page
5.1 Microphone Calibration Setup.	47
5.2 Microphone Setup within the Office.	48
6.1 Metro-R6 Body on Mounts.	61
6.2 Shaker Attachment.	61
6.3 Microphone Arrangement.	62
7.1 Impedance Tube and FFT Analyser.	85

**List of Tables.**

4.1 Metro-R6 Acoustic Modes.	40
5.1 Measured and Predicted Office Acoustic Natural Frequencies.	49
6.1 Measured and Predicted Metro-R6 Acoustic Modes.	63

## **Acknowledgements.**

There are several people whose contributions to this work should be recognized. Firstly, my supervisor Dr Denise Morrey for her help and support throughout the duration of the project. Phillip Woolley (Dynamics Technician) for the manufacture of the equipment and help in preparing the experiments. Colin Peachey and John Lofts, of the Body Refinement section at Rover Group's Cowley operations, for providing much of the background information and practical insight into the testing of vehicle structures. Finally (and certainly not least) my wife, Eileen, for generally putting up with three years of structurally induced automobile interior noise and undertaking the onerous task of proof reading this thesis.

## **Nomenclature.**

### **Numbering**

The numbering system used for equations, figures and tables uses the chapter number followed by sequential numbering (for each feature) after the decimal point. Figures and tables have their numbers included in their title whilst notes and numbers relating to equations are on the line below each equation.

### **Units.**

A consistent set of standard SI units is assumed throughout this work.

### **Abbreviations.**

ASTM	American Society for Testing and Materials
BEM	Boundary Element Method.
dB	Decibel
FEA	Finite Element Analysis
FFT	Fast Fourier Transform
FRF	Frequency Response Function
Lh	Left Hand
MDOF	Multi Degree Of Freedom
MPH	Miles Per Hour
NTF	Noise Transfer function
Rh	Right Hand
RPM	Revolutions Per Minute
SDOF	Single Degree Of Freedom
SAE	Society of Automotive Engineers
SI	Système International

### **Mathematical Symbols.**

{}	Column Matrix
[]	Rectangular Matrix
[I]	Identity Matrix
$\nabla$	$\partial/\partial x + \partial/\partial y + \partial/\partial z$

### **Notation.**

c	Damping Coefficient; Velocity of Sound
f	Force, Frequency
{f}	Force Vector
j	Imaginary number ( $\sqrt{-1}$ )
k	Spring Stiffness , Wave Number
[k]	Generalized Stiffness Matrix
m	Mass
[m]	Generalized Mass Matrix
p	Acoustic Pressure



$t$	Time
$(t)$	Time Domain
$u$	Particle Velocity
$x$	Displacement
$\{x\}$	Displacement Vector
$z$	Specific Acoustic Impedance.
$rA_{jk}$	Modal Constant $r^{\text{th}}$ Mode
$A(\omega)$	Inertance
$[C]$	Damping Matrix
$H$	Transfer Function
$[K]$	Stiffness Matrix
$[M]$	Mass Matrix
$N$	Element Shape Function
$Q$	Source Volume Velocity
$R$	Acoustic Flow Resistance, Reflection Coefficient
$U$	Particle Velocity
$Y(\omega)$	Mobility
$Z$	Acoustic Impedance
$\alpha$	Acoustic Absorption Coefficient
$\alpha(\omega)$	Receptance
$[\alpha(\omega)]$	Receptance Matrix
$\lambda$	Wavelength
$\rho$	Density
$\rho_0$	Static Density
$[\Phi]$	Mass Normalized Modeshape Matrix
$\eta$	Structural Loss Factor
$\omega$	Circular Frequency
$[\omega]$	Matrix Of Natural Frequencies
$(\omega)$	Frequency Domain
$[\psi]$	Unnormalized Modeshape Matrix

### **Subscripts.**

$b$	Boundary
$e$	Element
$fe$	Felt Backed Carpet
$fo$	Foam Backed Carpet
$i$	Incident
$r$	Reflected, $r^{\text{th}}$ Mode
$se$	Seats
$T$	Total
$x,y,z$	Cartesian Co-ordinate Axis Labels
$jk$	Matrix Row And Column Identifier

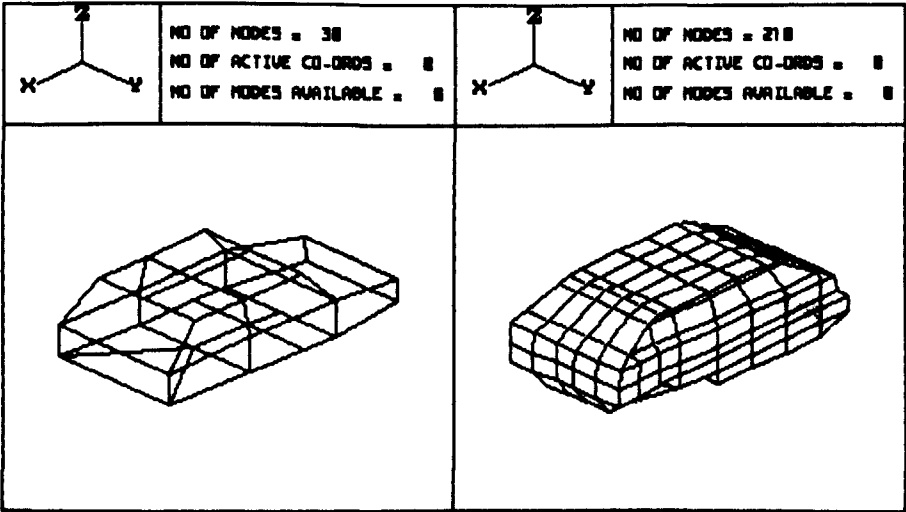
1. Introduction.

The study of noise and vibration in passenger cars is becoming an area of increasing importance for motor vehicle manufacturers. This is due to a number of different factors, such as the introduction of more stringent legislation, and an increasing emphasis on environmental issues. As a result, there are significant pressures to improve both fuel economy and performance, and the reduction of vehicle weight is seen as a key factor in achieving these. The main areas where weight savings can be made are in the engine, and the monocoque body shell. However, as these components become lighter, there is a tendency for them to be inherently noisier. This can have the effect of increasing the noise levels, and hence the quality of ride experienced by the occupants. One particular problem, which is the subject of this work, is that of low frequency cavity boom.

In order to explain this further, it is firstly necessary to consider some fundamental concepts. The dynamic behaviour of an engineering structure or a fluid cavity is characterised by its natural frequencies and the corresponding mode shapes. When a structure or cavity is excited at these frequencies the resulting measure of the amplitude of noise or vibration e.g. pressure or acceleration, is at its maximum value. At each of these frequencies, the structure or cavity of interest takes on a particular mode shape. This is a description (usually graphical) of how the structure or fluid cavity oscillates when it is driven at this natural frequency. Because of the increase in noise and vibration levels in the region of resonance, this is an important aspect to consider in characterising the behaviour of a vehicle. Structural modes are normally found by exciting a car body with an electromagnetic shaker and measuring the resulting accelerations at points on a mesh such as that shown in Fig. 1.1a. Acoustic modes describe the behaviour of the air space within the passenger compartment and can be determined numerically by considering a mesh such as that shown in Fig. 1.1b.

Fig. 1.1a Structural measurement mesh for the Rover Metro body (left hand figure)

Fig. 1.1b Acoustic mesh for the Rover Metro passenger compartment (right hand figure)



Cavity boom occurs when coupling of a structural mode of the body and an acoustic mode of the enclosed air volume of the passenger compartment (or cavity) causes a high interior sound level at a particular frequency. This causes two undesirable effects which depend on the driving conditions. The first is directly associated with engine noise which provides excitation at a single frequency and multiples thereof. During the acceleration of the vehicle, the sound level initially increases as the boom frequency is approached. It then decreases after this frequency is passed, and starts to increase again at higher frequencies. Occupants find increasing interior car noise with increasing speed acceptable, but not fluctuation in the manner just described. Secondly, when the car is driven at the speed at which boom is excited, the interior noise is dominated by a low frequency hum or drone. This is not only annoying, but can also increase driver fatigue. This can be a significant problem in motorway driving, where long distances are often covered at a constant speed. There is therefore a need for further study of the interaction between the structural and acoustic behaviour of the motor car vehicle.

In order to address the problem of cavity boom, it is necessary to consider in more detail two important areas, firstly the development process for a new vehicle which is currently used within the motor industry, and secondly the software and test techniques which are available and being used in the noise, vibration and harshness field.

### **1.1 The Development and Manufacture of new Motor Cars**

The development of a new car body from the point of view of dynamic behaviour is an iterative process. The first bodies to be tested are hand built prototypes, followed by proving bodies when the press tooling is completed. Final production bodies are analysed at the end of the development process. However, because of the long lead times involved in the manufacture of large press tools significant changes in panel design are only possible in the early stages of the whole process. Currently the major car manufacturers are striving to reduce development times on new models as they are faced with an increasingly competitive market and a shorter product life. This has led to an increased emphasis on acoustic considerations in the early stages of the development process. At this stage there is only a bare body shell available for analysis, and this has significant differences in its acoustic characteristics from a fully trimmed car. Hence there is a need for modelling techniques to be utilized in the very early stages, in order to predict the final noise spectra experienced by the occupants, and hence to decide upon any necessary modifications.

This project has been sponsored by the Rover Group from their Cowley operations. At present Rover carry out structural modal tests of untrimmed car bodies up to 100 Hz in order to identify the major structural modes, and up to 200 Hz in order to study the main panel modes. Acoustic modelling is limited to predicting the acoustic natural frequencies and modes of the passenger compartment cavity up to 200 Hz in order to identify the most responsive frequencies. The results of these tests are used to refine the dynamic characteristics of the structure in order to meet specified criteria. These criteria give ranges of values for the frequencies of the major structural

modes and the mobility levels of individual panels. Modifications can be made to shift the frequencies of the major structural modes away from that of any relevant excitation, and the vibration levels in car body panels are reduced by changing the design of the panel or applying palliative treatments to the problem areas. The main acoustic development work is done on running vehicles later in the development process.

The application of palliative treatments can be relatively ineffective at low frequencies. Damping materials and acoustic treatments not only add weight, but are relatively ineffective at the low frequencies where boom problems occur. There are therefore two main approaches to overcoming this problem. One is the use of active noise and vibration control. Although effective it adds significantly to the cost and complexity of each car produced. The other is to achieve a greater understanding of how interior noise is generated in a particular vehicle and produce a body shell that is effectively tuned to give acceptable noise levels. This is best achieved through the use of robust modelling tools which can be used to arrive at solutions prior to the production of the final press tooling. This is the major focus of this work.

Since it is the noise levels generated in the fully trimmed production vehicle which is of primary interest, any modelling techniques used in the early stages of development should be able to allow the effects of adding trim to be predicted, and compared with the behaviour of a bare body shell.

## **1.2 Available modelling and test techniques**

In order to arrive at a solution which could be implemented at the early stages of the development process, it is necessary to consider the available modelling and test techniques which could be used in this application, and to look at the ways in which they are currently used.

The main problem in predicting the low frequency acoustic characteristics of the passenger compartment has been the difficulty in predicting the response of the cavity, with its complex geometry to the boundary forcing function of the car body. The rapid development in the computing power available has made several powerful numerical tools, which are capable of modelling this type of problem, readily available to engineers. Two techniques that particularly lend themselves to this area of work are the finite element method, which can be used to predict both the modal properties and the forced response of complex air volumes, and experimental modal analysis, where the natural frequencies and associated mode shapes of structures can be determined from experimental data.

Although the finite element method can be used to predict the dynamic behaviour of vehicle structures, it is difficult to achieve accurate results without the use of very detailed models. Structural test data, on the other hand, is very reliable and repeatable, and can be obtained using a relatively coarse mesh of measurement points.

### **1.3 Programme of work undertaken**

This thesis sets out a methodology based on the use of the finite element method and experimental modal analysis to predict the structure-borne, engine-induced noise spectrum experienced by car occupants.

The thesis is broadly divided into four main sections. These main areas of research are described below with the relevant chapter numbers. The work was carried out on a production Metro-R6 body and trim items supplied by the Rover Group.

1. In order to study the dynamic behaviour of the acoustic cavity of the car passenger compartment, the acoustic modes were predicted using the finite element method (Chapter 4).

2. In order to have confidence in the modelling tools used, it is necessary to carry out an adequate programme of verification using experimental methods. In order to achieve this, an experimental method to determine the natural frequencies and mode shapes of acoustic cavities was developed (Chapter 5). This was then used to carry out a modal survey of the car passenger compartment (Chapter 6).

3. In order that the effects of trim could be included in the later models of the structure and cavity, it was necessary to measure the acoustic properties of various trim materials (Chapter 7).

4. Using structural test data, the forced response of the car passenger compartment to excitation by vibration of the body structure, for vehicles with and without interior trim, was predicted using the finite element models of the cavities which had been verified in earlier chapters (Chapter 8). The noise spectra generated were verified by comparison with experimental noise transfer functions obtained using the same form of excitation.

The output from this work is intended for use in a vibration test department and the following considerations are taken into account throughout the project. The techniques developed need to fit in with existing vibration test procedures and if possible use the same experimental results as these. The degree of detail used should be a compromise between accuracy and the time involved to acquire and process the data.

## **2 Review Of Previous Work.**

This section looks at work which has already been undertaken in the major areas relevant to this project. Published work relating to the cavity boom problem is discussed in relation to more general considerations of motor car interior noise. The development of finite element and experimental modal analysis methods for studying the acoustics of cavities are charted to establish the necessary background. Some consideration is given to the measurement of the acoustic properties of trim materials and noise control methods. However experimental structural modal analysis is not discussed in this chapter since for this project it is implemented with a proprietary software package. The relevant theory is covered in the next chapter.

### **2.1 Noise In Cars.**

Several papers have dealt extensively with interior car noise, Jha (1976), Jennequin (1971) and Wood & Joachim (1984 & 1986), producing a broad understanding of the sources and characteristics of the sound field. The following section discusses this work in relation to the cavity boom problem.

The noise (or rather lack of) experienced by the occupants of motor cars is an important factor in deciding the subjective quality of the vehicle and should give the impression of a solid well engineered product. Green pressures and the increasing price of fuel have forced the car manufacturers to produce more economical vehicles. Weight reduction has been used, mainly in the areas of the body shell and engine, to help meet the economy constraints without excessive reduction in the vehicles driving performance. These lighter structure vehicles tend to suffer from higher levels of vibration and (hence) interior noise. One particular problem is that of cavity boom where the coupling of structural and acoustic resonances leads to high interior sound levels at certain frequencies. This manifests itself as either as sudden rise and fall in the noise level as the boom frequency is swept through during acceleration or a continuous drone if the car is driven at a speed where the resonances are excited. Jha (1976) identifies the second harmonic of the engine crank speed in an in-line four cylinder four stroke engine as the dominant factor causing boom. This is a single frequency characteristic necessary to excite a single resonance. A typical four cylinder engine car engine does not usually have a rotational speed higher than 6000 RPM giving a maximum second order frequency of 200 Hz. Conversely the idle speed is around 850 RPM with a second order component of 28 Hz. These limits of engine speed have been used to define the frequency range of interest for this project as 30 to 200 Hz.

Current legislation is aimed at reducing the impact of traffic noise on the environment. The increasingly strict drive by noise laws used to achieve this have led to reduction in the interior noise generated by the tyres. Jha (1976) discusses the sources and characteristics of interior noise. The two main sources of noise are identified as the tyres and the engine. Tyre noise is generated by the road surface and is random in nature. This random component of interior noise does much to

mask the engine noise with its discrete components. Improvements in tyre design to meet exterior noise regulations have reduced this masking effect making any booms present more pronounced.

Jha (1976) identifies the first three acoustic modes as being the most significant for boom, as these have antinodes in the vicinity of a seating position, giving a typical frequency range of interest of 80 to 160 Hz for a saloon car (acoustic modes at 80-90 Hz, 130-140 Hz and 150-160 Hz). This coincides with the range of greatest structural sensitivity from 70 to 200 Hz where ring modes of the body can be shown to play a significant part in the generation of interior noise. Jennequin (1971) in modelling the interior sound field identifies a similar overlap between the acoustic modes of the cavity and large panel modes associated with noise generation. Whilst the exact relationship between the structural and acoustic modes is dependent on the particular design of a vehicle these results suggest a trend of low acoustic modal density in the region of highest structural sensitivity hence increasing the likelihood of a boom problem. As the effects of an acoustic resonance can be felt over a speed range of 5-7 MPH (Jha(1976)) the car cavity is a heavily damped acoustic system. The main source of this damping is the trim materials, carpets, seats, etc, which although capable of attenuating the cavity boom characteristic generated noise is not sufficient to remove it all together.

Noise is transmitted from its point of generation (engine,wheels,etc.) to the passenger compartment either through the structure or by the surrounding air. Below 400 Hz it is the structure-borne as opposed to air-borne, (Jha (1976)) transmission of noise that is the most significant making structural analysis important in understanding noise generation within this frequency range. At higher frequencies the air-borne component of interior noise is dominant. The interior noise is generated or transmitted (depending on the frequency) by vibrations of the surrounding structure. Below 200 Hz there are two main noise generating mechanisms: structural ring modes as identified by Jha (1976) and the major panel modes occurring between 40 and 250 Hz (Jennequin (1971)). It is the structural excitation of the ring and low order panel modes coupling with the acoustic modes of the passenger compartment that causes cavity boom. The noise generated by individual panels cannot be calculated by considering a panel in isolation as the sound level at any given point in the car is the sum of all relevant panel contributions and is dependent on their relative amplitude and phase (Jennequin (1971)).

Below 200 Hz the density of the structural and acoustic modes of a car is such that a modal representation of both systems is usually used (Nefske et al (1982)). However the interaction of the structural and acoustic systems affects both the acoustic natural frequencies and mode shapes. If at the frequency of an acoustic mode the dominant panel resonance is mass controlled the acoustic natural frequency is raised, conversely a stiffness controlled boundary lowers it (Nefske Wolf & Howell (1982)). The effect of the acoustic absorption of the trim materials is to lower the natural frequency (Craggs & Burna (1989)), and this affects the mode shape by producing an apparent antinode beyond the boundary.

Nominally identical cars can have a variation in interior noise levels of up to 10 dB. Wood & Joachim (1984 & 1986) investigated this characteristic and found it to be a frequency dependent characteristic. Up to 50 Hz, in the range of global structural modes, variation in the dynamic behaviour of car bodies is minimal. However in the range 100 to 200 Hz where the main modes of individual panels dominate the dynamics of a car body there can be a 15 dB variation in amplitude and 180° phase shift in the panel modes between individual cars. The variation in the behaviour of structural members was found to be significantly less. The body panels are responsible for the majority of noise generation and with the major cavity acoustic modes associated with boom problems occurring in this range the identification and control of boom problems for all the cars produced is difficult. This variation in behaviour limits the effective range of finite element models of car body natural frequencies and mode shapes to an upper limit of 100 Hz. Beyond this the finite element results represent only one possible solution. The variation in behaviour between hand built prototype and mass produced production bodies further complicates the issue. Slight shifts in the natural frequencies of the structural modes can cause a boom which was not evident during the development of the model.

The two main causes of scatter are variations in the behaviour of the various components that provide excitation for the body structure and variations in the behaviour of the structure itself. The former is beyond the scope of this project leaving variations in the relative phase of body panels and damping levels in the structure as the main causes of noise scatter pertinent to this work. Phase and damping characteristics are particularly difficult to model accurately making experimental data of the body's behaviour more relevant than finite element predictions. It must still be borne in mind that any results apply only to that particular body. Thus any noise control measures taken in the development stages of a new model only reduce the likelihood of the final product being unacceptable.

## **2.2 The Use Of Finite Elements For Studying Car Interior Acoustics.**

The finite element method has been developed from its early application to structural problems in the early 1960s to cover a wide range of boundary value problems including the analysis of acoustic problems. Other methods for studying the acoustics of cavities with complex boundary conditions such as the finite difference method have been employed, notably by Jennequin (1971), Jha & Cheilas (1977), Succi (1987) and Suzuki, Maruyama & Ido (1989). However the finite element method is the most widely used analysis tool and is available in affordable commercial packages.

Zienkiewicz and Newton (1969) developed a finite element formulation for solving structural-acoustic interaction problems. This was initially applied to modelling the behaviour of ships vibrating in a finite or infinite fluid. The governing equations for the behaviour of the structure of the ship and the fluid were developed in finite element form. These were then linked by a coupling matrix that describes the relationship between the fluid pressure and the structural displacement.



The main drawback to this approach is that the resulting matrices are asymmetric and are expensive to solve in terms of memory and computer time. The situation considered by Zienkiewicz and Newton is the reverse of a car passenger compartment where the fluid is bounded by a vibrating structure. However, the same equations apply for the solution of the problem. Once the significance of this work for modelling the interior acoustics of automobiles was realized there followed several publications detailing different formulations of acoustic elements and their experimental verification, the following references being typical of the work: Craggs (1972) using tetrahedron and cuboid elements, Shuku & Ishihara (1973) using triangular elements, Petyt Lea & Koopman (1976) using 20 node isoparametric element and Richards & Jha (1979) using triangular elements. Initially only the undamped natural frequencies and mode shapes of simplified cavities were considered with experimental data taken within wood or perspex scale models of car passenger compartments.

Nefske & Howell (1978) extended the scope of the method to link a finite element model of the air volume within the car to measured panel vibration data as a boundary condition. This was used to produce plots for ranking the noise contributions of individual panels at particular locations within the cavity with polar plots as defined by Jennequin (1971) at a given frequency.

Later papers (Nefske Wolf & Howell (1982), Sung & Nefske (1984) and Nefske & Sung (1985)) outline the full range of structural-acoustic interaction problems considered for the analysis of low frequency interior noise in cars. The finite element model of the cavity volume is analysed as though surrounded by a rigid reflective boundary for the extraction of the acoustic modes. A dynamic boundary is imposed from experimental data from a car body (Nefske Wolf & Howell (1982)) or a finite element model of the structure (Sung & Nefske (1984)) is used to produce a finite element model of the combined structural-acoustic system. Damping is included either by specifying the modal damping (structural and acoustic) or the absorption coefficient of boundary trim materials (Nefske & Sung (1985)). The models are used to predict noise spectra at particular locations within the cavity or the sound field at a particular frequency. Panel noise generation and absorber effectiveness plots can also be produced (Nefske & Sung (1985)).

The most descriptive way to describe the dynamics of a structure is as a modal model. The finite element method can be used to determine the structural modes of the car body shell and acoustic modes of the air cavity separately. The degree of interaction between individual structural and acoustic modes is dependent on their relative frequencies and mode shapes. Damping is also important as it affects the range of frequencies over which a mode can be excited. Determining this degree of interaction enables the most significant structural modes in terms of noise generation to be obtained. Richards (1982) uses a two dimensional model of the car cavity and surrounding body shell to study the degree of interaction between the structural ring modes and acoustic modes. A coupling coefficient based on a surface integral formulation of the product of a structural and acoustic eigenvector was defined this allows the degree of interaction between individual structural and acoustic modes to be determined. Sung et al (1991) extended this work to consider a three dimensional situation using the same coupling coefficient. The acoustic modes were found by the

finite element method and compared with experimentally determined structural modes. In both cases significant reduction in the peak values of the noise spectra were achieved by localized stiffening of panels.

A different approach was utilized by Yashiro et al (1985). The finite element formulation for the coupled behaviour of the combined structural-acoustic system without damping as developed by Zienkiewicz and Newton (1969) was modified. The acoustic pressure was assumed to have little effect on the structural modes. This allowed the original asymmetric matrix equation to be broken down into two separate equations with symmetric matrices. The first allows the acceleration of the body panels to be calculated and in turn these are used as a boundary condition for the acoustic model via the coupling matrix. From this the sound spectrum experienced by occupants can be predicted and the major noise generating panels at a problem frequency determined.

Shippen and Dunn (1988 and 1991) concentrate on the concept stage of vehicle design. Noise Transfer functions were calculated from a finite element model of the car structure and passenger compartment volume. Structural modes that did not affect the acoustics were determined by comparing their orthogonality to the acoustic modes through the coupling matrix and the reduced mode set was shown to give good correlation with experimental data with only half the structural modes included.

### **2.3 Experimental Analysis Of Acoustic Modes.**

A knowledge of the acoustic natural frequencies and mode shapes of a car passenger compartment is essential for the control of low frequency interior noise. Until the advent of frequency analysers the experimental measurement of acoustic modes involved finding the natural frequencies of the cavity of interest by comparing the relative phase of the source acceleration (measured with an accelerometer) and the pressure signal from a microphone. The mode shapes could then be determined by plotting the pressure distribution for each natural frequency of interest independently by exciting the cavity with a single frequency. Petyt et al (1976) describe this process in detail.

Smith (1976) utilized a Fourier analyser to determine the transfer functions between the acceleration of an acoustic source (speaker with an accelerometer attached) and the pressure response of a cavity measured by a microphone. The response was measured at ten locations along the centre line of the car allowing the first four longitudinal modes to be extracted. Whilst this allows simple acoustic mode shapes to be determined by assigning the measured pressure transfer functions an arbitrary direction for processing and displaying with structural modal software more complex three dimensional acoustic modes cannot easily be treated in this way.

An impedance based method has been developed and applied initially to ducts and lumped acoustic systems using coincident quadrature extraction (Nieter & Singh (1982)). This was then applied to annular cavities with three dimensional acoustic modes using vector diagram extraction

(Kung & Singh (1985)). Transfer function data is taken between the volume velocity of an acoustic source and microphone pressure measurements at various locations within the cavity of interest. Although mode shapes were successfully determined the technique is not suitable for direct implementation on a modern structural modal analysis package because of the lack of directionality in the transfer functions obtained.

The relationship between the pressure gradient, which is a vector, of a mode and particle acceleration has been used to determine the particle motion mode shapes of a cavity by a number of authors. It has been implemented by using a curve fit on a series of single microphone pressure transfer functions (Byrne (1985)), and by a finite difference calculation using a microphone pair with subsequent processing by structural modal analysis software (Knittel & Oswald (1987)). The method is relatively easy to implement with existing hardware and software. The input is provided from an accelerometer attached to the source speaker and the output from a pair of microphones. Processing the resulting transfer functions with a Fast Fourier Transform analyser and computer with structural modal software allows unambiguous three dimensional mode shapes to be determined. The drawback is that particle acceleration is spatially in quadrature with pressure in a standing wave. Thus the antinodes and nodes of the measured data are interchanged with those of the pressure mode shapes making comparison with finite element results difficult particularly for cavities with complex geometry.

#### **2.4 Measurement Of The Absorption Coefficient Of Trim Materials.**

The sound absorption provided by the trim materials is the major source of damping for the acoustic modes of a vehicle interior. It is necessary to include this in any finite element model as shown by Nefske & Sung (1985). The measurement of the absorption coefficient of automotive trim materials at low frequencies has been difficult until recently, the two main methods used elsewhere proving to be unsuitable. The reverberation room (Kuntruff (1979)) requires a large sample that is difficult to obtain for automotive materials whilst the impedance tube (ASTM (1990)) needs to be at least one quarter of a wavelength long. At 20 Hz this gives a length of 4.3 metres. In practice two minima should be measured for greater accuracy. Such a tube has recently been constructed (Swenson (1993)) for measurements in the range 20 to 100 Hz with an overall length of some 8.6 metres. The size and construction cost make such a piece of equipment unsuitable for general laboratory use.

Several alternative methods have been developed which allow the ranking of materials (Powers & Rudinoff (1975), Saha & Davis (1982)) at low frequencies. The advent of the Fourier analyser led to the development of twin microphone impedance tube techniques overcoming the previous length requirements (Chung & Blaser (1980), Elliott (1981), ASTM (1986), Højberg (1991)). These methods gives good results down to around 50 Hz. Below this the speaker is unable to generate sufficient noise for a good coherent transfer function between the microphones to be measured. A variation is given by Fahy (1984) using a single microphone in two positions within the impedance tube. The transfer function of the microphone outputs referenced to the speaker driving signal is

taken. This overcomes the need for calibrating the microphone pair. The two microphone method has been adapted as a free field technique by Allard and Sieben (1985). Tone burst techniques (Powell & Houten (1970), Yuzawa (1975)) are unsuitable because of the long wavelengths occurring at low frequencies.

## **2.5 Noise Control Methods.**

Having found the source of any unwanted cavity boom the next stage is to control it. As the main component of interior noise below 400 Hz is structure borne the most common approach which is used industrially is to reduce the amplitude of the panel vibration by applying a damping material. An alternative is to stiffen the panel to move its natural frequencies away from those of the acoustic mode (Jha (1976), Richards (1982)). Care must be exercised in this due to the significance of phase relationships between panels in noise generation. At low frequencies acoustic damping in the form of absorbent sheet or heavy carpets is ineffective because of the ratio of the acoustic wavelength to the thickness of the absorbent material (Jha (1976)). This makes the use of acoustic absorbers impractical.

Other methods that have been implemented have been changing the geometry of the car to shift the acoustic natural frequencies (Kojic et al (1984)) and the use of a luggage compartment resonator (Franco (1991)). Although effective these techniques require major alterations to the car design. Reducing the level of input to the structure would involve a major redesign of the main sources of excitation such as the engine or suspension. Modifying such items would be a major undertaking and this would not be allowed to affect ride, handling, economy etc. which form the main design criteria of these items and are fixed at a very early stage of the development process. Since the form of the body has already been established by aerodynamic and style (fashion) considerations the design changes that can be introduced in the noise and vibration test environment are minor and only available in the very early stages of the development process. Also later in the development of a vehicle work has often begun on producing the dies for forming the body panels making any major changes impractical at this stage. Consequently vibration and noise control methods are often limited solely to the use of palliative treatments.

### 3 Theory.

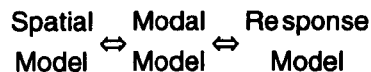
The background theory relevant to this project will now be covered. The equations describing structural and acoustic modal behaviour are developed and used as an introduction to finite element techniques and experimental modal analysis methods.

NB A harmonic solution for all equations is assumed throughout as this is the type of excitation provided by the out of balance forces.

#### 3.1 Modelling System Dynamics.

There are three ways in which the dynamics of a system (structural or acoustic) can be modelled, by the spatial, modal or response models. Each of these has different characteristics making it suitable for a different type of analysis. The process of modal analysis involves generating or measuring one model (usually spatial or response) and processing to determine the properties of another. This relationship is shown in figure. 3.1.

Fig. 3.1 Spatial, Modal and Response Models.



The spatial model is formed from the mass, stiffness and damping matrices of the system. Modal properties can be extracted from these and in turn used to predict the frequency response functions at specific locations. This represents the analytical route of modal analysis as is used by the finite element method and other numerical techniques. The alternative (experimental) approach is to measure the frequency response at several locations and use numerical algorithms to determine the natural frequencies and mode shapes. Converting the modal model to a spatial model is rarely successful because of the difficulties in creating mass and stiffness matrices from the incomplete modal model. Fortunately this is seldom a problem as the modal model is the most useful for noise and vibration control.

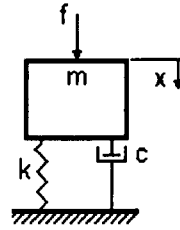
#### 3.2 Structural Modal Theory.

The spatial, modal and response models are formulated for both single degree of freedom systems (SDOF) then the multidegree of freedom (MDOF) case.

##### 3.2.1 Single Degree Of Freedom System.

Figure 3.2 shows the classical viscously damped SDOF system.

Fig. 3.2 SDOF System.



The equation of motion for this can be written as:

$$m\ddot{x}(t) + c\dot{x}(t) + kx(t) = f(t) \quad (3.1)$$

Assuming a sinusoidal input and response of the form  $f(t) = Fe^{j\omega t}$  and  $x(t) = Xe^{j\omega t}$  with  $F$  and  $X$  being complex to account for phase difference equation 3.1 can be rewritten as:

$$((k - \omega^2 m) + j\omega c)Xe^{j\omega t} = Fe^{j\omega t} \quad (3.2)$$

From this undamped free vibration can be expressed as:

$$(k - \omega^2 m) Xe^{j\omega t} = 0 \quad (3.3)$$

Giving a natural frequency of

$$\omega_n = \sqrt{\frac{k}{m}} \quad (3.4)$$

Below the natural frequency the response is dominated by the stiffness of the spring, and above it the inertia of the mass is dominant.

The response of a system is expressed as its displacement per unit input. From equation 3.1 this can be expressed as

$$\frac{X}{F} = \frac{1}{(k - \omega^2 m) + j(\omega c)} \quad (3.5)$$

and is termed the receptance ( $\alpha(\omega)$ ) and is independent of the form of the excitation. This response can also be defined in terms of the velocity (mobility  $Y(\omega)$ ) and acceleration (inertance  $A(\omega)$ ). In practice only one of these needs to be determined as they are related by an integral relationship

$$Y(\omega) = j\omega(\alpha(\omega)) \quad (3.6)$$

$$A(\omega) = -\omega^2(\alpha(\omega)) \quad (3.7)$$

### 3.2.2 Multi Degree Of Freedom System.

Systems having more than one degree of freedom are described using matrix methods. An equation of motion is written for each degree of freedom and these are combined in the mass,

stiffness and damping matrices. This gives for harmonic analysis an expression which is similar to equation 3.2

$$([K] - \omega^2[M] + j\omega[C])(X)e^{j\omega t} = \{F\}e^{j\omega t} \quad (3.8)$$

There are now as many natural frequencies as there are degrees of freedom. These can be found from the eigensolution of the characteristic equation

$$|[M]^{-1}[K] - \omega^2[I]| = 0 \quad (3.9)$$

Associated with the diagonal matrix of natural frequencies, the spectral matrix  $[\omega^2]$ , is the modal matrix  $[\psi]$  which has as its columns the eigenvectors,  $\{\psi\}$  of the system which describe the individual mode shapes.  $[K]$  and  $[M]$  are the spatial model of the system and the matrices  $[\omega^2]$  and  $[\psi]$  form the modal model.

For the forced response analysis the receptance can be written as

$$\frac{\{X\}}{\{F\}} = ([K] - \omega^2[M] + j\omega[C])^{-1} = [\alpha(\omega)] \quad (3.10)$$

The receptance matrix  $[\alpha(\omega)]$  forms the response model of the system.

### 3.2.3 Damping.

There are several models of damping used in structural analysis namely, viscous, proportional and hysteretic (Ewins (1986)). The classical model is a viscous damper with the force generated by damping being proportional to velocity. Hence the level of damping increases with frequency (equations 3.5 and 3.10). MDOF systems more usually show a damping level that is inversely proportional to frequency ( $c = b/\omega$  where  $b$  is a constant) giving a slightly different loss term in the response model of a system. However for the purposes of this chapter viscous damping has been assumed for simplicity. However, In practice more than one damping mechanism may be acting.

### 3.3 Modal Normalization.

The eigenvector associated with a particular mode  $\{\Psi\}_r$  describes the relative displacements of points on the system and as such is not a unique solution. Normalization is almost always used for computation and display purposes. There are several methods available, but mass normalization is described here as it is applied to the mode shapes presented later in this work.

Mass normalization results in a unique eigenvector  $\{\Phi\}$ . The advantage of this method is that mass normalization can be implemented on modes obtained either from spatial or response models making it useful for comparing analytical and experimental data. The method is based on the orthogonality properties of the modal model (Ewins (1986)).

From the spatial model the orthogonal properties of the eigenvectors with respect to the mass and stiffness matrices can be expressed as

$$[\psi]^T [M] [\psi] = [m] \quad (3.11)$$

and

$$[\psi]^T [K] [\psi] = [k] \quad (3.12)$$

where  $[m]$  and  $[k]$  are diagonal and termed the generalized mass and stiffness matrices. The mass normalized mode shapes are defined as having the properties

$$[\Phi]^T [M] [\Phi] = [I] \quad (3.13)$$

$$[\Phi]^T [K] [\Phi] = [\omega^2] \quad (3.14)$$

Thus the mass normalized mode shapes can be found from

$$[\Phi] = [\psi][m]^{-0.5} \quad (3.15)$$

Mass normalization from the response model is achieved by considering the response of the model at a given frequency  $\omega$  as the sum of the contribution from all modes. For the undamped case the receptance between two points can be expressed as

$$\alpha(\omega)_{jk} = \sum_{r=1}^N \frac{r A_{jk}}{\omega_r^2 - \omega^2} = \sum_{r=1}^N \frac{(r\Phi_j)(r\Phi_k)}{\omega_r^2 - \omega^2} = \sum_{r=1}^N \frac{(r\psi_j)(r\psi_k)}{m_r(\omega_r^2 - \omega^2)} \quad (3.16)$$

Where  $A$  is the modal constant for the  $r^{\text{th}}$  mode for excitation at  $j$  and response at  $K$ . For a point measurement the modal constant can be expressed as

$$r A_{jj} = (r\Phi_{jj})(r\Phi_{jj}) \quad (3.17)$$

From this the mass normalised mode shapes can be found by dividing each column of the modal matrix  $[\psi]$  by the square root of the modal constant of its point measurement to give the mass normalized modal matrix  $[\Phi]$ .

### 3.4 Experimental Modal Analysis.

Experimental modal analysis involves the extraction of modal properties from measured FRF data. For structures the most usual measurement is inertance with force transducers and accelerometers. Two SDOF modal extraction methods, peak-amplitude and circle fit (Ewins (1986)), are discussed in detail. The available MDOF modal extraction methods are based on multiple curve fitting (Smiley, Whey & Hogg (1984)) and matrix manipulation (Fillod et al (1985)).



### 3.4.1 Peak Amplitude Method.

Figure 3.3 shows the frequency response function for a single degree of freedom system. The resonant frequency  $\omega_r$  is assumed to be at the point of peak amplitude  $\alpha_{\max}$ . The frequencies of the half power points ( $\alpha_{\max}/\sqrt{2}$ ),  $\omega_a$  and  $\omega_b$  are then used to estimate the damping. For a lightly damped system this can be expressed as

$$\eta_r = \frac{(\omega_b^2 - \omega_a^2)}{\omega_r^2} \approx \frac{\Delta\omega}{\omega_r}$$

where  $\eta_r$  is the modal loss factor for the  $r^{\text{th}}$  mode (3.18)

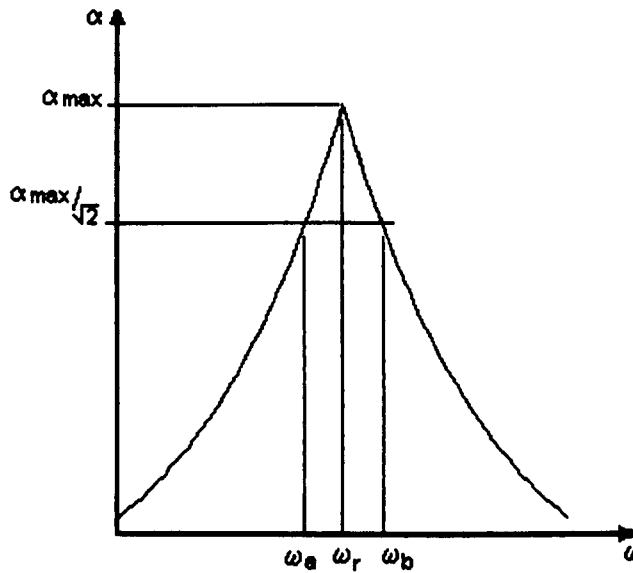
The general relationship for receptance given in 3.16 can be modified to suit a single degree of freedom system with the loss term  $\eta_r$  included.

$$\alpha(\omega) = \frac{A_r}{(\omega_r^2 - \omega^2 + j\eta_r\omega_r^2)} \quad (3.19)$$

The strength of the modal constant can be estimated from

$$A_r = \alpha_{\max}\omega_r^2\eta_r \quad (3.20)$$

Fig. 3.3 SDOF Resonance



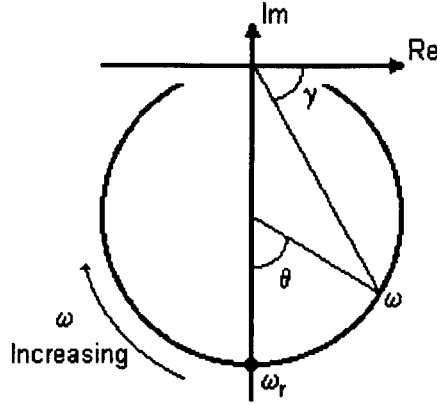
The peak amplitude method does not give any phase information and has now been superseded by extraction methods using complex information.

### 3.4.2 Circle Fit Method.

The circle fit method was the first to use complex FRF data to extract modal properties. This is a SDOF modal extraction method based in the characteristics of Nyquist plots of FRF data. In this case the theory is developed for structural damping as this is the general form used in the majority

of commercial software applications. It can be shown that for a SDOF system with structural damping a Nyquist plot of the receptance forms a true circle in the frequency range  $0-\infty$  (Ewins (1986)). This characteristic is used to extract modal properties. Figure 3.4 shows the Nyquist plot of inertance for a structurally damped SDOF system

Fig. 3.4 Nyquist Plot.



The receptance for a SDOF system with structural damping can be written as

$$\alpha = \frac{1}{\omega_r^2 (1 - (\omega / \omega_r)^2 + j\eta_r)} \quad (3.21)$$

From this it can be seen that for any frequency,  $\omega$ , the ratio of the imaginary to real part of the receptance is given by

$$\tan \gamma = \frac{\eta_r}{1 - (\omega / \omega_r)^2} \quad (3.22)$$

Using trigonometric relationships

$$\tan \left( \frac{\theta}{2} \right) = \tan (90 - \gamma) = \frac{1 - (\omega / \omega_r)^2}{\eta_r} \quad (3.23)$$

Hence

$$\omega^2 = \omega_r^2 \left( 1 - \eta_r \tan \left( \frac{\theta}{2} \right) \right) \quad (3.24)$$

Differentiating equation 3.24 with respect to  $\theta$  gives.

$$\frac{d\omega^2}{d\theta} = \frac{-\omega_r^2 \eta_r}{2} \sec^2 \left( \frac{\theta}{2} \right) = \left( \frac{-\omega_r^2 \eta_r}{2} \right) \left( 1 + \frac{(1 - (\omega / \omega_r)^2)^2}{\eta_r^2} \right) \quad (3.25)$$

$$\sec^2 \theta = 1 + \tan^2 \theta$$

The reciprocal of this quantity gives the rate at which the locus sweeps around the circle. This reaches a maximum value when  $\omega = \omega_r$ . It is this characteristic that is used to determine the natural frequency from experimental data by finding the greatest sweep rate between data points

on the FRF. Equation 3.25 can also be used to estimate the modal loss factor  $\eta_r$  if  $\omega_r$  is known since at  $\omega = \omega_r$  the expression reduces to

$$\left( \frac{d\omega^2}{d\theta} \right)_{\omega=\omega_r} = -\frac{\omega_r^2 \eta_r}{2} \quad (3.26)$$

Once the natural frequency  $\omega_r$  is known equation 3.25 can be used to analyse any variations in damping around the resonance.

For fitting on MDOF FRFs the residual effects of any other modes can be shown to cause the circle to be displaced from the origin (Ewins (1986)).

### 3.5 Acoustic Modal Theory.

The wave equation is developed for three dimensional acoustic regions and this is then extended to find the natural frequencies and mode shapes of a simple rectangular rooms. Initially rigid reflective boundaries are considered then non-rigid absorbent walls.

#### 3.5.1 Travelling And Standing Waves.

The human ear responds to variations in pressure as a compression wave passes. Associated with this variation of pressure is a motion of the gas in addition to its normal molecular motion. These perturbations are sufficiently small for the relationship between the particle motion and acoustic pressure to be considered as linear. The following assumptions also apply.

- 1.The fluid is compressible
- 2.Internal losses are negligible
- 3.There is no flow of the fluid
- 5.The mean density and pressure are uniform throughout the fluid

For an arbitrary set of cartesian coordinates the particle velocity of a gas as an acoustic wave passes can be written as the vector sum of its component along each axis

$$\bar{u}_T = \bar{u}_x + \bar{u}_y + \bar{u}_z \quad (3.27)$$

Hence the total acoustic pressure can be described by the scalar sum of the pressures associated with the particle motions along each axis

$$p_T = p_x + p_y + p_z \quad (3.28)$$

This allows the analysis of acoustic waves to be considered along a single axis simplifying the analysis.

The behaviour of compression waves in three dimensions is described by the wave equation

$$c^2 \nabla^2 p = \frac{\partial p}{\partial t}$$

Where  $c$  is the velocity of sound for the gas (3.29)

For a single Cartesian ( $x$ ) axis this can be rewritten as

$$c^2 \frac{\partial^2 p_x}{\partial x^2} = \frac{\partial^2 p_x}{\partial t^2} \quad (3.30)$$

Neglecting subscripts this has the solution

$$p = Ae^{j(\omega t - kx)} + Be^{j(\omega t + kx)} \quad (3.31)$$

Where  $k$  is the wavenumber and the right hand side represents two sinusoidal waves of magnitude  $A$  and  $B$  (travelling in opposite directions).

Considering the effects of the forward travelling wave

$$p = Ae^{j(\omega t - kx)} \quad (3.32)$$

in isolation. The relationship between the acoustic pressure and the particle velocity is given by

$$\frac{\partial p}{\partial x} = -\rho_0 \frac{\partial \bar{u}_T}{\partial t}$$

Where  $\rho_0$  is the mean fluid density. (3.33)

This relationship gives the particle velocity of a forward travelling wave as

$$\bar{u} = \frac{1}{\rho_0 c \omega} Ae^{j(\omega t - kx)} \quad (3.34)$$

Comparing equations 3.31 and 3.34 it can be seen that pressure and particle velocity are spatially and temporally in phase in a propagating acoustic wave.

An idealized acoustic mode is formed from two waves of equal magnitude and frequency but opposite directions combining with constructive interference. i.e.

$$p = Ae^{j(\omega t - kx)} + Ae^{j(\omega t + kx)} \quad (3.35)$$

$$p = Ae^{j\omega t} (e^{-jkx} + e^{jkx}) \quad (3.36)$$

Equation 3.33 gives

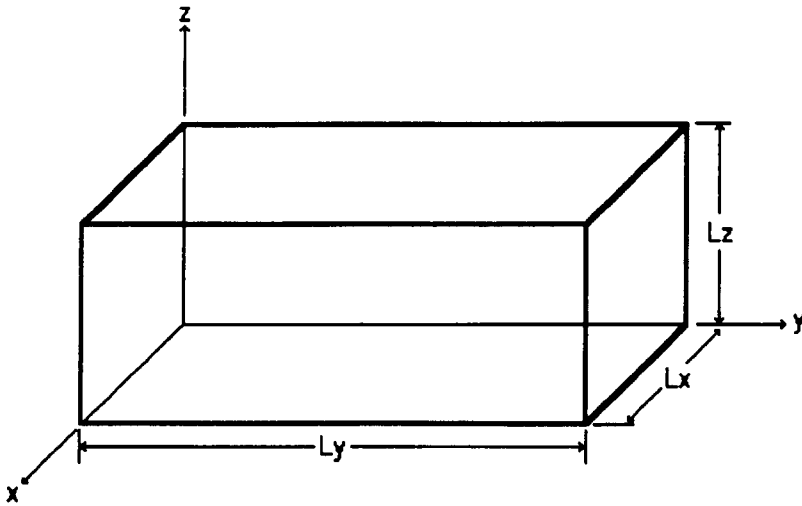
$$\bar{u} = \frac{1}{\rho_0 c \omega} - jA(jke^{jkx} - jke^{-jkx})e^{j\omega t} \quad (3.37)$$

Hence, the pressure and particle velocity are spatially and temporally in quadrature in a standing wave. It is this interchange of energy that enables the wave to exist without propagation.

### 3.5.2 Normal Modes Of Rectangular Cavities.

In enclosed volumes of gas the acoustic modes are standing waves formed by reflection at the boundaries. At certain frequencies the wavelength (or multiples thereof) is the same as the dimensions of the cavity and a standing wave is formed. The frequencies at which this occurs is affected by the geometry of the cavity. Although this is usually too involved for an exact analysis the simple case of a rectangular cavity can be considered. The walls are considered as rigid and perfectly reflective with the absorption of the air itself being negligible over short distances at low frequencies. Such a cavity is shown in figure 3.5.

Fig. 3.5 Rectangular Cavity.



The wave equation (3.29) can be expressed in time independent form as

$$\nabla^2 p + k^2 p = 0 \quad (3.38)$$

Where  $k$  is the wavenumber ( $1/\lambda$ )

Considering pressure variation in just the  $x$  direction equation 3.38 reduces to

$$\frac{d^2 p_x}{dx^2} + k_x^2 p_x = 0 \quad (3.39)$$

Rigid walls give a boundary condition of

$$\begin{aligned} \bar{u}_x &= 0 \text{ at } x = 0 \text{ and } x = L_x \\ (\therefore \frac{\partial \bar{u}_x}{\partial t} &= 0 \text{ at } x = 0 \text{ and } x = L_x) \end{aligned} \quad (3.40)$$

From equation 3.33 this gives

$$\frac{dp_x}{dx} = 0 \text{ at } x = 0 \text{ and } x = L_x \quad (3.41)$$

Equation 3.39 has a general solution of the form

$$p_x = A_x e^{jk_x x} + B_x e^{-jk_x x} \quad (3.42)$$

Considering a wave travelling in the x positive direction and expressing it in trigonometric form equation 3.42 can be reduced to

$$p_x = A_x \cos(k_x x) + B_x \sin(k_x x) \quad (3.43)$$

In order to satisfy equation 3.41  $B_x$  must equal zero as a sine term does not have a zero gradient at  $x = 0$ . For the gradient to equal zero at  $x = L_x$  the term  $\cos(k_x L_x)$  must equal  $\pm 1$ . Thus  $k_x L_x$  must be an integer multiple of  $\Pi$

$$k_x = \frac{n_x \Pi}{L_x} \quad (3.44)$$

Where  $n_x$  is an integer

Similar arguments hold for the other axes giving

$$k_y = \frac{n_y \Pi}{L_y} \quad (3.45)$$

$$k_z = \frac{n_z \Pi}{L_z} \quad (3.46)$$

The wavenumber of each axis has a trigonometric relationship with the global wavenumber

$$k_x^2 + k_y^2 + k_z^2 = k^2 \quad (3.47)$$

Hence

$$k = \Pi \sqrt{\left(\frac{n_x}{L_x}\right)^2 + \left(\frac{n_y}{L_y}\right)^2 + \left(\frac{n_z}{L_z}\right)^2} \quad (3.48)$$

The natural frequencies of the room can be found from

$$f = \frac{ck}{2\Pi} \quad (3.49)$$

Hence

$$f = \frac{c}{2} \sqrt{\left(\frac{n_x}{L_x}\right)^2 + \left(\frac{n_y}{L_y}\right)^2 + \left(\frac{n_z}{L_z}\right)^2} \quad (3.50)$$

The pressure field for a given mode is then defined as the multiple of the three cosine functions that define the pressure along each axis

$$p_T = D \cos\left(\frac{n_x \Pi x}{L_x}\right) \cos\left(\frac{n_y \Pi y}{L_y}\right) \cos\left(\frac{n_z \Pi z}{L_z}\right)$$

Where  $D$  is a constant (3.51)

The boundary of a car passenger compartment has non rigid absorbent walls. The acoustic characteristics of any boundary can be described by its impedance ( $Z$ ). This is a complex quantity as it must account for the effects of both phase and magnitude on the reflected wave. A discussion of the various boundary conditions and their effects is beyond the scope of this section. The main consideration is the effect on mode shape of a flexible wall.

A simple example is considered in which the wall impedance is assumed to be uniform for any given wall and that the opposite wall has the same impedance at a given frequency.

The boundary conditions are now changed as the particle velocity is no longer zero at the wall. Again considering the  $x$  axis independently equation 3.33 gives

$$\bar{u}_x = -\frac{1}{j\rho_0\omega} \frac{dp_x}{dx} \quad (3.52)$$

Replacing  $u_x$  with  $p_x/Z_x$  where  $Z$  is the characteristic impedance

$$Z_x \frac{dp_x}{dx} + j\rho_0\omega p_x = 0 \quad (3.53)$$

However, as the specific acoustic impedance  $z = Z/(\rho_0 c)$  equation 3.53 can be rewritten as

$$z_x \frac{dp_x}{dx} + jk_x p_x = 0 \quad (3.54)$$

Assuming a solution of the same form as equation 3.43 the complex wave equation is

$$p_x = A_x \cos(k_x x) + B_x \sin(k_x x) \quad (3.55)$$

The wave number  $k_x$  is now complex and the impedance determines the ratio of the constants  $A_x$  and  $B_x$ . The boundary conditions at  $x=0$  and  $x=L_x$  need to be applied to equation 3.54. It can be seen that for a rigid reflective wall  $z = \infty$  and  $B_x = 0$  as was described previously. The main consideration pertinent to this work is the effect of the boundary impedance on mode shape. Using the general trigonometric identity

$$P \cos \theta + Q \sin \theta = R \cos(\theta - \alpha) \quad (3.56)$$

Where

$$R = \sqrt{P^2 + Q^2} \quad \alpha = \tan^{-1}\left(\frac{Q}{P}\right)$$

Thus equation 3.55 becomes

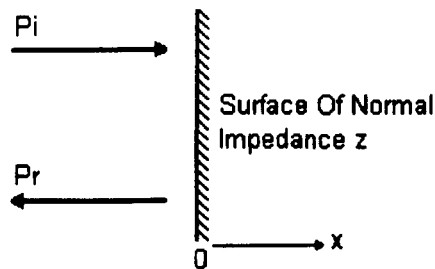
$$p_x = C_x \cos(k_x x - \alpha_x) \quad (3.57)$$

It can be seen that the mode shape is still a sinusoidal function. The phase shift,  $\alpha$ , shifts the antinode of the pressure wave away from the boundary shifting the natural frequencies and affecting the mode shapes.

### 3.6 Sound Absorption.

The main acoustic absorption in a car passenger compartment occurs at the boundary within the trim materials (seats, carpets, etc.), the absorption by the air itself being negligible. The absorption coefficient of a material is dependent on the frequency and angle of incidence of the acoustic wave. The majority of the acoustic modes associated with boom problems are axial modes allowing the consideration of waves which are only normally incident to a surface. Figure 3.6 shows the incident and reflected waves normal to such a surface.

Fig. 3.6 Reflection Of Normally Incident Sound At A Surface.



The sound field to the left of the surface can be described by the sum of the incident and reflected waves

$$\begin{aligned} p &= p_i + p_r \\ &= A e^{j(\omega t - kx)} + B e^{j(\omega t + kx)} \end{aligned}$$

Where A and B are complex constants (3.58)

The ratio of the reflected wave to the incident wave is termed the reflection coefficient R and is itself complex

$$R = \frac{B}{A} \quad (3.59)$$

The absorption coefficient is defined as the ratio of the absorbed energy to the incident energy. As the energy in a wave is a function of  $p^2$  the absorption coefficient can be expressed as

$$\alpha = 1 - |R|^2 \quad (3.60)$$

Impedance tube methods for determining the absorption coefficient and impedance of materials do this by determining the ratio of B/A (Kuntruff (1979)).

### 3.7 Finite Element Method.

The theory of acoustic modal analysis using the finite element method is covered. The partial discretization of acoustic systems is covered as this separates the spatial and temporal parts of the wave equation (3.29) into a form analogous to the structural multi degree of freedom system (equation 3.8). This is significant in the experimental analysis of acoustic modes with structural



modal analysis software (Knittel & Oswald (1987)). The detailed formulations of acoustic elements are not given as these are covered by several texts (Zienkiewicz & Taylor (1989)) and in the relevant software manuals.

### 3.7.1 Analysis types.

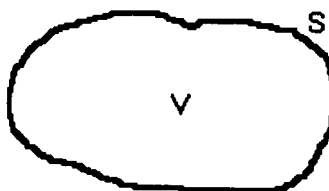
The finite element method offers two ways of studying the behaviour of acoustic and structural-acoustic systems in the frequency domain.

1. The natural frequencies and mode shapes of acoustic and structural-acoustic systems can be found by solving the spatial model using the finite element method. Thus the acoustic modes obtained are for boundaries with no absorption.
2. The steady state response of a system can be predicted by direct solution of the spatial model or by modal superposition at a given frequency for a specified input.

### 3.7.2 Discretization Of Acoustic Systems.

For acoustic systems to be modelled using the finite element method the actual continuous acoustic medium must be approximated by a discrete equivalent. Considering an arbitrary acoustic cavity of volume  $V$  and surface  $S$  as shown in figure 3.7 with unit depth and applying the assumptions defined in chapter 3.3.1.

Fig. 3.7 Defined Continuum.



The acoustics of the cavity are described by the wave equation

$$c^2 \nabla^2 p = \frac{\partial p}{\partial t} \quad (3.61)$$

As has been discussed (chapter 3.3.2) an exact solution to equation 3.61 is only possible for simple cases. To overcome this limitation numerical methods are used to obtain an approximate solution. In the finite element method the domain is broken down into nodes with interconnecting elements and a solution assumed of the form.

$$p \approx p_{\text{approx}} = \sum_i N_i p_i = [N][p]$$

Where  $[N]$  is the matrix of shape functions  
 $[p]$  is the matrix of nodal pressures

$$(3.62)$$

In this case a partial discretization is required separating the spatial and temporal parts of the wave equation. Spatial variations are included in the shape function and temporal considerations in the pressure term. i.e.

$$N = N_{(x,y,z)}, \quad p = p(t) \quad (3.63)$$

Substituting equation 3.62 in equation 3.61 gives

$$\{\nabla\}[N]\{\nabla\}^T[p] - (c^2)^{-1}[N]\{\ddot{p}\} = 0$$

Where  $\{\nabla\} = \left\{ \frac{\partial}{\partial x} \frac{\partial}{\partial y} \frac{\partial}{\partial z} \right\}$  (3.64)

Applying the Galerkin weighted residual method to equation 3.64 and integrating over the volume gives

$$-\frac{1}{c^2} \int_V ([N][N]^T) \{\ddot{p}\} dV + \int_V (\{\nabla\}[N][N]^T \{\nabla\}^T) dV \{p\} = 0 \quad (3.65)$$

From equation 3.65 the undamped natural frequencies and mode shapes can be extracted . However for an harmonic analysis any boundary losses must be included. The model of the boundary losses is based on the acoustic impedance of the surface or its absorption coefficient. Craggs (1986) gives a gives a boundary loss term for a rigid porous absorber based on its acoustic flow resistivity such that the loss term D can be expressed as

$$D = \frac{1}{c} \left( \frac{R}{\rho_0 c} \right) \dot{p} \quad (3.66)$$

Where R is the acoustic flow resistance

The term  $R/\rho_0 c$  can be shown to equal the acoustic absorption coefficient  $\alpha$  of the boundary. Using this relationship and applying the approximate solution and weighted residual, integrating over the surface area of the boundary gives

$$D = \frac{\alpha}{c} \int_S [N][N]^T dS \{\dot{p}\}$$

Where  $\alpha$  is the absorption coefficient of the boundary (3.67)

Thus equations 3.65 and 3.67 can be combined with an acoustic source at a single node expressed as a volume velocity to give

$$[M]\{\ddot{p}\} + [C]\{\dot{p}\} + [K]\{p\} = \{F\}$$

where

$$[M] = -(c^2)^{-1} \int_V ([N][N]^T) dV$$

$$[C] = \left(\frac{\alpha}{c}\right) \int_S ([N][N]^T) dS$$

$$[K] = \int_V (\nabla[N][N]^T \nabla^T) dV$$

$$\{F\} = \{0 \dots Q \dots 0\}^T$$

(3.68)

From this point the modes can be extracted. It should be noted that the form of equation 3.68 is similar to 3.8 making it analogous to a structural MDOF system.

For a coupled structural analysis equation 3.68 can be coupled to its structural equivalent to describe a fluid structure interface. This is done via a coupling matrix that relates pressure, displacement and force (Zienkiewicz & Newton (1969)).

#### 4. Modelling Car Cavity Acoustic Modes.

The construction of the finite element model of the acoustic cavity of a Rover Metro-R6 for predicting the acoustic natural frequencies and mode shapes of the passenger compartment is discussed and the results presented. The ANSYS finite element software has been used throughout this project for the acoustic modelling. A full discussion of the ANSYS element and analysis capabilities is given in the ANSYS manual (ANSYS (1992)).

##### 4.1 ANSYS Acoustic Elements.

The models created for this project have been three dimensional using the ANSYS FLUID30 eight noded brick acoustic element. This element also has prism and tetrahedron options available. The following assumptions and restrictions are applicable

1. The fluid is compressible (density changes due to pressure variations).
2. Inviscid fluid (no dissipative effect due to viscosity).
3. There is no mean flow of the fluid.
4. The mean density and pressure are uniform throughout the fluid.
5. Analyses are limited to relatively small acoustic pressures so that the changes in density are small compared with the mean density

Other options, relevant to the later forced response analysis is the analysis of structural-acoustic interaction via a coupling matrix giving a combined formulation (Zienkiewicz & Newton (1969)) and the inclusion of boundary losses as a specified absorption coefficient (Craggs (1986)).

##### 4.2 Finite Element Modal Extraction and Expansion.

The finite element method determines the modes of a system by generation and solution of the spatial model. An acoustic equivalent of equation 3.9 for a MDOF system with no forcing input can be written as

$$([K] - \omega^2[M])\{p\}e^{j\omega t} = 0$$

Where  $[M]$  and  $[K]$  are the acoustic mass and stiffness matrices defined in equation 3.68 (4.1)

Hence the natural frequencies can be found from

$$|[K] - \omega^2[M]| = 0 \quad (4.2)$$

and the pressure mode shapes determined by substitution of the natural frequencies in equation 4.1. This gives the undamped modes of the system which are then mass normalized as discussed in chapter 3.3.

There are several modal extraction algorithms available within ANSYS. The full subspace method with all the nodal pressures defined as master degrees of freedom was found to give the best results. This was established by comparing finite element predictions of the modes of a rectangular cavity with those calculated from equation 3.50 (see chapter 5).

#### **4.3 Construction of The Model.**

The geometry of the Metro passenger compartment was determined by measurement of the test body used for this project. This was necessary as Rover did not have the relevant data. To simplify the model curved surfaces (door panels etc.) were modelled as a flat surface at the mid point of the panels depth.

It was decided to extract the acoustic modes of the cavity up to 250 Hz to ensure that any modes above 200 Hz that may have significant residual effects in the frequency range of interest were not omitted. The ANSYS software specifies that the element edge length should be less than one sixth the wavelength,  $\lambda$ , at the maximum frequency of interest. Assuming the speed of sound in air to be  $344 \text{ ms}^{-1}$  this gives a maximum element edge length of 0.23 m.

The generation of the mesh was initially done interactively by automatic meshing of rectangular sub volumes and direct generation of prism elements where required. This was then converted to direct generation of nodes and elements via a batch file to facilitate transfer of the model to a new version of the ANSYS package (4.4A to 5.0). The structure of this batch file with the necessary commands to extract the natural frequencies and expand the mode shapes is given in Appendix 1.

#### **4.4 Metro-R6 Acoustic Modes Predicted By FEA.**

Table 4.1 shows the natural frequencies and mode shapes for the passenger compartment acoustic modes predicted by an ANSYS FEA. The mode shape is identified by the number of half waves in the x,y,z (longitudinal, lateral and vertical) directions respectively. Table 4.1 lists the first seven acoustic modes of the passenger compartment. As can be seen the first mode above 200 Hz occurs at 226 Hz. This is sufficiently above the frequency range of interest for these higher modes to be neglected.

A detailed discussion of the significance and accuracy of these results is given in chapter 6 where the predicted and experimental natural frequencies and mode shapes are compared.

Table 4.1 Metro-R6 Acoustic Modes.

Mode	Frequency (Hz)	Mode shape
1	73.4	1 0 0
2	138.2	2 0 0
3	141.5	0 1 0
4	162.1	1 1 0
5	176.3	0 0 1
6	190.4	1 0 1
7	198.0	2 1 0
8	226.3	2 0 1

Figures 4.1 to 4.7 show the ANSYS predicted pressure mode shapes for each of the above natural frequencies up to 200 Hz.

Fig. 4.1 Metro-R6 First Acoustic Mode.

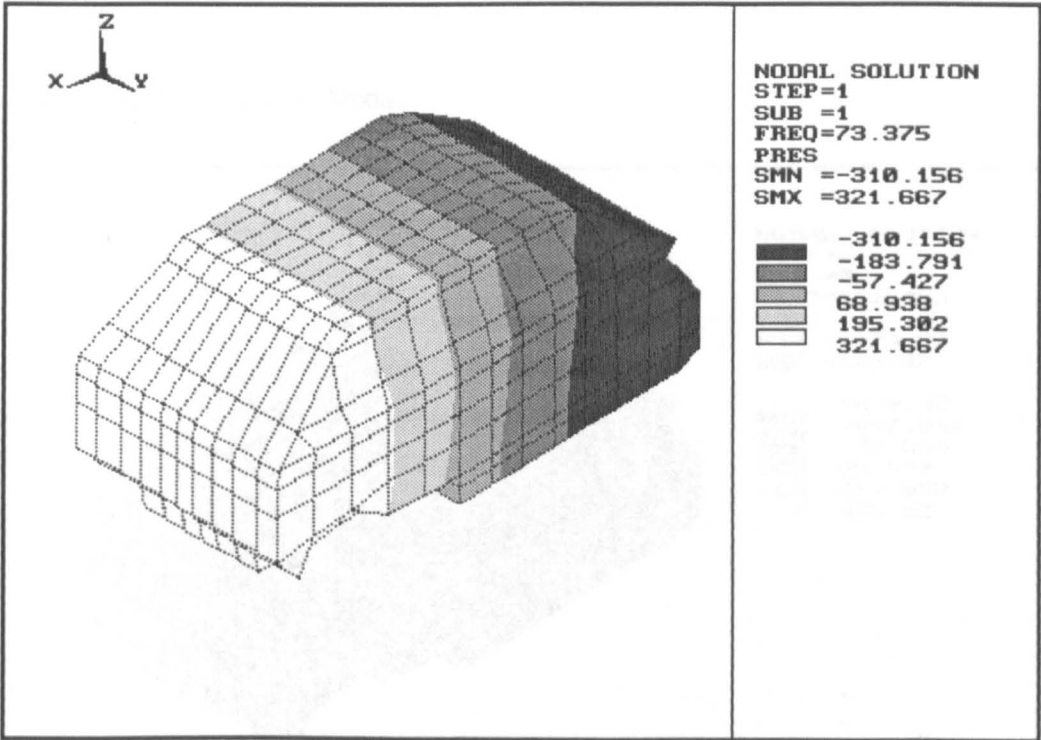


Fig. 4.2 Metro-R6 Second Acoustic Mode.

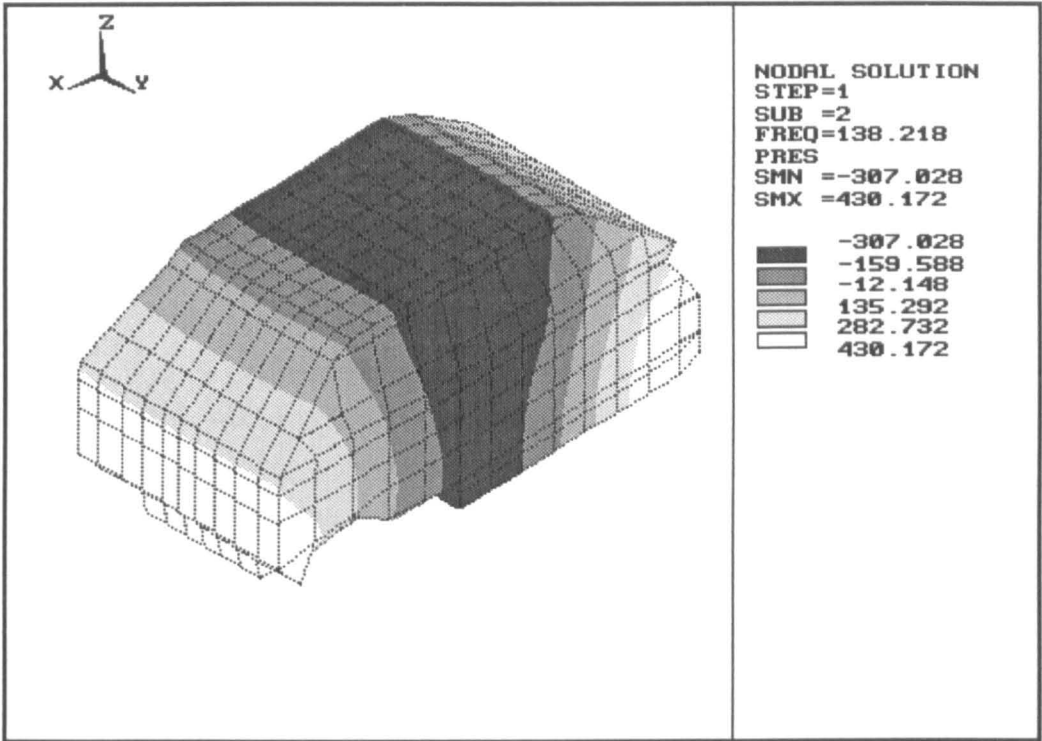


Fig. 4.3 Metro-R6 Third Acoustic Mode.

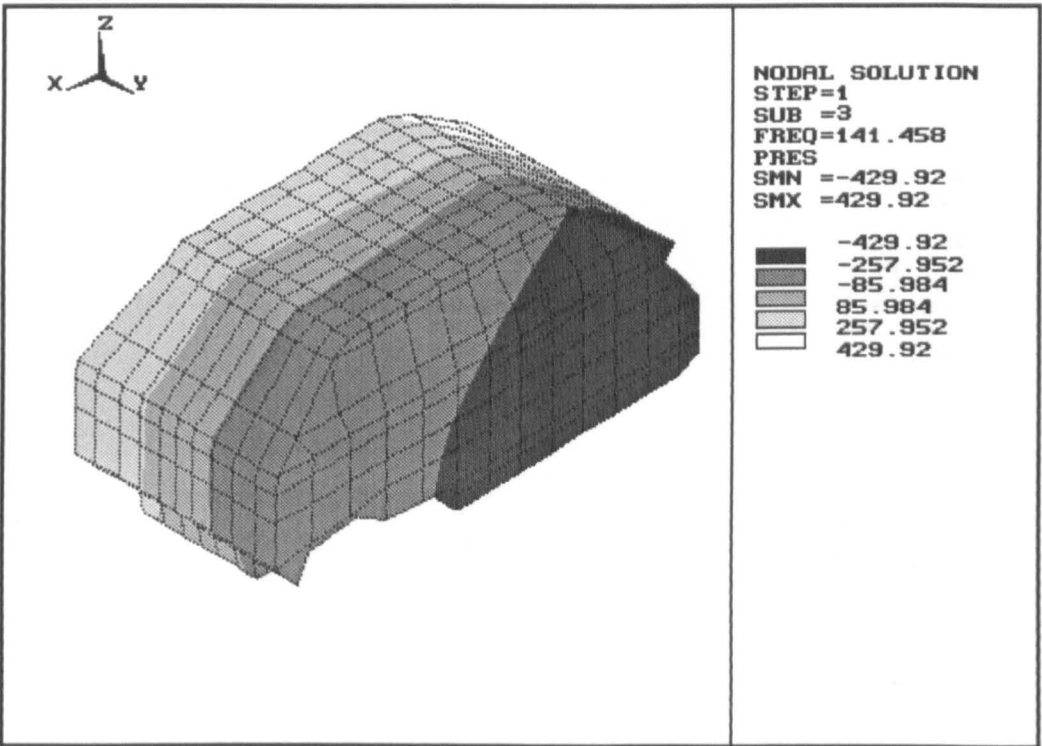


Fig. 4.4 Metro-R6 Fourth Acoustic Mode.

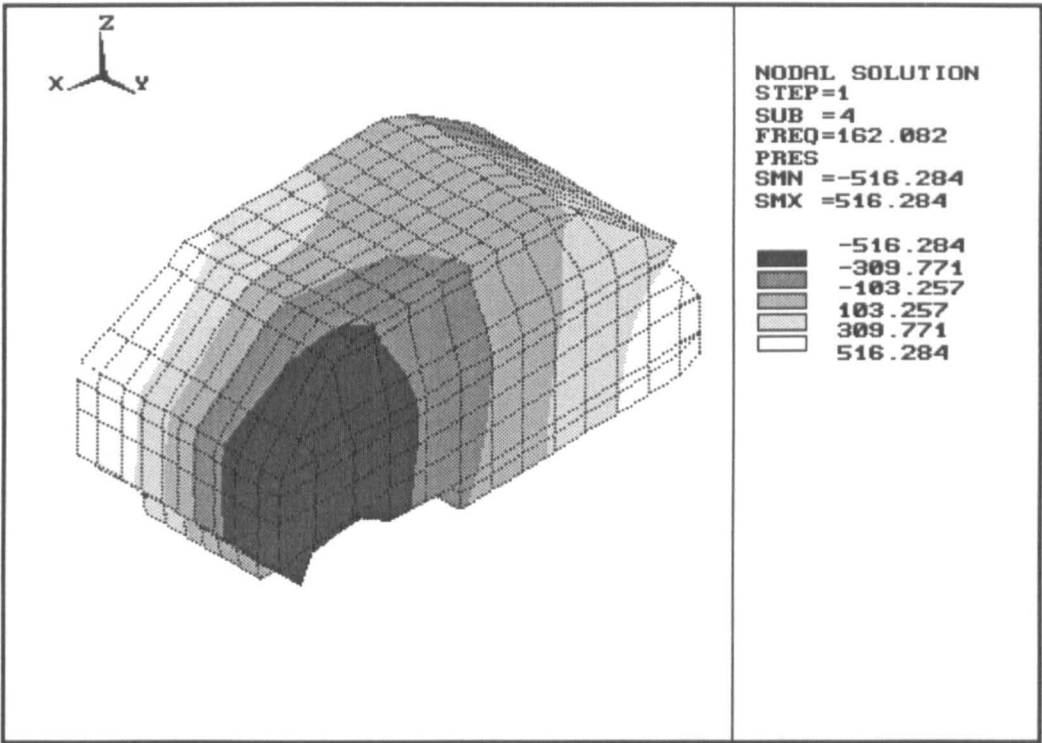


Fig. 4.5 Metro-R6 Fifth Acoustic Mode.

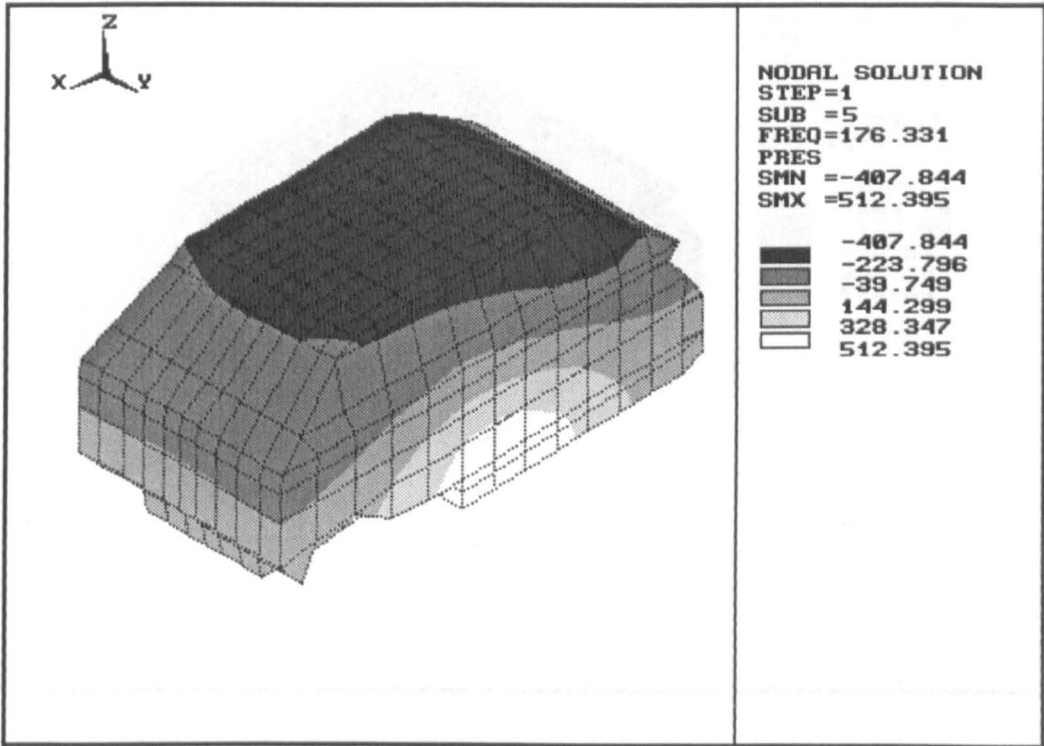




Fig. 4.6 Metro-R6 Sixth Acoustic Mode.

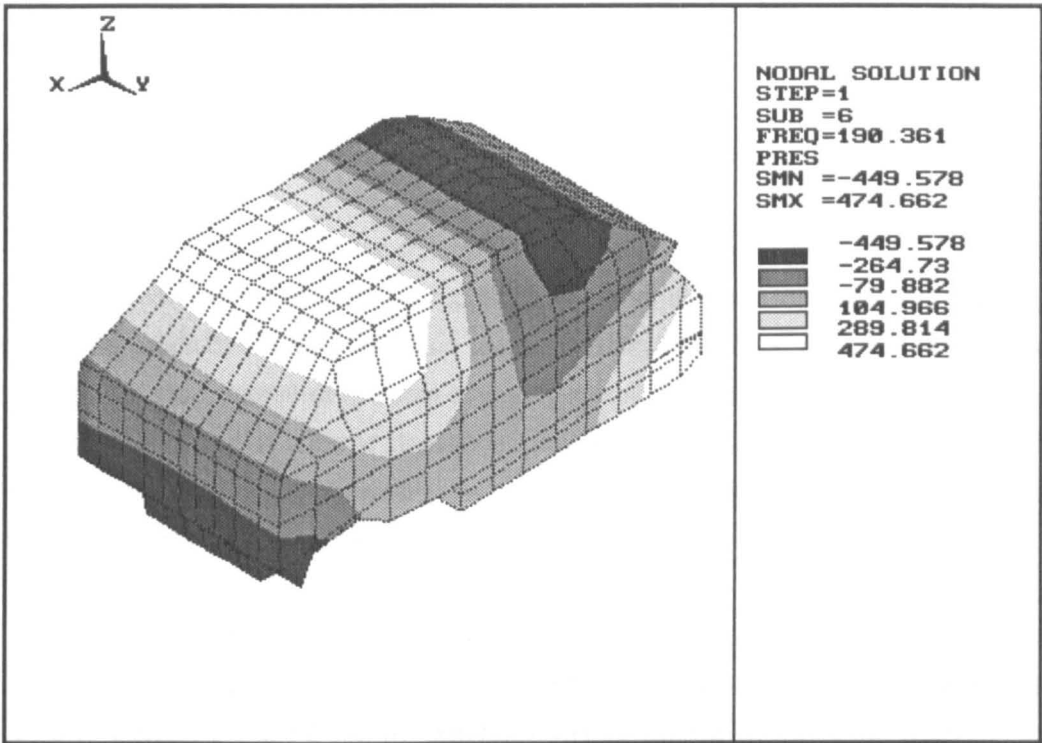
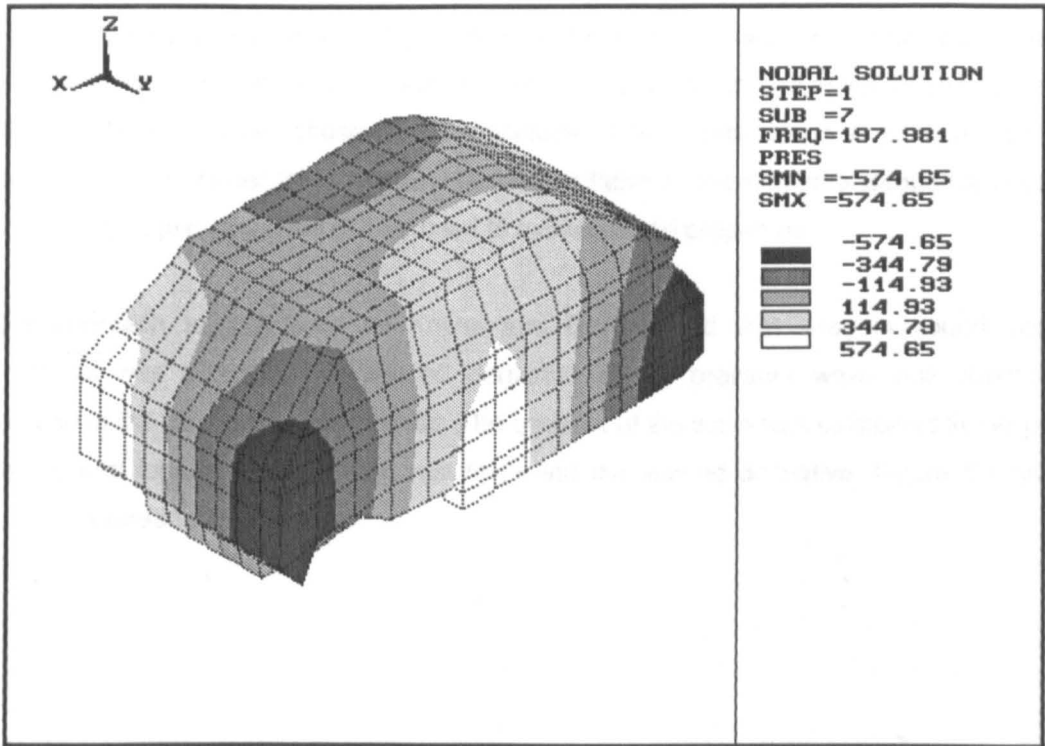


Fig. 4.7 Metro-R6 Seventh Acoustic Mode.



## **5. Experimental Method of Acoustic Modal Analysis.**

A new method for the experimental analysis of acoustic modes is presented with verification in a simple rectangular enclosure.

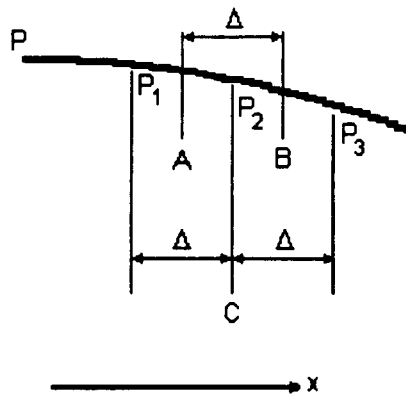
### **5.1 Theory.**

Knittel & Oswald's (1987) method for determining the low order particle modes of an acoustic cavity demonstrated the use of structural modal software for determining acoustic mode shapes. The semi discretization of the wave equation (equation 3.68) into a form analogous to that for the forced response of multi degree-of-freedom structural system (equation 3.8) was used as the basis for the method. Although this allowed directional properties to be assigned to the sound field for processing with structural modal analysis software the particle acceleration mode shapes obtained are spatially in quadrature to the pressure modes.

As the degree of coupling between low frequency structural and acoustic modes is of interest for this work an experimental method that allows the analysis of low order acoustic modes with the effects of any boundary panels clearly demonstrated is desirable. To achieve this Knittel & Oswald's work was extended here to allow the spatial variation of pressure in the three cartesian directions ( $p_x, p_y, p_z$ ) to be determined. This is achieved by calculating the second spatial derivative of the pressure wave along an axis. Equation 3.43 shows that an acoustic mode is a sinusoidal function which means that the second derivative of the original mode shape will be shifted through  $180^\circ$ . Since it is the relative phase of the amplitude of the mode shape at each node that is required for this work rather than its absolute value relative to the source a frequency response function of the type just described can be used to extract modal properties.

A similar approach to that used by Knittel and Oswald and that used in sound intensity measurements was adopted. The second derivative of the pressure wave was obtained by repeated use of the finite difference method. The gradient of the wave was calculated in two places and the process repeated using these results to find the second derivative. Figure 5.1 gives a diagrammatic representation of this.

Fig. 5.1 Finite Difference Calculation.



Three equispaced pressure measurements are taken along an axis separated with a spacing of  $\Delta$  and are denoted by  $p_1$ ,  $p_2$  and  $p_3$  respectively. Thus

$$\left(\frac{\partial p}{\partial x}\right)_{x=A} = \frac{p_1 - p_2}{\Delta} \quad \text{and} \quad \left(\frac{\partial p}{\partial x}\right)_{x=B} = \frac{p_2 - p_3}{\Delta} \quad (5.1)$$

From this

$$\left(\frac{\partial^2 p}{\partial x^2}\right)_{x=C} = \frac{\left[\frac{p_1 - p_2}{\Delta}\right] - \left[\frac{p_2 - p_3}{\Delta}\right]}{\Delta} = \frac{p_1 - 2p_2 + p_3}{\Delta^2} \quad (5.2)$$

$\Delta^2$  can be ignored as it is a constant and it is only the relative amplitudes of the FRFs which are of interest.

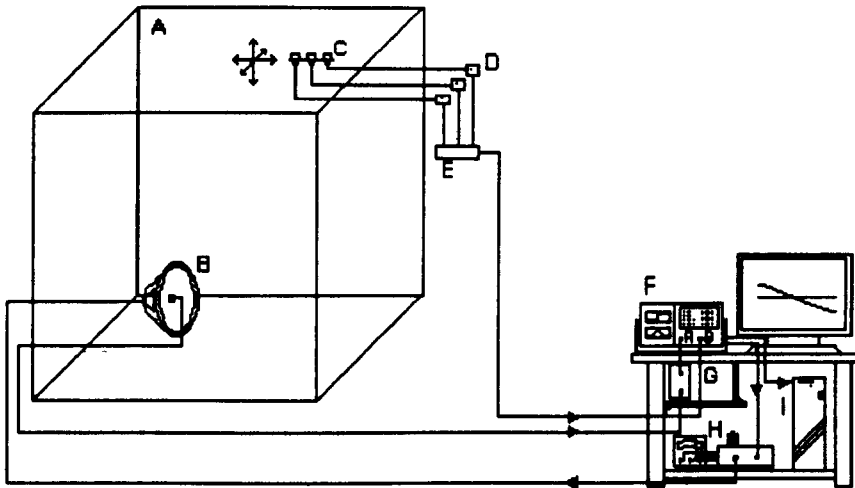
## 5.2 Method.

The finite difference calculation was performed using an analogue electronic circuit (Appendix 2). Gain compensation was included by calibrating each microphone by placing the three microphones in a standing wave tube and minimizing the transfer function for each pair of microphones (1-2, 2-3). Phase compensation was not included as the microphones responses were measured and found to be accurate to within  $1^\circ$  of each other. The requirements for sound intensity measurements (Bruel and Kjaer (1986)) were used to determine the microphone pitches. These requirements specify that to be accurate to within 1 dB on a sound intensity measurement the microphone spacing must be less than one sixth the wavelength at the highest frequency of interest and that the phase change of the pressure wave over the spacing should be more than five times the phase mismatch. Applying these criteria gave microphone pitches of 400 mm for the measurement of the office acoustic modes and 150 mm for measurements inside the car.

The equipment used is shown in figure 5.2 with Plate 5.1 showing the set up for calibrating the microphone probe. A single accelerometer attached to the cone of a speaker can be used to

determine its characteristics as an acoustic source at frequencies below the first mode of the cone (piston region). The piston region for the speaker used was determined using the methods described by Biering (1) and was found to extend well beyond the frequency range of interest.

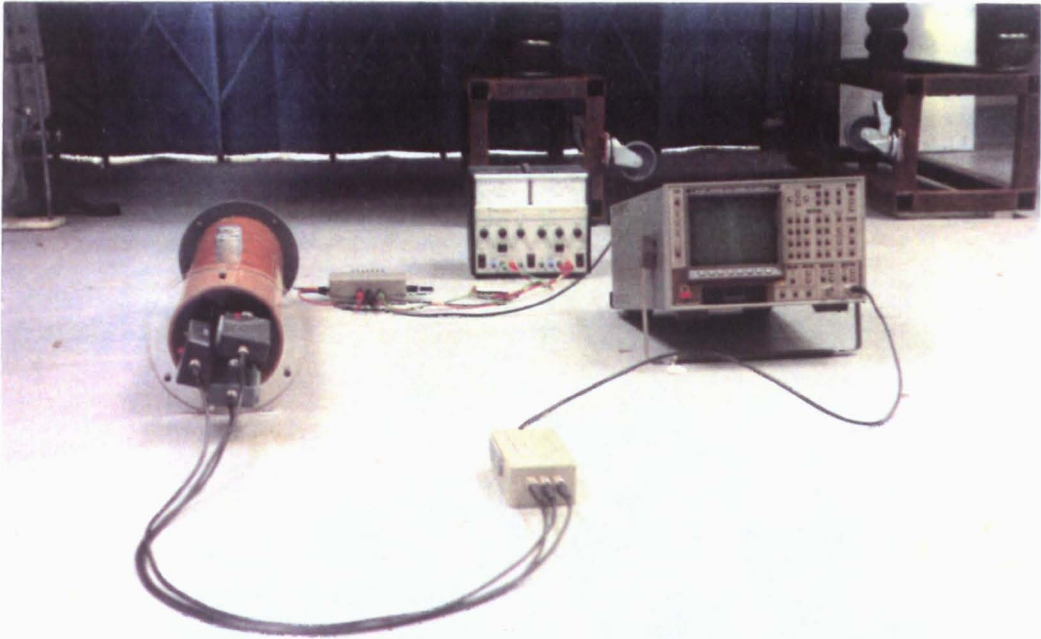
Fig. 5.2 Experimental Setup.



- A: Cavity Of Interest.
- B: Speaker With Accelerometer Attached (with a screw fitting glued to the cone).
- C: 3 Microphone Array (rotatable about x,y,z axis).  
1" Condenser Microphones Grade 2
- D: Microphone Power Supplies.
- E: Differential Amplifier (P1-2P2+P3).
- F: Ono-Sokki Twin Channel FFT Analyser With:  
Noise Board to H (Providing Signal Output).  
GPIB Bus To I (Data Transfer From FFT Analyser to PC).
- G: Bruel and Kjaer Charge Amplifier Type 2635.
- H: Speaker Driver And Power Supply.
- I: REM 486 Personal Computer (PC).

## Plate 5.1 Microphone Calibration Setup.

Original In Colour



## 5.3 Verification.

To prove this method for the determination of acoustic modes experimentally, the acoustic modes of a bare office were analysed up to 100 Hz. This was the best representation of a rectangular volume with rigid reflective walls available. The speaker was located in one corner to excite all the modes (see equation 3.51) and a swept sine excitation was employed. The acoustic response was measured along three mutually perpendicular axes (corresponding to length, width and height) at twenty six locations within the room. This mesh was sufficient for the basic node-antinode relationships to be established for the first six acoustic modes of the room and is shown in figure 5.3. The natural frequencies and mode shapes were extracted from the FRF data using ICATS modal analysis software. The natural frequencies and mode shapes were also calculated from the wave equation using equation 3.48 and modelled numerically with the ANSYS finite element software. Plate 5.2 shows the three microphone set up within the office.

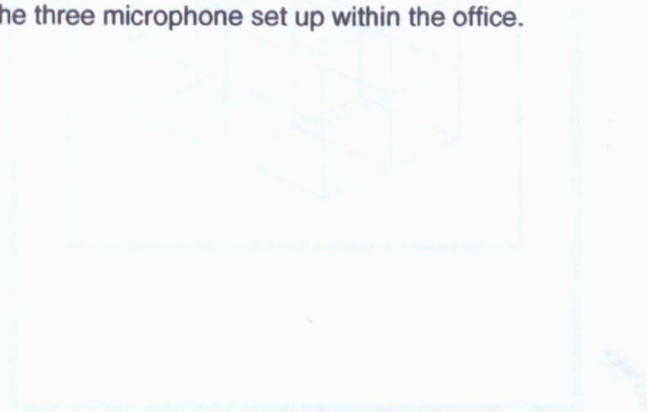


Plate 5.2 Microphone Setup Within The Office.  
Original In Colour

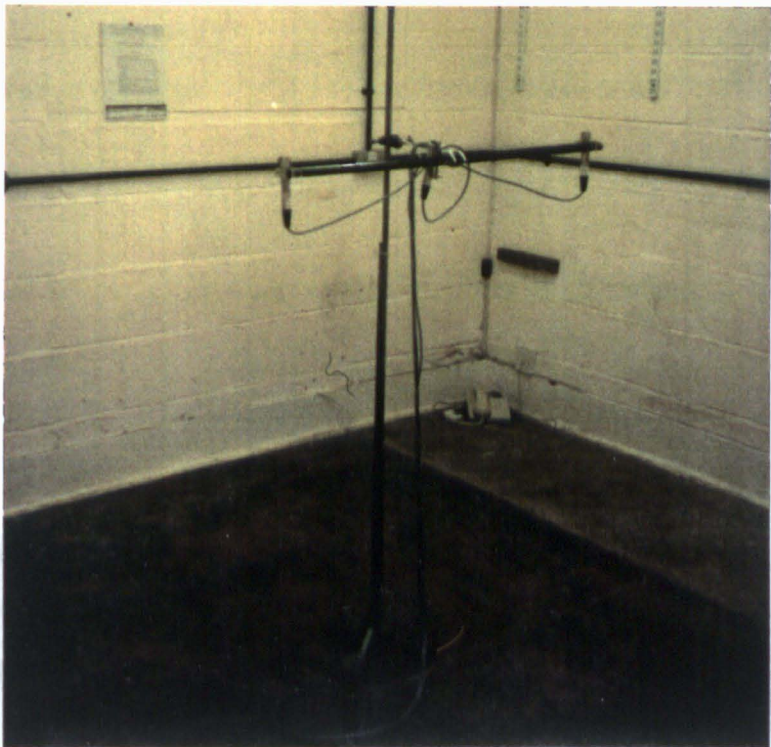
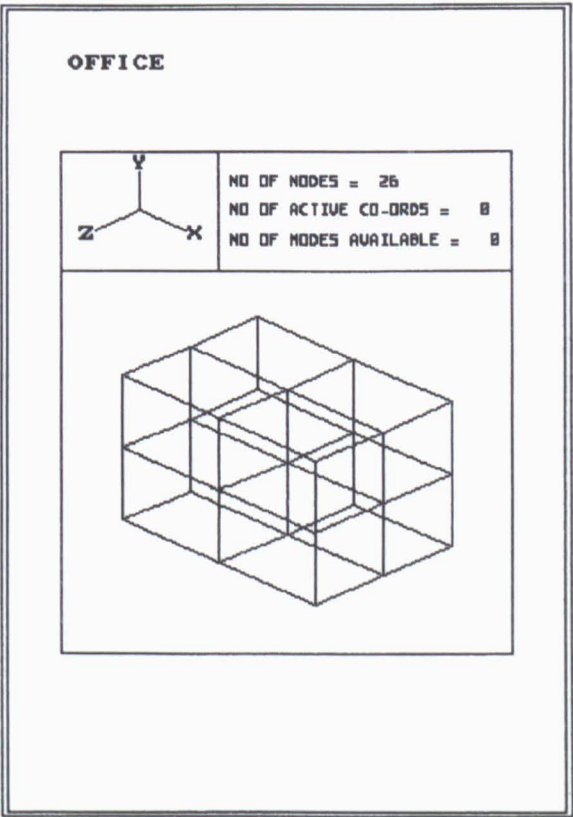


Fig. 5.3 Modal Mesh.



## 5.4 Results.

Table 5.1 shows the three sets of results.

Table 5.1 Measured and Predicted Office Acoustic Natural Frequencies.

Office Dimensions 3.2 x 2.82 x 2.36 m

Speed Of Sound 344 ms<sup>-1</sup>

<u>Mode</u>	<u>ANSYS</u> (Hz)	<u>Calculated</u> (Hz)	<u>Experimental</u> (Hz)
1 0 0	54.0	53.8	54.2
0 1 0	61.2	61.0	62.6
0 0 1	73.2	72.8	71.6
1 1 0	81.6	81.3	81.6
1 0 1	90.9	90.1	88.5
0 1 1	95.4	95.0	93.2

Figures 5.4 and 5.5 show acoustic FRF data for the three microphone arrangement along each axis and a single microphone pressure measurement measured at the diagonally opposite corner from the speaker.



Fig. 5.4 Sample Office Acoustic FRFs (Directional)

Original in colour

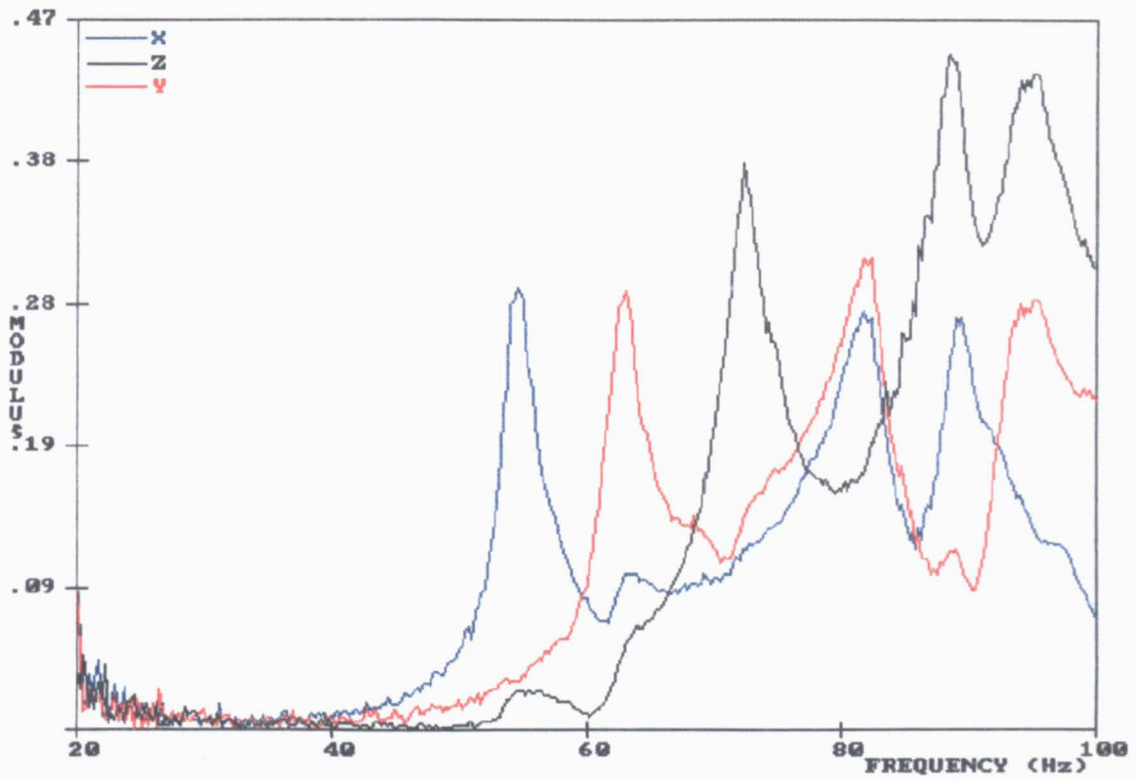


Fig. 5.5 Single Microphone Pressure Transfer Function.

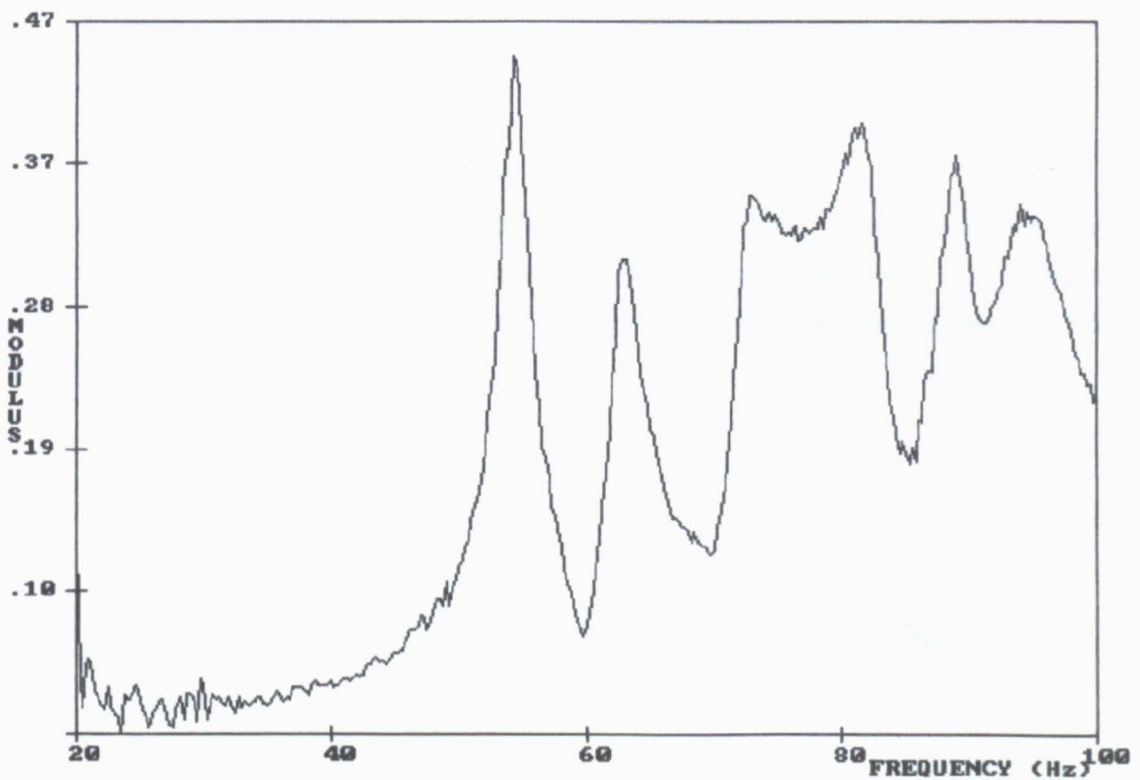
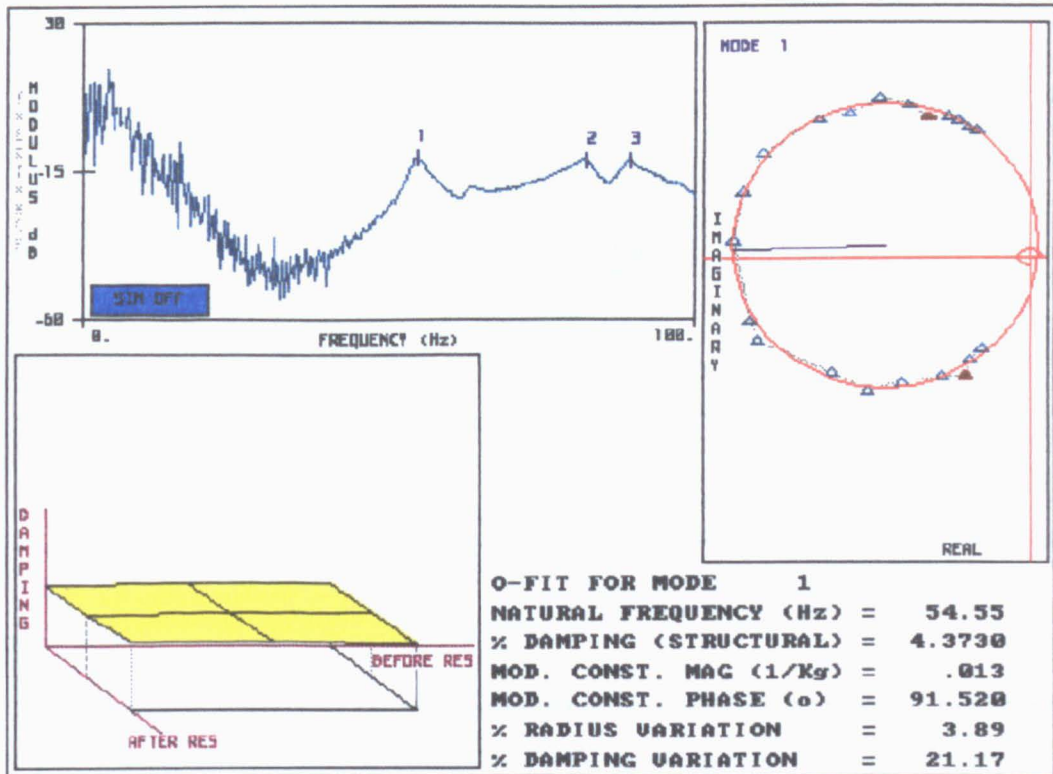




Figure 5.6 shows the results of an ICATS circle fit on the first mode of the x-axis FRF shown in figure 5.4.

Fig. 5.6 Circle Fit Results.

Original In Colour

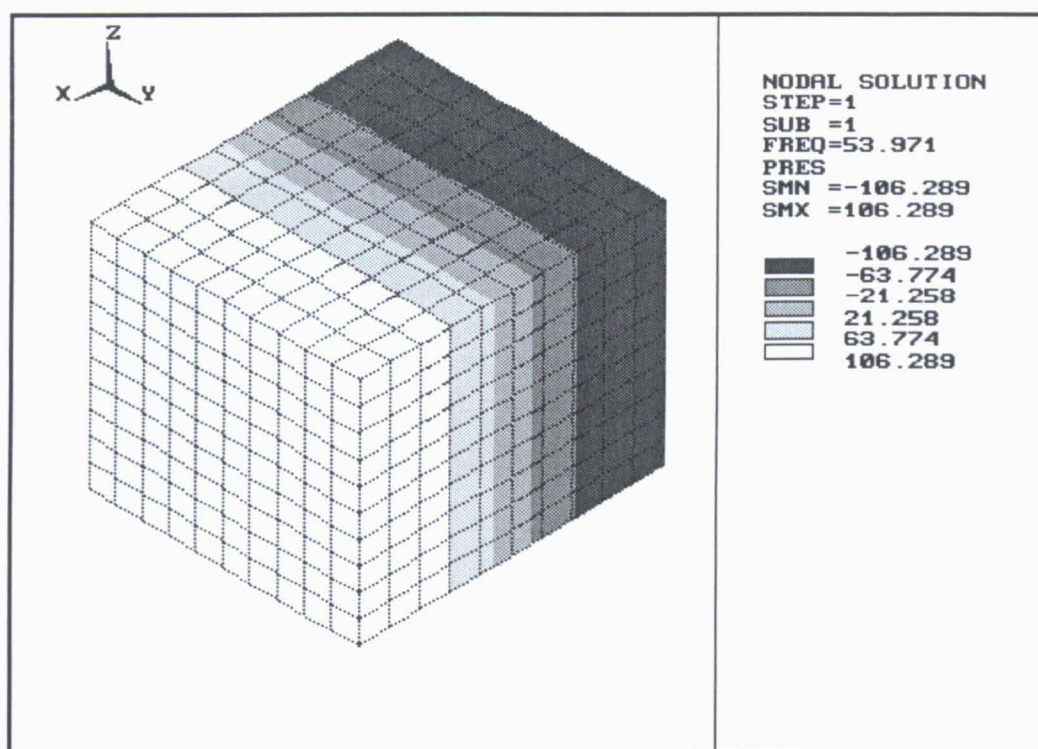


The remaining figures show the acoustic mode shapes predicted by the ANSYS finite element software and the experimental mode shapes.

The finite element analysis results show the pressure contours with a key. The displacement of the nodes on the experimental mesh indicate the amplitude of the component of pressure along the axis that the displacement occurs and the direction of that displacement indicates the relative sign of the acoustic pressure.

Fig. 5.7 First Office Acoustic Mode (1 0 0).

Predicted



Experimental

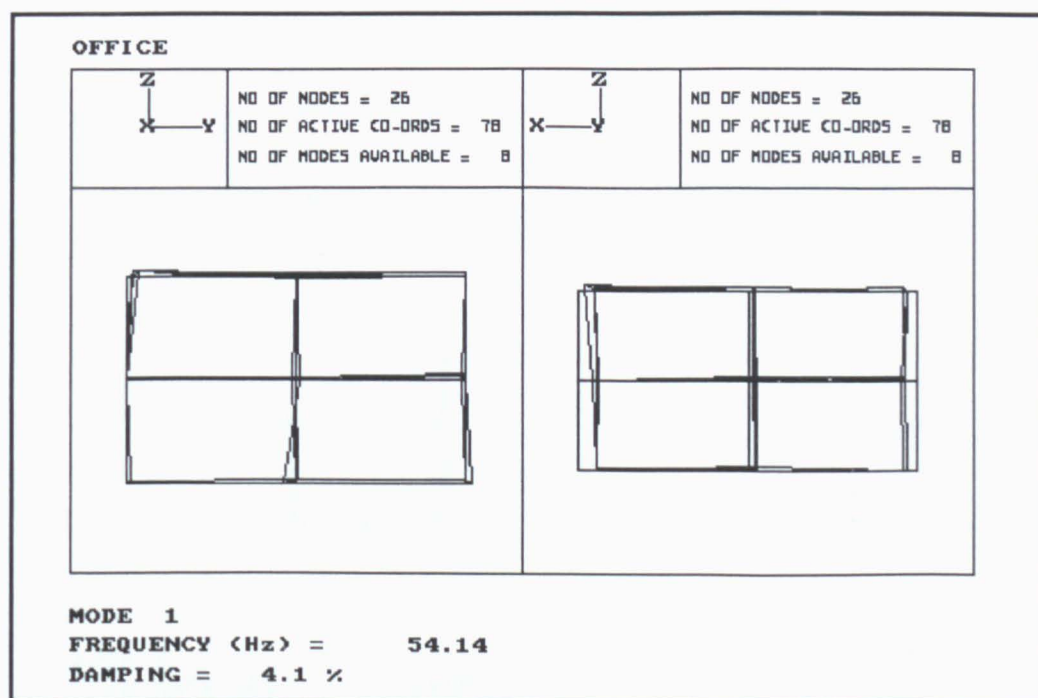
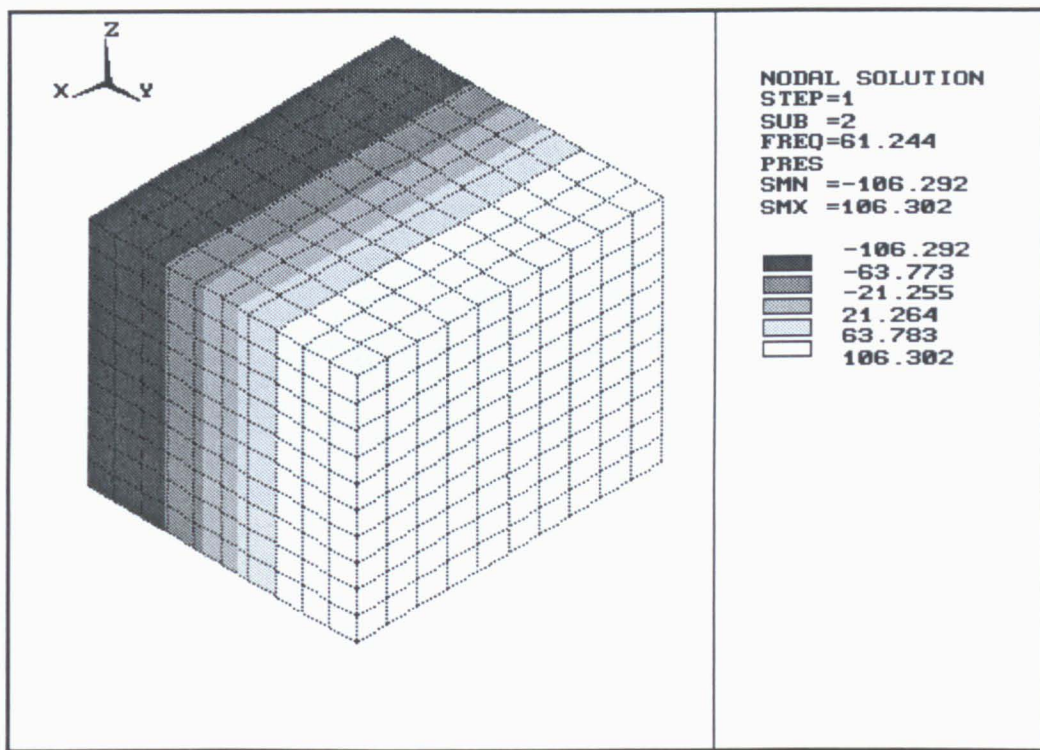


Fig. 5.8 Second Office Acoustic Mode (0 1 0).

Predicted



Experimental

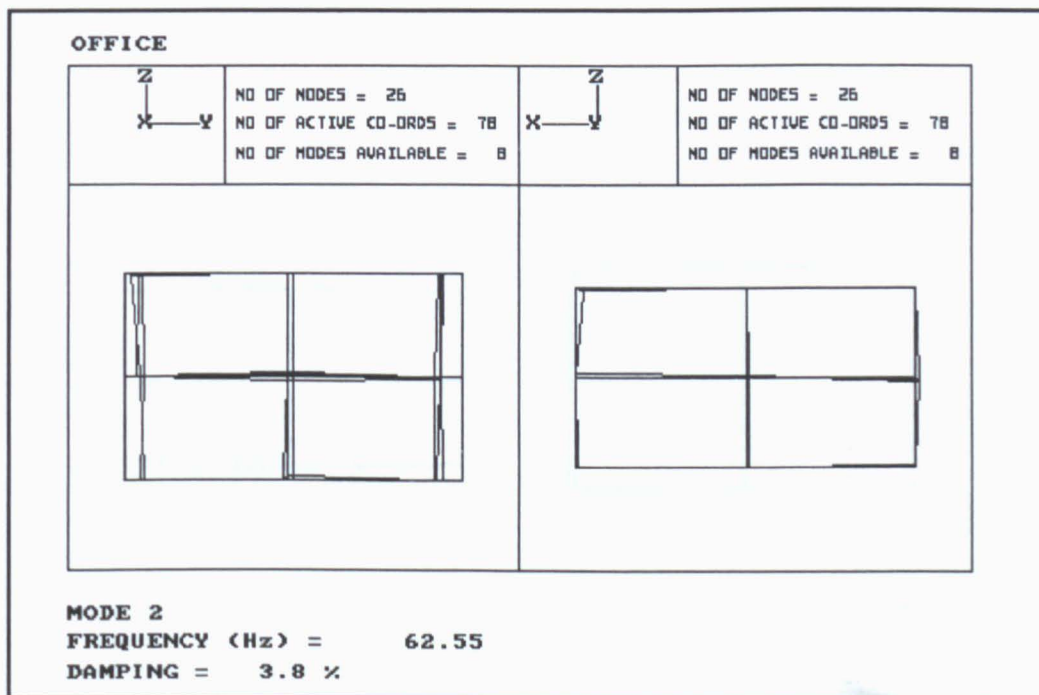
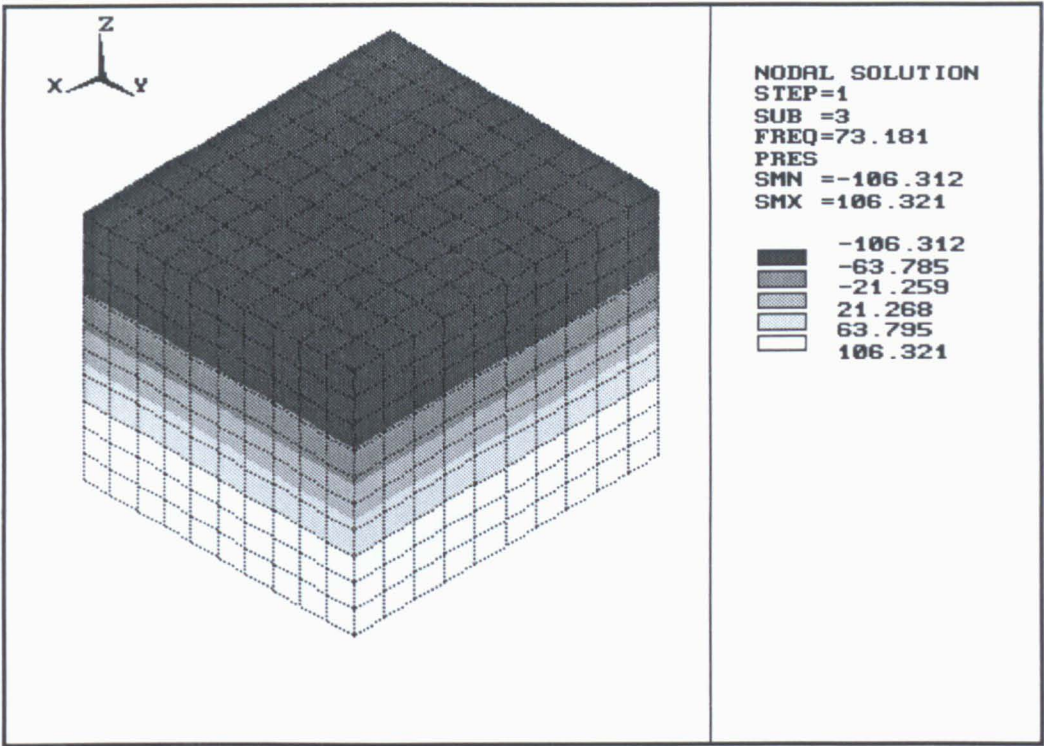


Fig. 5.9 Third Office Acoustic Mode (0 0 1).

Predicted



Experimental

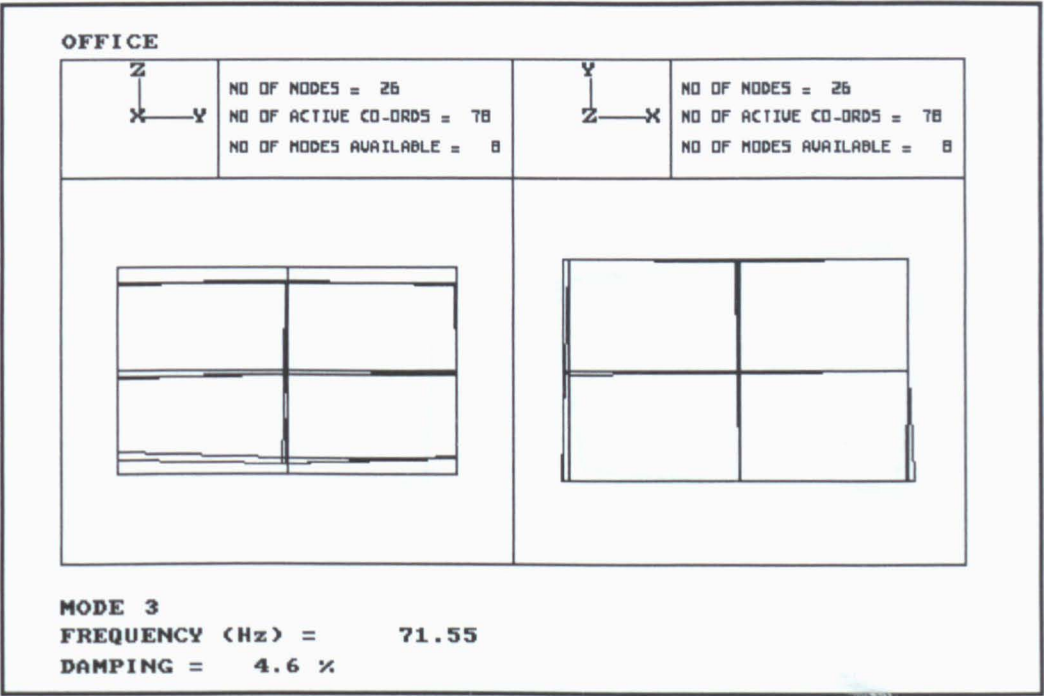
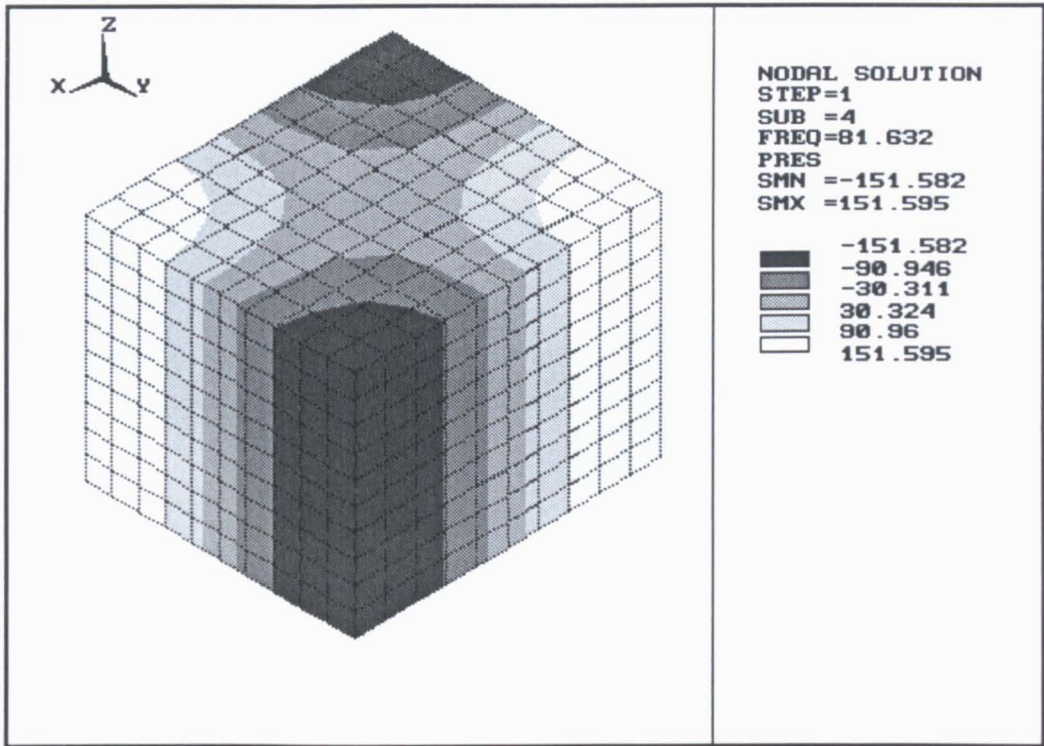




Fig. 5.10 Fourth Office Acoustic Mode (1 1 0).

Predicted



Experimental

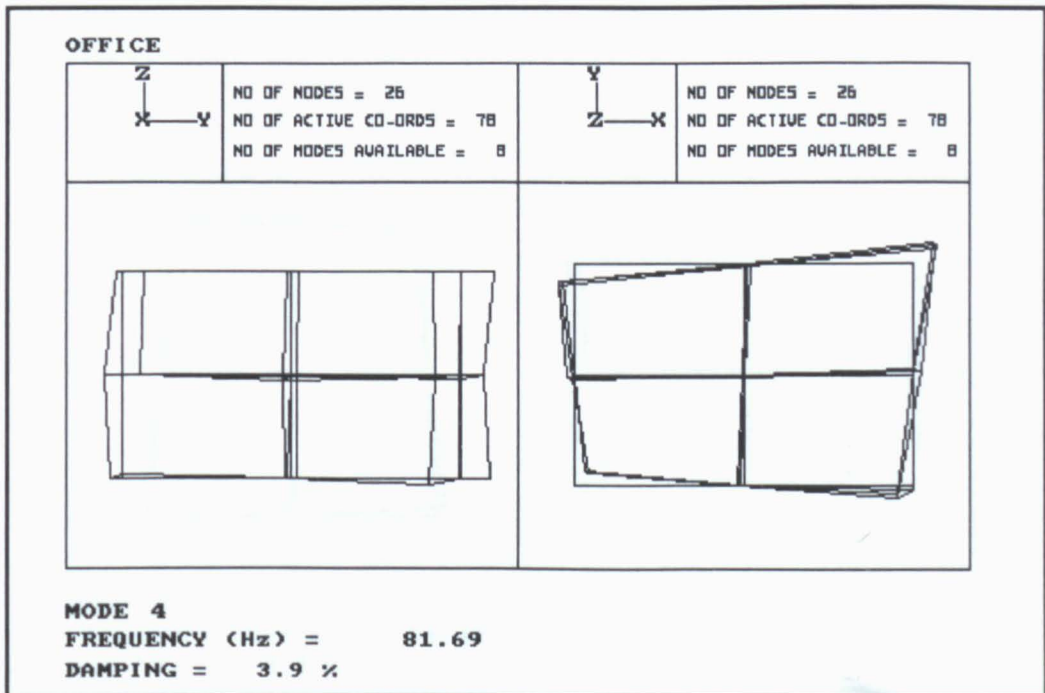
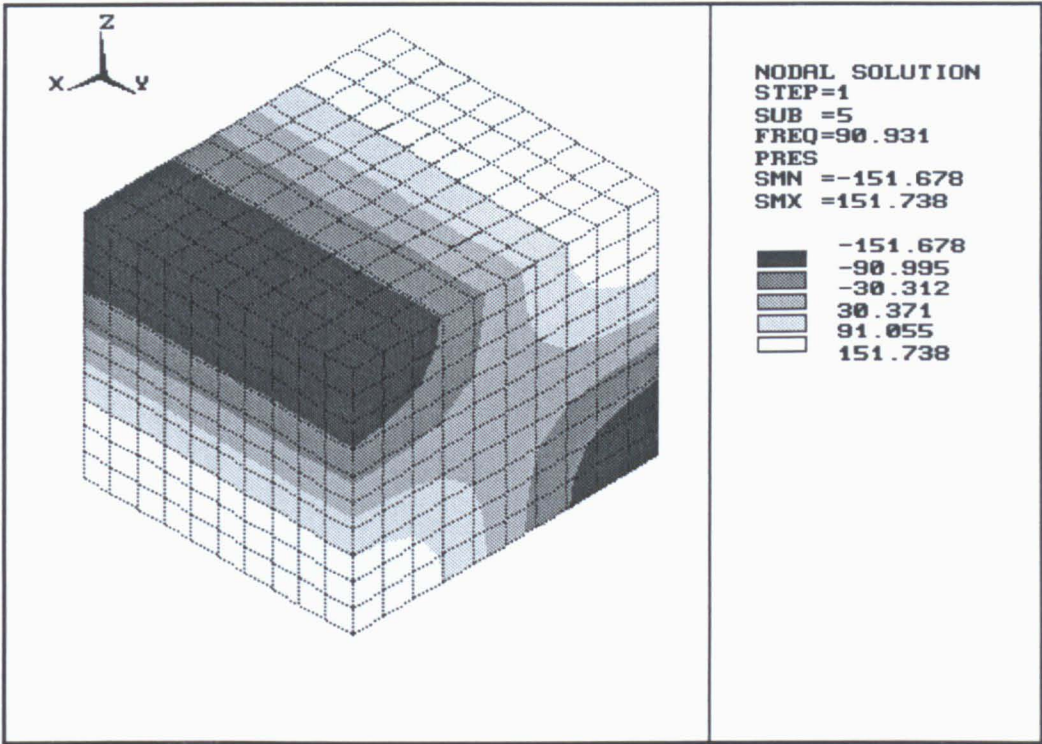


Fig. 5.11 Fifth Office Acoustic Mode (1 0 1).

Predicted



Experimental

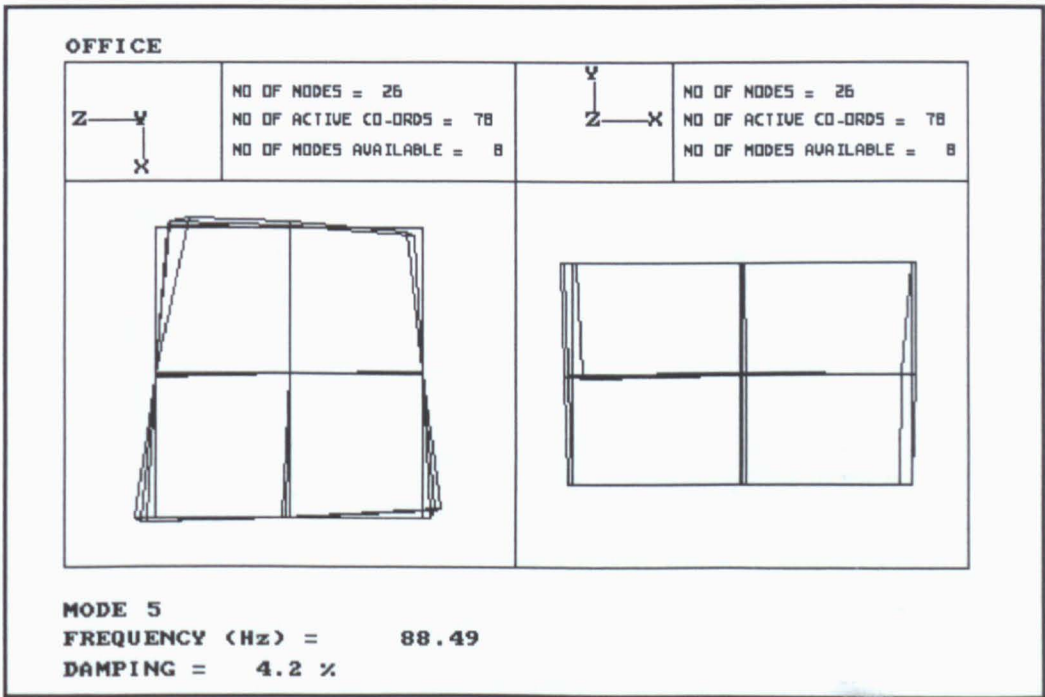
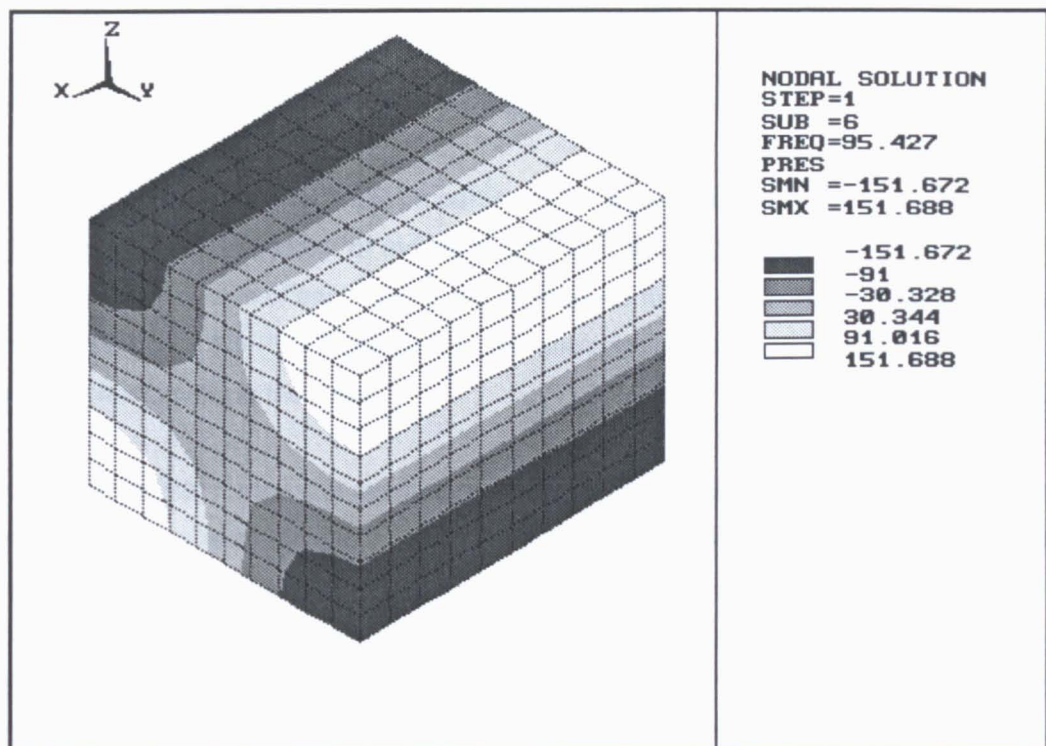
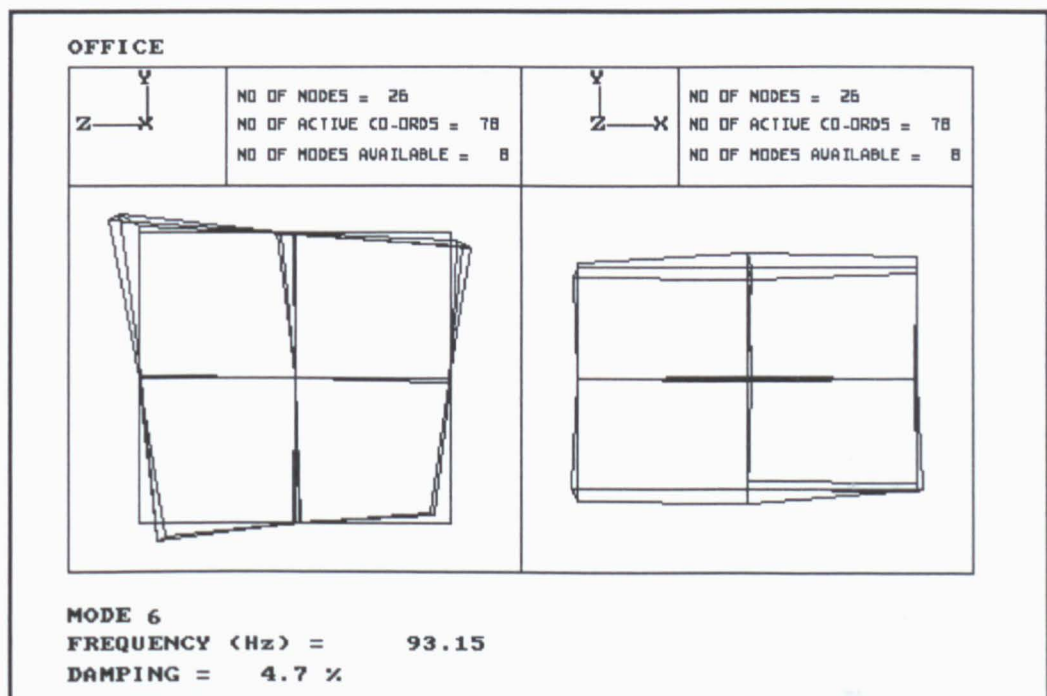


Fig. 5.12 Sixth Office Acoustic Mode (0 1 1).

Predicted



Experimental



## 5.5 Discussion.

As can be seen from table 5.1 the natural frequencies show good agreement. This verifies the accuracy of the finite element modelling procedure and the new experimental technique. No general trends were discernible from the differences between the results. Both the finite element and experimental mode shapes agree with the analytical predictions given.

Figure 5.4 clearly shows the directional properties of the three microphone method. The peaks are clearly defined with good rejection of modes occurring in the perpendicular axes at any point on each FRF. The components of each resonance correspond to the mode shapes given in table 5.1. Comparison with figure 5.5 (FRF data for a single microphone pressure measurement) shows no spurious or omitted peaks in the curve.

The circle fit (figure 5.6) for the first mode on the sample FRF (which corresponds to figure 5.4 -x) has been included to reinforce the analogy between the behaviour of acoustic and structural systems. There is little variation in radius indicating a good comparison with structural modal behaviour and little variation in damping before and after the resonance as indicated by the flatness of the damping plot. One possible source of error is the assumption of a structural damping model which is made by the ICATS modal analysis software, rather than the viscous model usually assumed for acoustic systems.

All the mode shapes show little displacement along the axes not involved in that particular mode with the central node of the mesh forming the node of all the modes as predicted by equation 3.51.



**6. Acoustic Modal Analysis of a Rover Metro Passenger Compartment.**

Having verified the technique of experimental acoustic modal analysis the next stage was to determine the acoustic modes of a car passenger compartment. This is a more complex situation with the non-rigid boundary affecting both the natural frequencies and mode shapes (equation 3.57). The chapter has two main sections. In the first the acoustic modes of the Metro-R6 passenger compartment as predicted in chapter four are analysed. The results are presented for the acoustic modes of the passenger compartment below 200 Hz and discussed in relation to the results of the finite element predictions in chapter four. The second section covers an investigation of peaks in the interior noise spectra not associated with the acoustic modes.

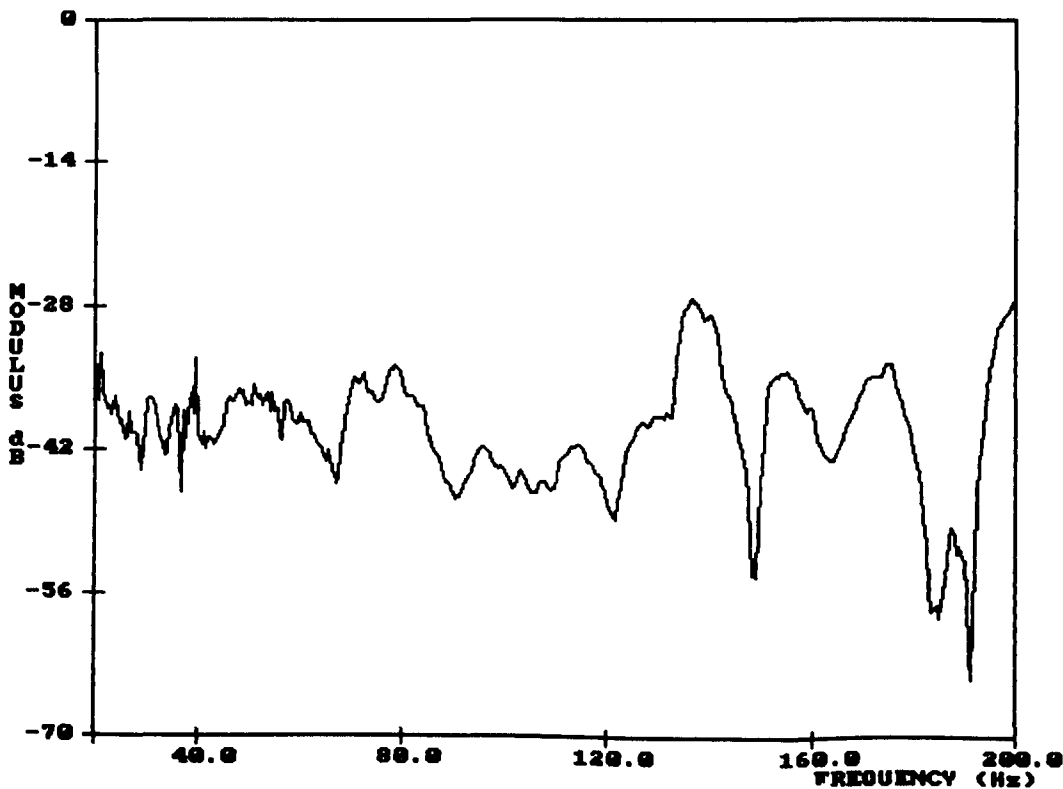
**6.1 Measurement of Acoustic Modes.**

The choice of the method of excitation is discussed followed by a description of the procedure.

**6.1.1 Excitation.**

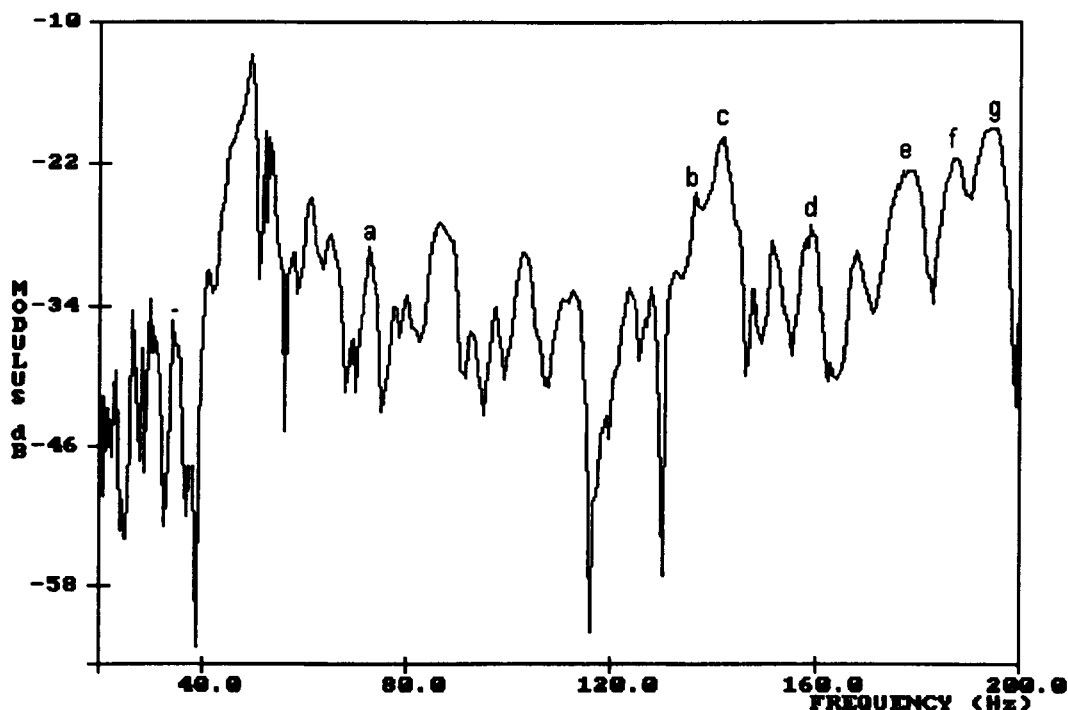
Previous workers in this field (Knittel & Oswald (1987)) excited the cavity with a speaker located in the driver's side footwell. Of the mode shapes in chapter four all except the 0 0 1 mode at 176 Hz have an antinode located in the corners of the footwell. The pressure response at the driver's head to this method of excitation is shown in figure 6.1 as a transfer function referenced to the acceleration of the speaker cone.

Fig. 6.1 Cavity Response at Driver's Head to Excitation by a Loud Speaker.



However the response from this form of excitation is quite different to that provided by excitation of the body with an electromagnetic shaker. Figure 6.2 shows the pressure response at the drivers head for excitation of the body with an electromagnetic shaker attached to the torsional engine mount (this was selected as it is attached directly to the body shell and is particularly good at giving coherent noise transfer functions). The peaks on this FRF associated with the acoustic modes identified in chapter four are labelled a to g. The other peaks are discussed later in this chapter.

Fig. 6.2 Cavity Response to Structural Excitation with an Electromagnetic Shaker.



The response shown in figure 6.2 has more clearly defined peaks than those in figure 6.1 making the extraction of modal properties easier. The clearly defined peaks at frequencies other than those associated with the acoustic modes of the cavity requires that the interaction of the structural and acoustic responses be studied. It was therefore decided that for the acoustic modal test the excitation would be provided by an electromagnetic shaker attached to the torsional engine mount.

#### 6.1.2 Method.

The car body was mounted on air bellows to represent a free body as shown in plate 6.2. The stiffness of the mounts was adjusted to give rigid body modes lower than 5 Hz. The experimental set up is similar to that shown in figure 5.2 with the speaker, accelerometer and speaker driver (with power supply) being replaced with an electromagnetic shaker, force transducer and a power amplifier. The attachment of the shaker to the torsional engine mount is shown in plate 6.2.

Plate 6.1 Metro-R6 Body on Mounts.

Original In Colour



Plate 6.2 Shaker Attachment.

Original In Colour



To minimize acoustic losses any holes in the car body were plugged with perspex sheet. The three microphone array was mounted on a rotatable mechanism which in turn could be positioned in the three mutually perpendicular directions required within the car as shown in plate 6.3. The cavity response was measured at forty locations as shown on the mesh in figure 6.3. A swept sine excitation was used with the FRF data recorded along the three axes at each node up to 200 Hz

and the modes extracted with the Global multi degree-of-freedom extraction method (ICATS (1993)).

Plate 6.3 Microphone Arrangement.

Original In Colour

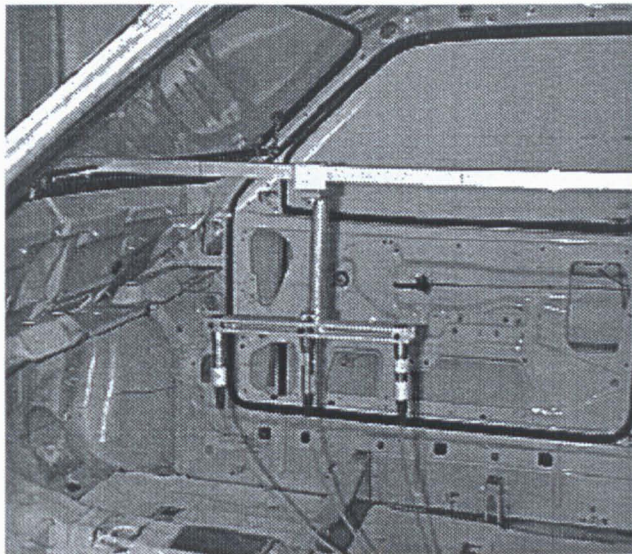
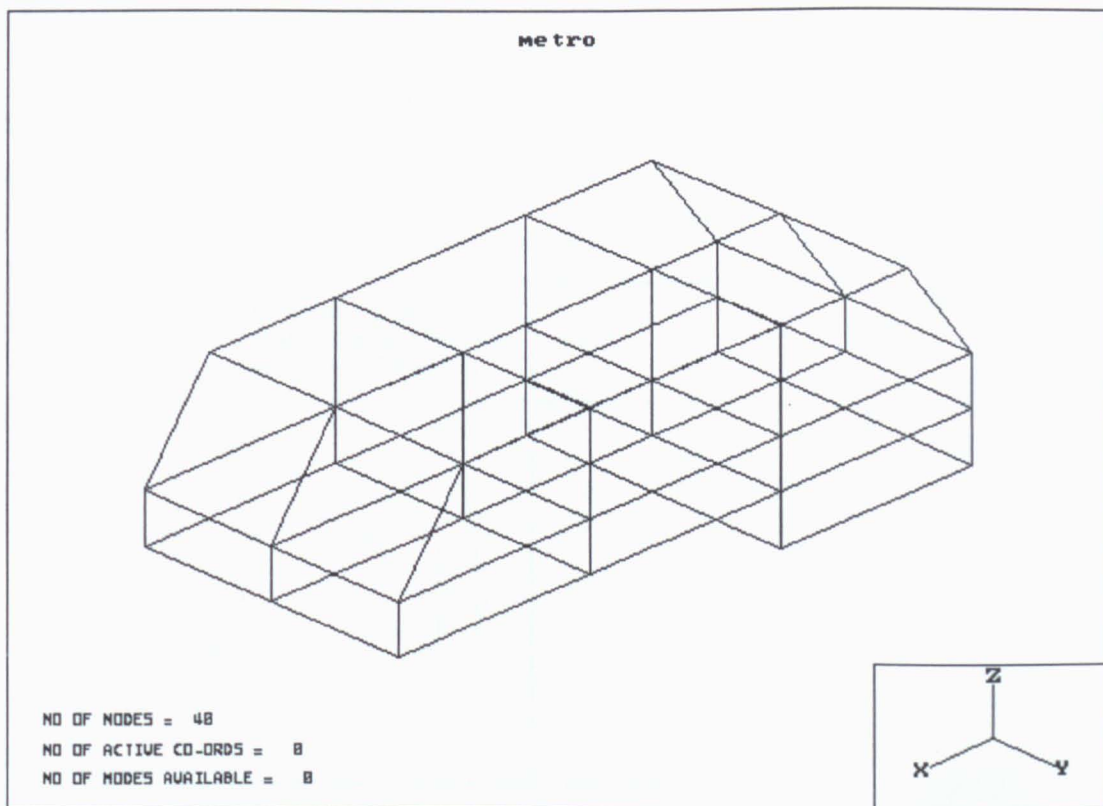


Fig. 6.3 Modal Mesh



6.1.3 Results.

Table 6.1 shows the measured and predicted acoustic modes (ANSYS FEA chapter 4) of the Metro-R6 passenger compartment. The following figures (6.4 to 6.10) show the measured mode shapes.

Table 6.1 Measured and Predicted Metro-R6 Acoustic Modes.

Mode	Measured Frequency (Hz)	Predicted Frequency (Hz)	% Difference
1 0 0	72.6	73.4	1.10
0 1 0	136.4	141.5	3.74
2 0 0	141.8	138.2	2.54
1 1 0	159.5	162.1	1.63
0 0 1	176.9	176.3	0.34
1 0 1	188.7	190.4	0.79
2 1 0	196.1	198.0	0.96

Fig. 6.4 First Metro-R6 Acoustic Mode (1 0 0).

Original In Colour

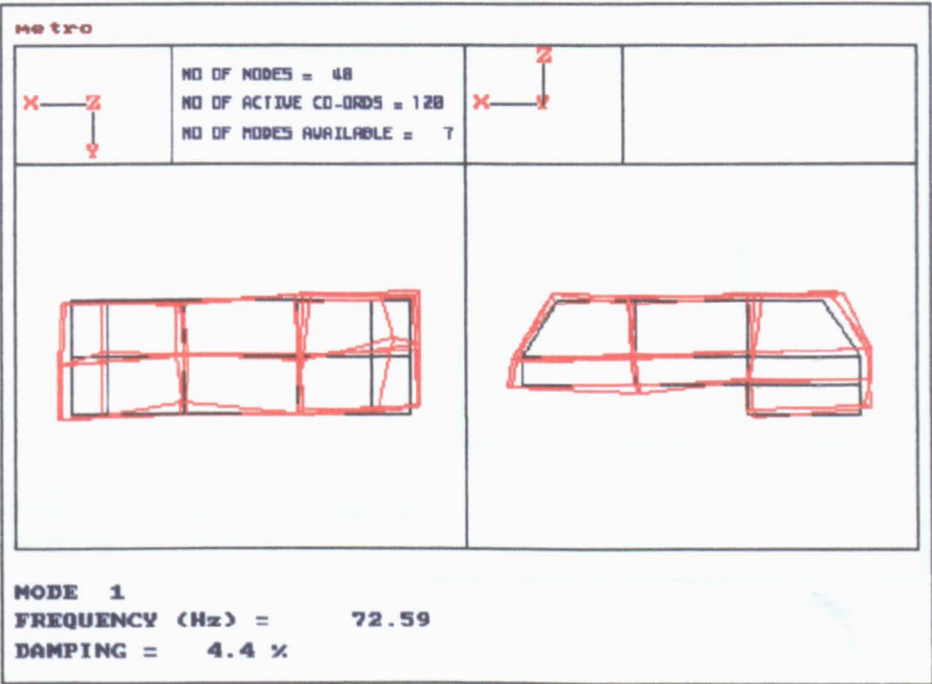




Fig. 6.5 Second Metro-R6 Acoustic Mode (0 1 0).

Original In Colour

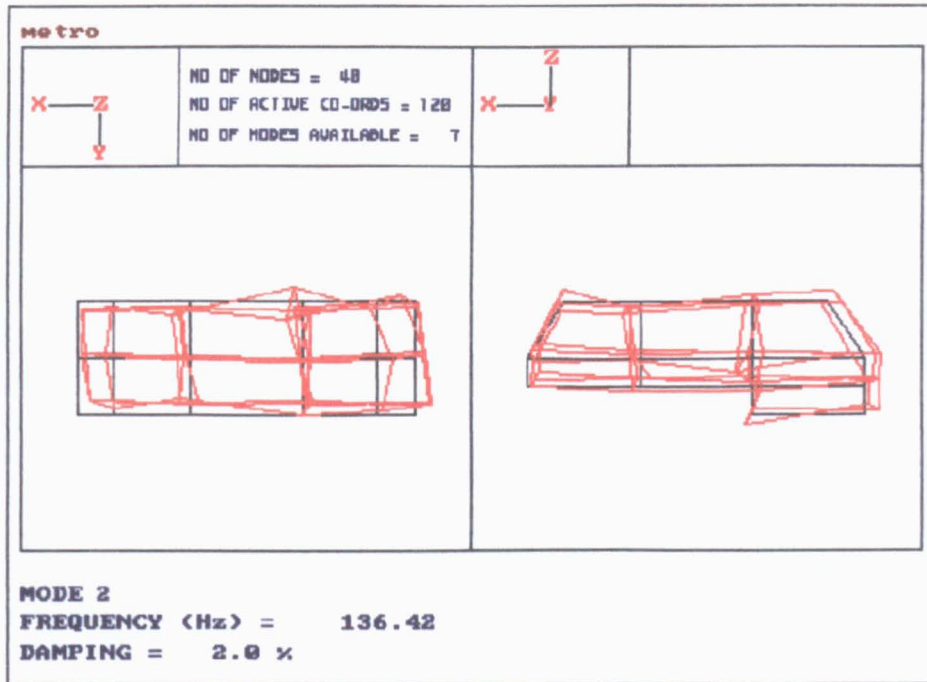


Fig. 6.6 Third Metro-R6 Acoustic Mode (2 0 0).

Original In Colour

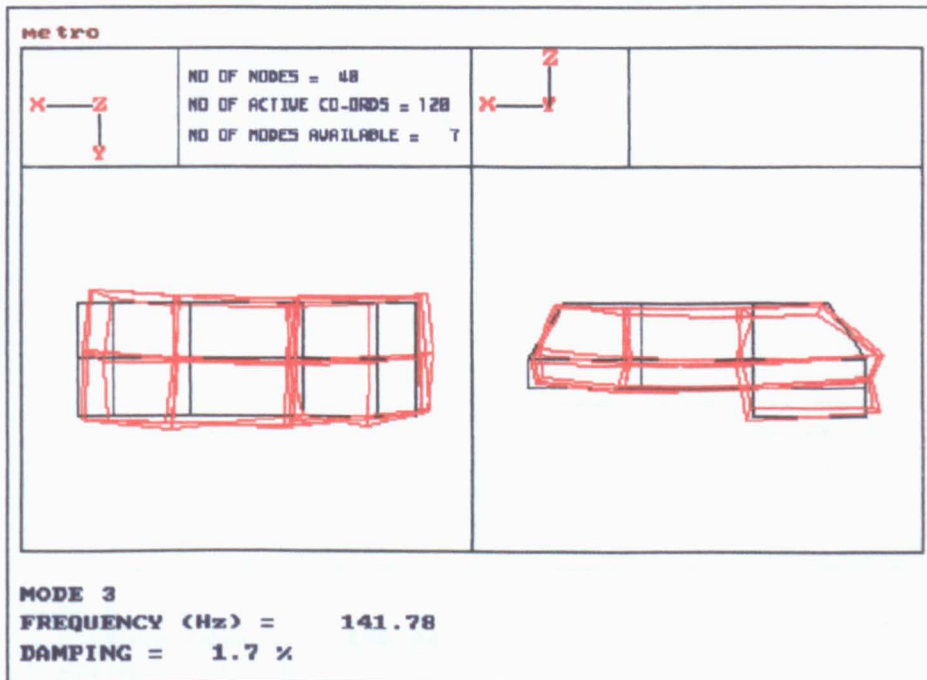


Fig. 6.7 Fourth Metro-R6 Acoustic Mode (1 1 0).  
Original In Colour

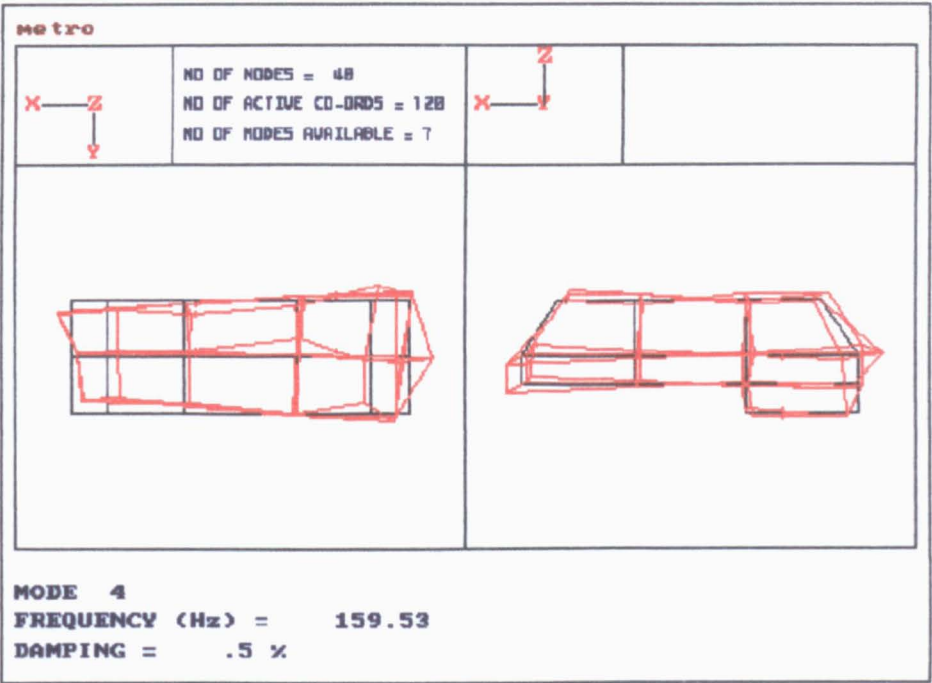


Fig. 6.8 Fifth Metro-R6 Acoustic Mode (0 0 1).  
Original In Colour

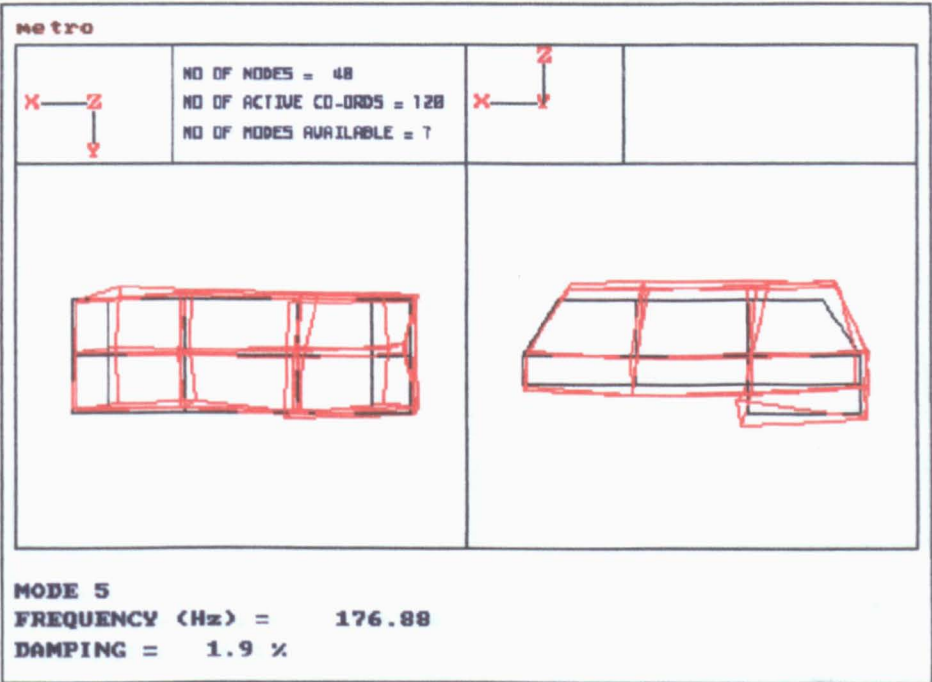


Fig. 6.9 Sixth Metro-R6 Acoustic Mode (1 0 1).

Original In Colour

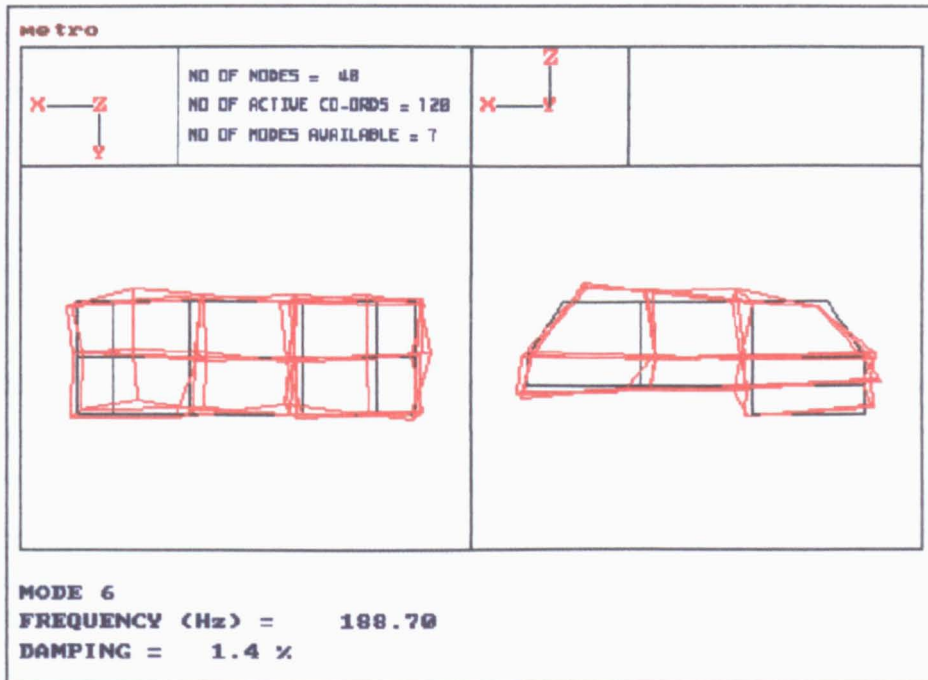
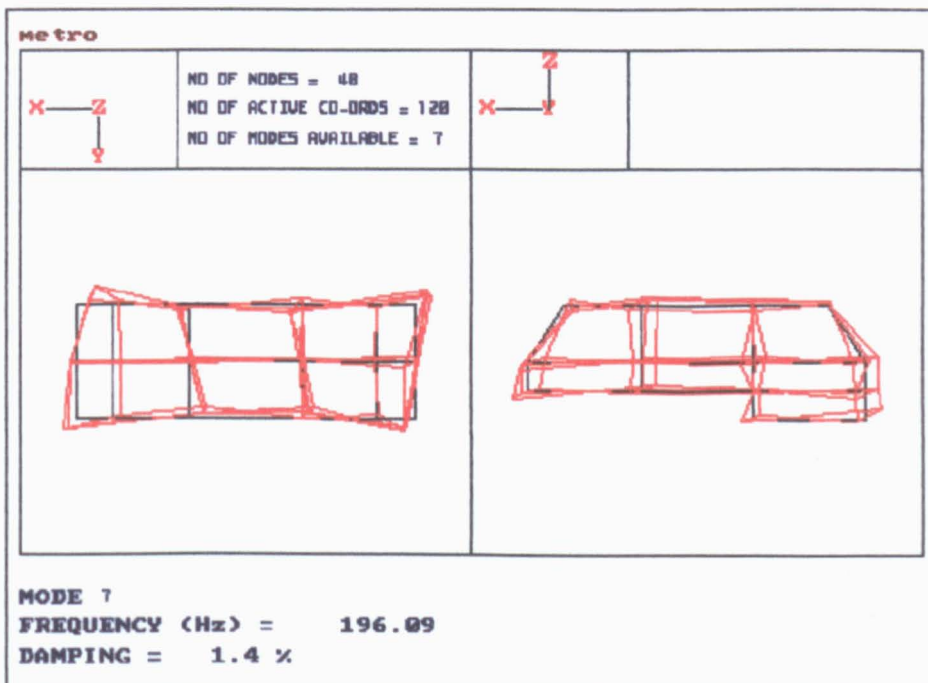


Fig. 6.10 Seventh Metro-R6 Acoustic Mode (2 1 0).

Original In Colour





#### **6.1.4 Discussion.**

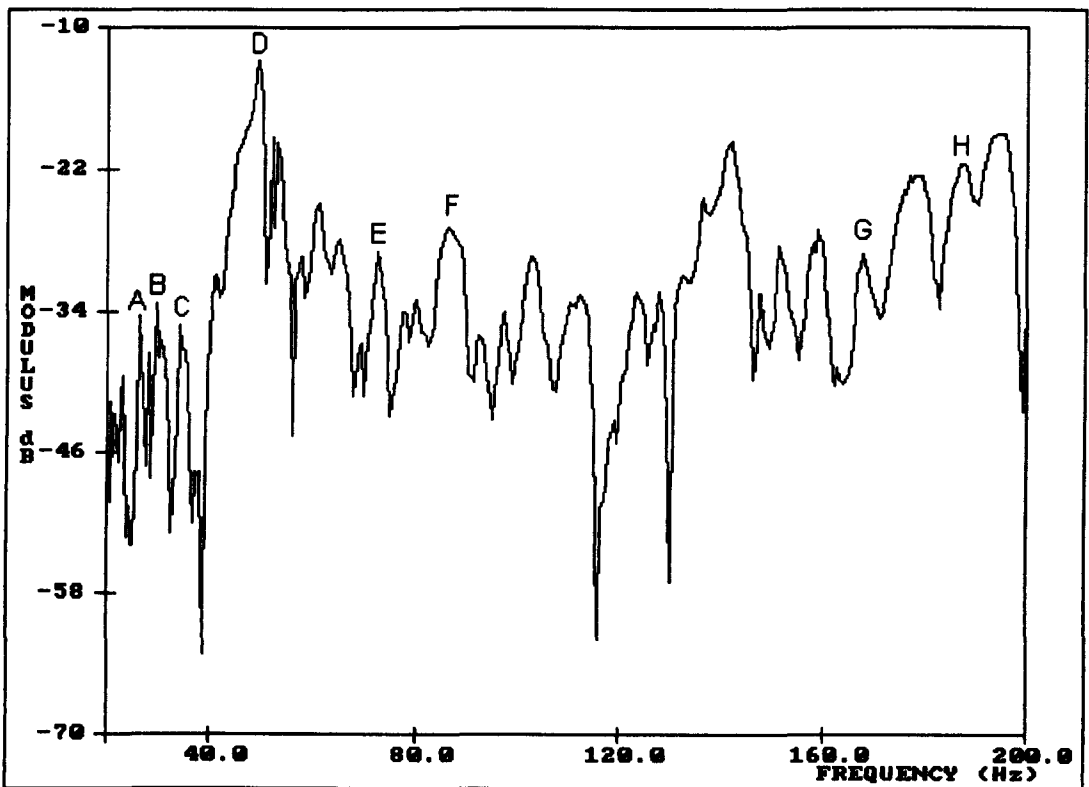
The results show good agreement between the predicted and experimental natural frequencies indicating that the boundary impedance has little effect on the acoustic natural frequencies of the cavity. However, the experimental mode shapes do not match the predicted shape as well as for the examples in chapter five. It is likely that this is due to the influence of the vibrating boundary causing pressure gradients within the cavity other than those associated with the acoustic modes. Despite this it was possible to clearly identify the acoustic modes and the modal extraction software gave repeatable results. The two close modes (0 1 0 and 2 0 0) are the least clearly defined as the software has been unable to separate them completely.

These results show that modelling the modal characteristics of the acoustics of untrimmed car passenger compartments can be done without including the effects of the boundary impedance on the natural frequencies and shapes of the acoustic modes. This is particularly useful for the body-in-white (untrimmed) testing of vehicles where the prediction of the acoustic modes is often used to define frequencies of interest for the control of low frequency interior noise.

## 6.2 Investigation of Structural-Acoustic Interaction.

The remainder of this chapter considers the use of experimental structural and acoustic modal data to study the interaction of the vehicle structure and the air within the passenger compartment. It was found that the FRF data used for determining the acoustic modes of the Metro-R6 cavity also yielded modal data at frequencies not associated with the acoustic modes of the cavity. This data was then used to experimentally study the behaviour of the vehicle structure and the passenger compartment acoustic response. Several representative peaks on the pressure FRF shown in figure 6.2 are considered and these are labelled A to H on figure 6.11. These are used to show the nature of structural-acoustic interaction.

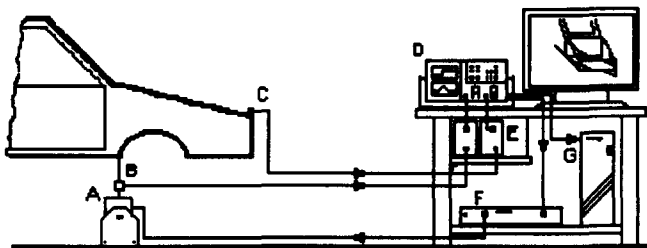
Fig. 6.11 Cavity Response to Structural Excitation with an Electromagnetic Shaker.



### 6.2.1 Method.

In addition to the acoustic FRF data used in the previous section two sets of structural data were taken with the equipment shown in figure 6.12.

Fig. 6.12 Structural Modal Analysis Equipment.



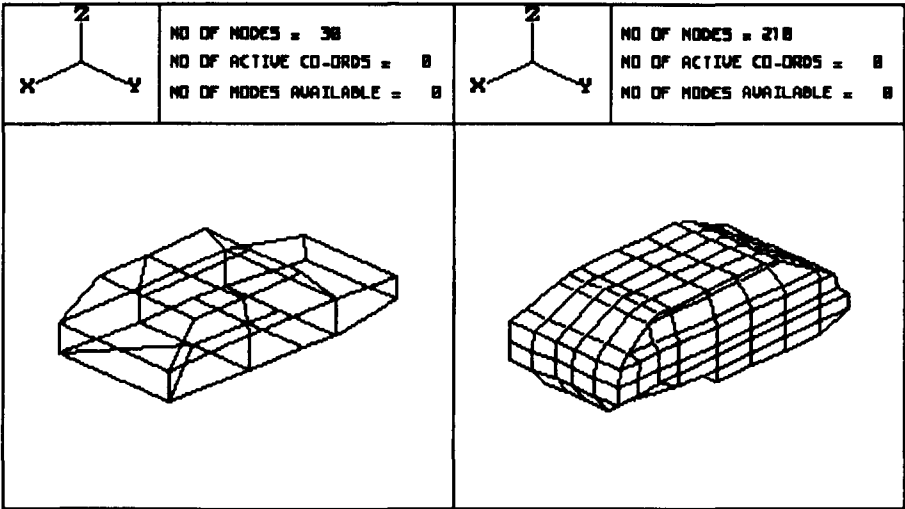
#### Key

- A Environmental Equipments 1501 Electromagnetic Exciter.
- B Kistler 9331-A Force Transducer.
- C Accelerometer (assorted)
- D Ono-Sokki CF350 Twin Channel FFT Analyser with:  
Noise Board To F (Providing a signal output)  
GPIB Bus To G (Data transfer to P.C.).
- E Bruel and Kjaer Charge Amplifiers Type 2635.
- F Environmental Equipments 1531 Power Oscillator.
- G REM 486 Personal Computer.

A thirty node tri-axial modal test recording FRF data up to 100 Hz was used to determine the major structural modes of the body. The excitation was applied at the front passenger side subframe attachment point as it proved particularly useful for exciting the major body modes.

The second set of FRF data was recorded from 0 to 200 Hz at 210 locations normal to the body surface, except for the front and rear windscreens where the results were taken along the longitudinal and vertical axes. These meshes are shown in figure 6.13.

Fig. 6.13 30 And 210 Node Modal Meshes.



The modes for all three sets of data (30 and 210 node structural and 40 node acoustic meshes) were then extracted around the frequencies of the peaks in the pressure response at the drivers head location shown in figure 6.11. The results for the selected peaks labelled A-H are shown in the next section.

### 6.2.2 Results.

A circle fit is shown in figure 6.15 of an arbitrary selection of those peaks not associated with the acoustic modes of the cavity to demonstrate their modal properties. These correspond to the peaks labelled 1 to 6 in figure 6.14. This is followed by the extracted mode shapes for each of the peaks labelled A to H in figure 6.11.

The extracted modes at each of these frequencies are of three types, namely structural modes using the 30-node mesh, structural surface modes extracted using the 210-node mesh and the acoustic modes extracted using the 40-node mesh of the interior cavity.

Fig. 6.14 Sample Peaks Not Associated With Acoustic Modes.

(Pressure FRF at drivers head location using electromagnetic excitation)

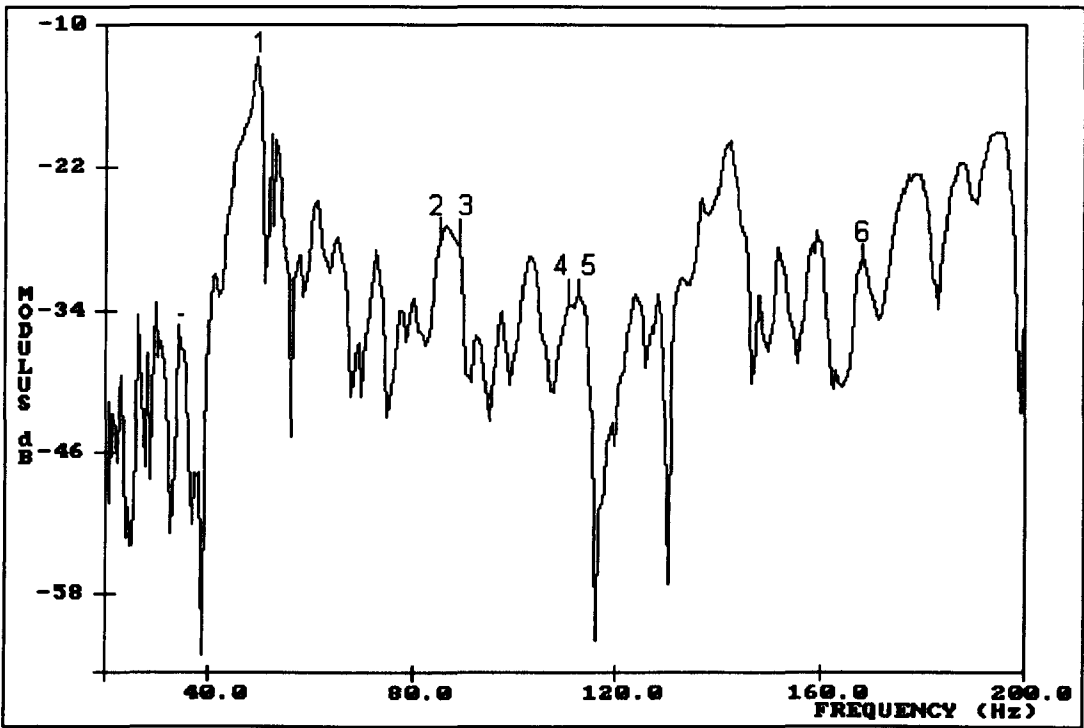
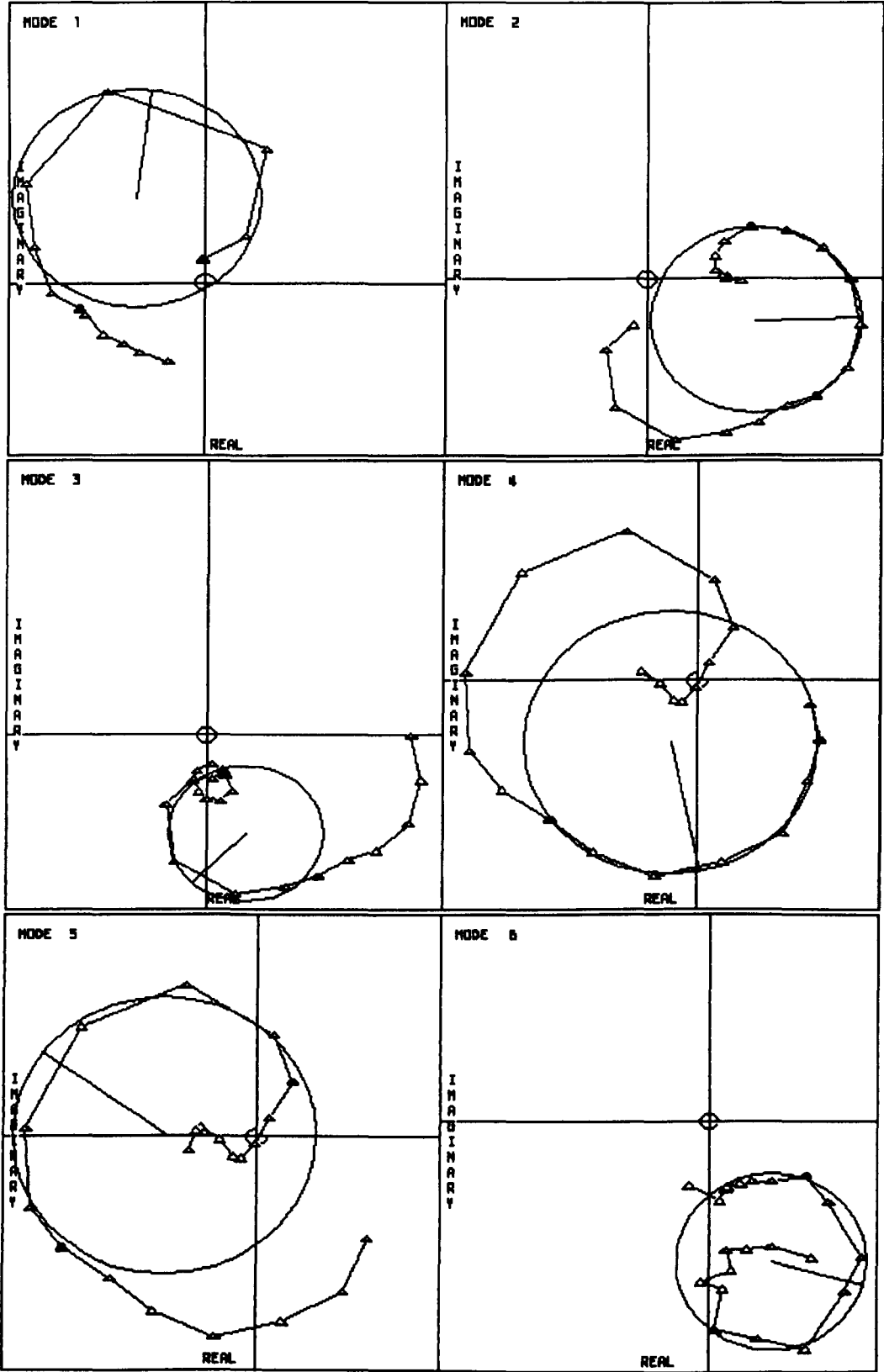


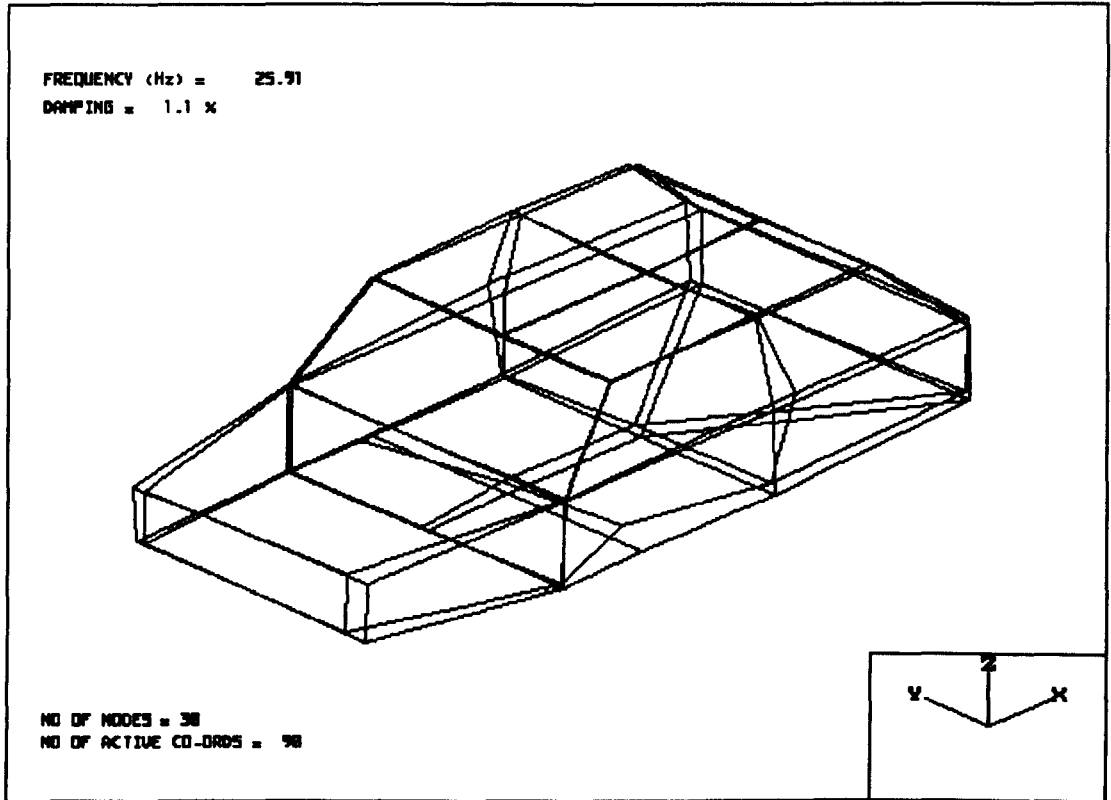
Fig. 6.15 Circle Fits for Peaks Shown in Figure 6.14.



Peak A.

This corresponds to the front lateral and side frame beat mode occurring at 26 Hz

Fig. 6.16 Structural Mode Associated with Peak A.

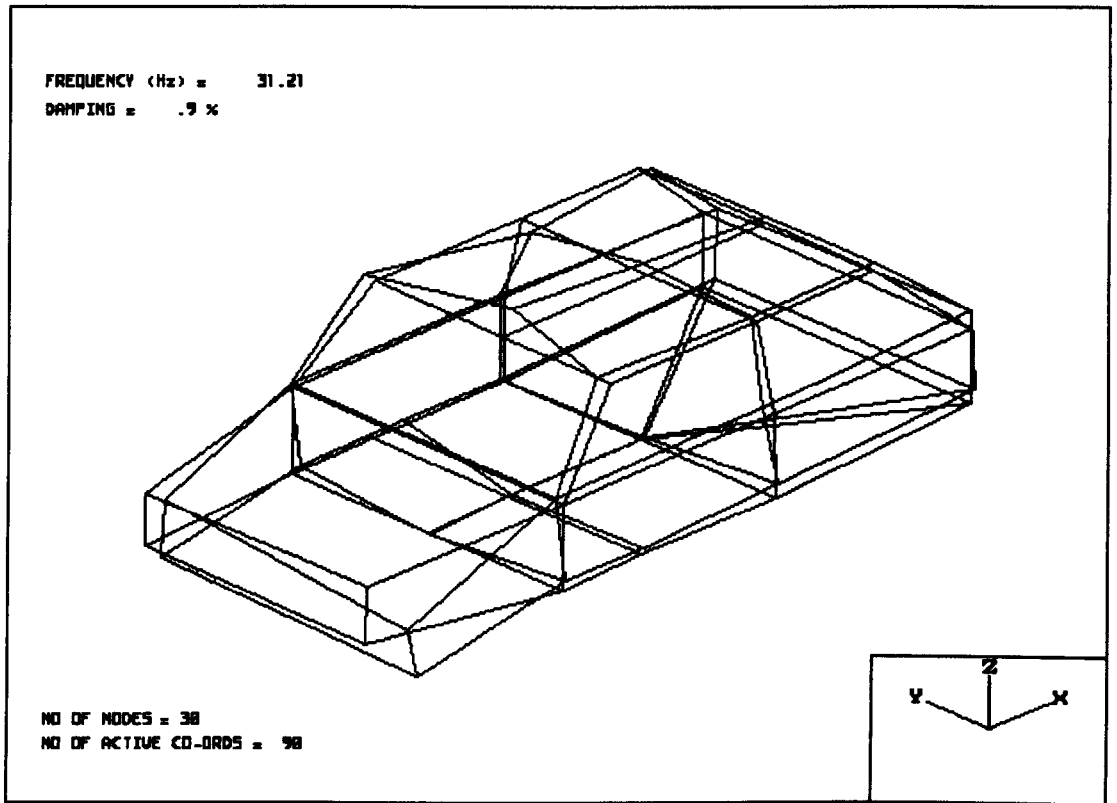


It was not possible to extract an acoustic modal response for this peak.

Peak B.

Associated with flexing of the front passenger side engine bay member at 31 Hz.

Fig. 6.17 Structural Mode Associated with Peak B.



It was not possible to extract an acoustic modal response for this peak.



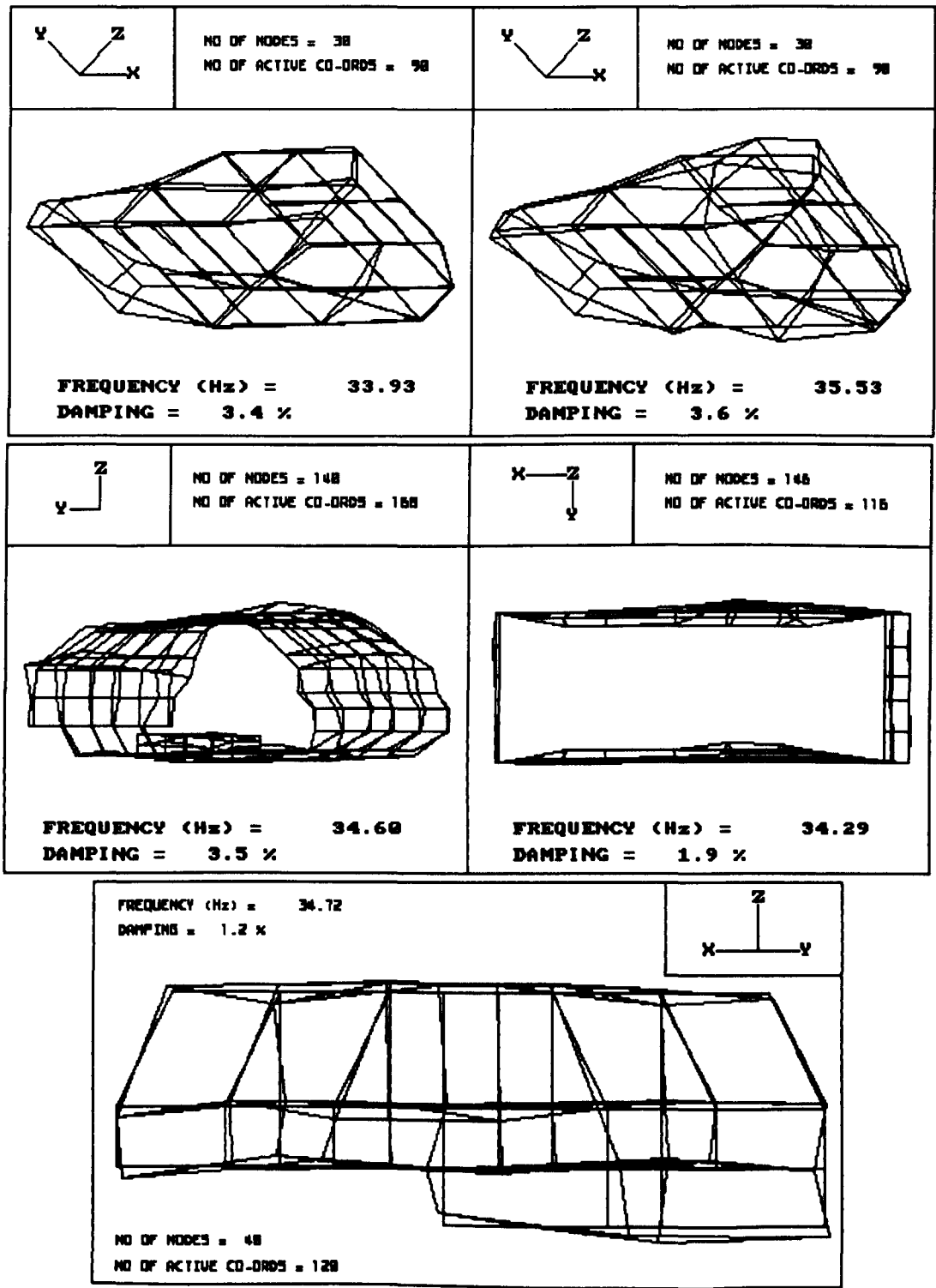
Peak C.

Occurs in the region of two close structural modes.

33.9 Hz First lateral bending/front end torsional.

35.5 Hz First body torsional.

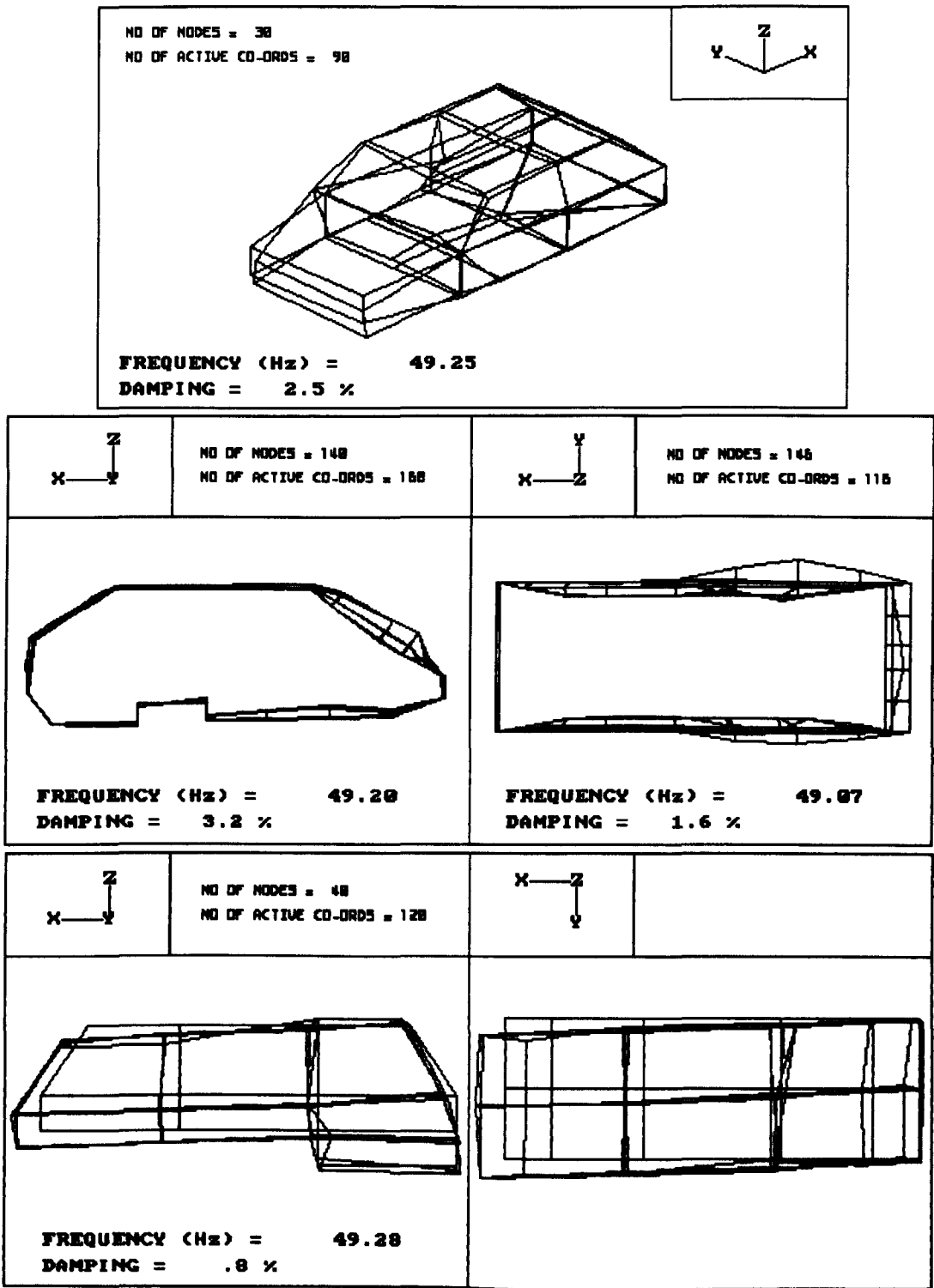
Fig. 6.18 Modes Associated with Peak C.



Peak D.

Associated with the front end bending mode at 49 Hz.

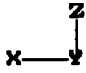
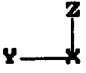

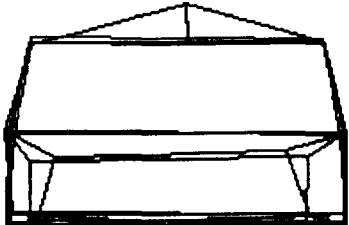
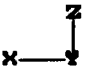
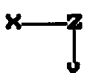

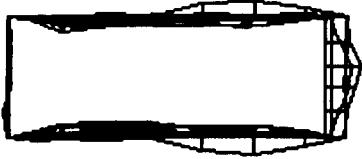
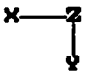
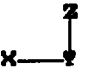
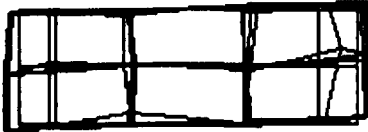

Fig. 6.19 Modes Associated with Peak D.



Peak E.

Associated with first acoustic mode (1 0 0).

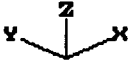

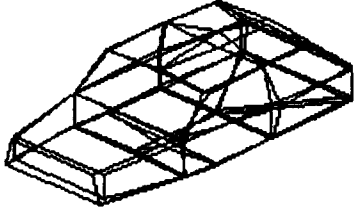
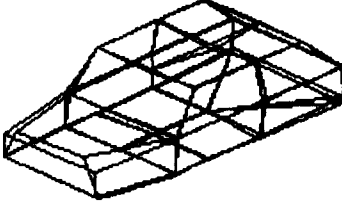
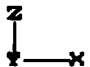
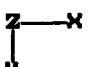


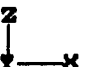
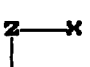
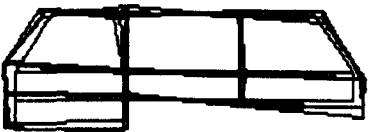
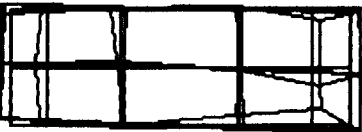
Fig. 6.20 Modes Associated with Peak E.

	NO OF NODES = 38 NO OF ACTIVE CO-ORDS = 98		
  FREQUENCY (Hz) = 72.61 DAMPING = 2.3 %			
	NO OF NODES = 148 NO OF ACTIVE CO-ORDS = 188		NO OF NODES = 148 NO OF ACTIVE CO-ORDS = 115
  FREQUENCY (Hz) = 73.13 DAMPING = 3.7 %		  FREQUENCY (Hz) = 72.74 DAMPING = 1.1 %	
	NO OF NODES = 48 NO OF ACTIVE CO-ORDS = 128		
  FREQUENCY (Hz) = 72.59 DAMPING = 4.4 %			

Peak F.

Occurs in the region of two close structural modes at 85.9 and 87.8 Hz.

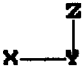
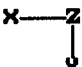
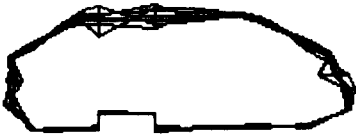

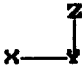
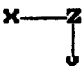
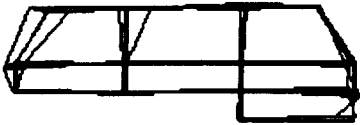
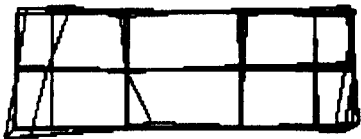
Fig. 6.21 Modes Associated with Peak F.

	NO OF NODES = 38 NO OF ACTIVE CO-ORDS = 98		NO OF NODES = 38 NO OF ACTIVE CO-ORDS = 98
			
FREQUENCY (Hz) = 85.86 DAMPING = 3.6 %		FREQUENCY (Hz) = 87.79 DAMPING = 2.9 %	
	NO OF NODES = 148 NO OF ACTIVE CO-ORDS = 188		NO OF NODES = 148 NO OF ACTIVE CO-ORDS = 118
			
FREQUENCY (Hz) = 85.51 DAMPING = 2.5 %		FREQUENCY (Hz) = 85.30 DAMPING = 2.2 %	
	NO OF NODES = 48 NO OF ACTIVE CO-ORDS = 128		
			
FREQUENCY (Hz) = 85.29 DAMPING = 1.2 %			

Peak G.

Associated with a region of high mobility in the rear roof.

Fig. 6.22 Modes Associated with Peak G.

	NO OF NODES = 148 NO OF ACTIVE CO-ORDS = 168		NO OF NODES = 146 NO OF ACTIVE CO-ORDS = 115
	<b>FREQUENCY (Hz) = 166.53</b> <b>DAMPING = 1.5 %</b>		<b>FREQUENCY (Hz) = 166.06</b> <b>DAMPING = 2.0 %</b>
	NO OF NODES = 48 NO OF ACTIVE CO-ORDS = 120		
	<b>FREQUENCY (Hz) = 166.63</b> <b>DAMPING = 1.2 %</b>		

Peak H.

Associated with the sixth acoustic mode (2 1 0)

Fig. 6.23 Modes Associated with Peak H.

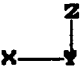
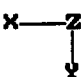
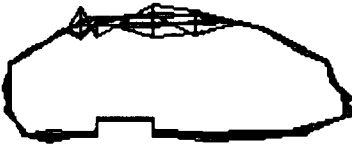
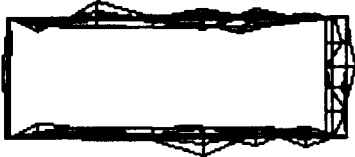
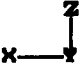
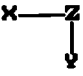
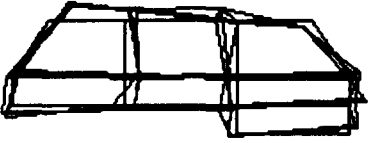
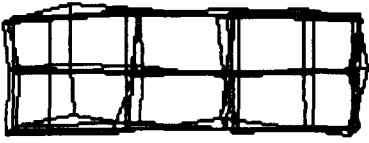
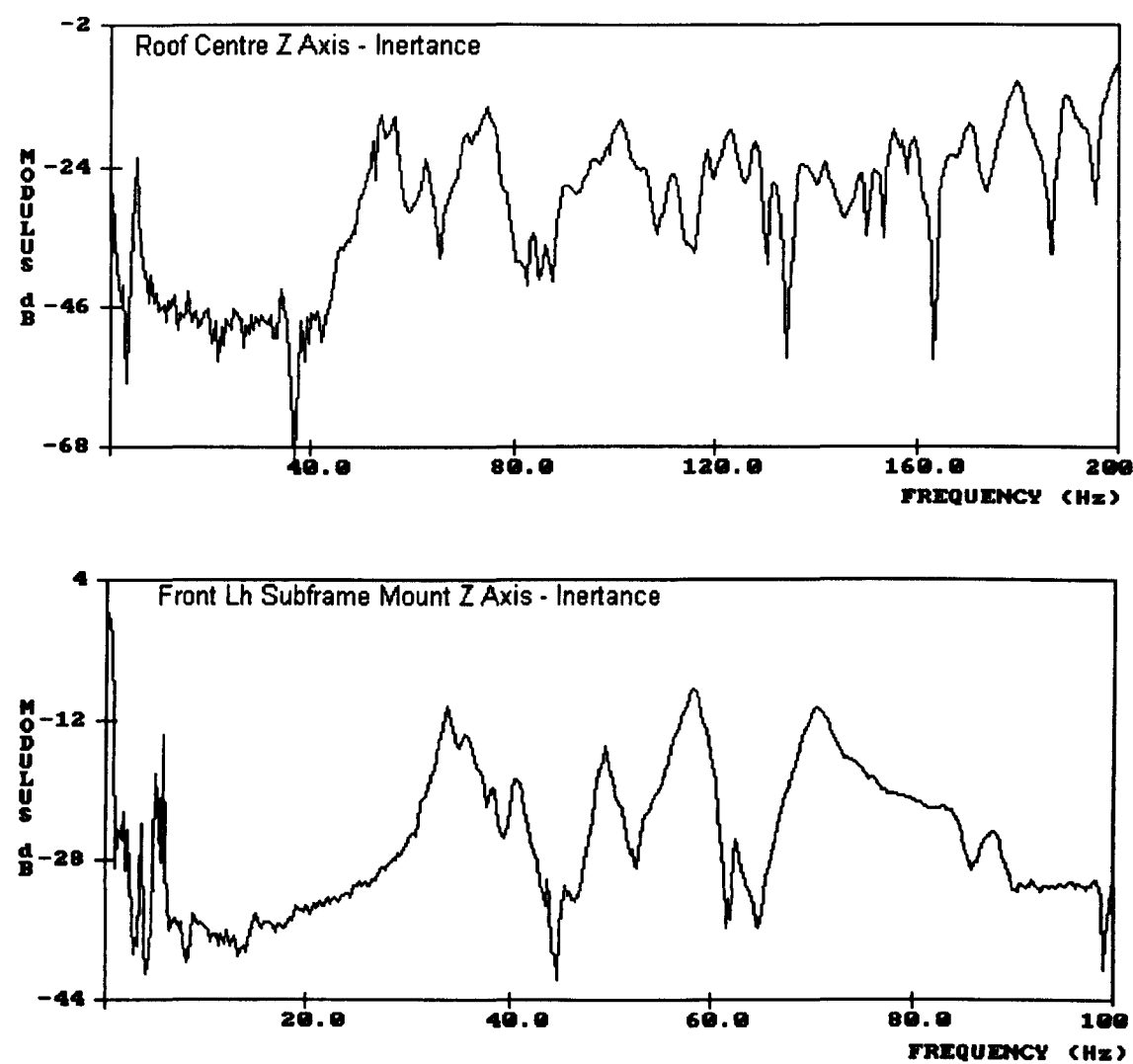
	NO OF NODES = 148 NO OF ACTIVE CO-ORDS = 168		NO OF NODES = 148 NO OF ACTIVE CO-ORDS = 115
	<b>FREQUENCY (Hz) = 188.43</b> <b>DAMPING = 1.1 %</b>		<b>FREQUENCY (Hz) = 187.80</b> <b>DAMPING = 1.6 %</b>
	NO OF NODES = 48 NO OF ACTIVE CO-ORDS = 128		
	<b>FREQUENCY (Hz) = 188.70</b> <b>DAMPING = 1.4 %</b>		

Figure 6.24 shows a comparison of the FRF data for the centre of the roof panel (up to 200 Hz) and a structural member (up to 100 Hz).

Fig. 6.24 Comparison of Structural FRF Data for a Body Panel and a Structural Member.



### 6.2.3 Discussion.

The interaction of the structural and acoustic systems is discussed in relation to the experimental results shown in the previous section. The peaks in the noise transfer function not associated with the acoustic modes shown in figure 6.14 demonstrate a modal response as shown by the circle fits in figure 6.15. This shows that the FRF data for the response of the air within the cavity is directly related to the excitation provided by the structural modes. Spatially the sound field will be sinusoidal in nature as the excitation was provided by a swept sine input. This is an important consideration for the application of the three microphone method at these frequencies as the finite difference calculation is dependent on a sinusoidal wave form. The swept sine input is pertinent to this work as it is the control of the noise generated by second order component of the engine vibration that is of interest.

Figure 6.24 shows FRF data for the front left hand subframe mount and the centre of the roof panel. As can be seen the first mode of the structural member is at a considerably lower frequency than that of the panel. This trend is reflected in figure 6.11 where the first three peaks of interest (A, B and C) occur below the lowest frequency where there is a panel mode. These first modes are dominated by the motion of the engine bay members rather than the body panels. This shows that at frequencies below the first panel modes the acoustic response is dominated by the major structural modes of the vehicle.

The amplitude of the acoustic response at 49 Hz (D figure 6.11) is considerably higher than for the previous three peaks. This corresponds to the bending mode of the engine bay members (figure 6.19) with the interior noise being generated by an out of phase motion of the floor pan and front windscreen with some motion of the door panels. Comparison of figures 6.11 and 6.24 show that the increase in the level of acoustic response closely matches the panel behaviour at these low frequencies.

The relationship between the dimensions of the cavity and the wavelength of sound at a given frequency now become significant. At frequencies where the dimensions of the cavity are much smaller than the wavelength of sound the enclosed air behaves (acoustically) as a rigid body. However once the a dimension of the cavity is equal to one quarter of the wavelength ( $\lambda/4$ ) it is possible to have a node and antinode of a standing wave along that axis provided one of the walls is not reflective. At 49 Hz  $\lambda/4$  is approximately 1.75 m which corresponds to the mean distance between the front and rear windscreens of a Rover Metro. As can be seen from figure 6.19 the pressure level is greatest at the rear of the car and a minimum at the front. The motion of the floor panel and front windscreen are in phase with the acoustic pressure and do not present a reflective boundary. Thus the acoustic response at this frequency is analagous to the first mode of a pipe with one open end effectively causing a  $\frac{1}{2} 0 0$  acoustic mode. The z and y axis components show rigid body behaviour as the dimensions of these axes are considerably less than  $\lambda/4$ .



Peak E is the first acoustic mode at 72.6 Hz (1 0 0). The side and plan views of the structure show structural ring modes at 73.13 and 72.74 Hz which show a high degree of interaction between the structural and acoustic systems. The roof mode shown by the 30-node structural mesh provides excitation near the node of the acoustic mode

The following peak (F) at 86 Hz again shows a high degree of interaction between the structural and acoustic systems. There are well defined ring modes in both the vertical longitudinal and horizontal planes. The acoustic mode shape shows strong residual effects from the first acoustic mode at 72 Hz superimposed with displacement in the remaining axes that matches the structural mode shape.

At higher frequencies the dominant structural modes are more localized and more likely to be associated with individual panels. Peak G (166 Hz) demonstrates this characteristic with a localized acoustic response in the region of high levels of structural vibration of the roof panel.

The final peak to be considered (H) is the sixth acoustic mode (1 0 1) at 189 Hz. The structural and acoustic systems no longer show a high degree of interaction. The structural modal behaviour is largely restricted to single panel modes which provide excitation for the acoustic mode of the cavity.

#### **6.2.4 Conclusion.**

The three microphone method can not only be used to determine the mode shapes of acoustic cavities but also allows the experimental study of fluid-structure interaction. A logical extension of this work would be to use numerical methods to quantify the degree of interaction or coupling between the structural and acoustic modes such as those described by Richards (1982) or Shippen & Dunn (1991).

## 7. Measurement of Acoustic Absorption Coefficient of Trim Materials.

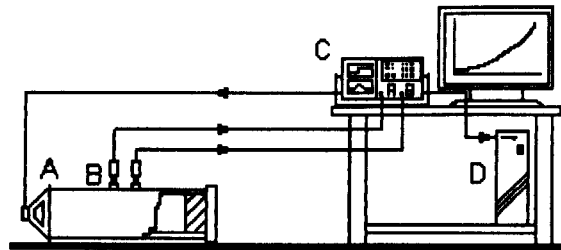
The modelling of cavity acoustics requires the accurate definition of any loss mechanisms present. Typical automotive trim materials are porous absorbers whose acoustic characteristics can be represented by a frequency dependent absorption coefficient.

After investigating the available methods for measuring the absorption coefficient of automotive trim materials at low frequencies it was decided to utilize the impedance tube method with two microphones and an FFT analyser (Chung & Blaser (1980)). This allows the measurement of the absorption coefficient normal to the material surface down to approximately 50 Hz (Højberg (1991)). The normal incidence absorption coefficient is applicable in this instance as the main acoustic modes of interest (those below 150 Hz) are axial and the absorbent surfaces are therefore normal (or nearly so) to the axes of the acoustic modes.

### 7.1 Method.

A tube was constructed in accordance with the specification given in ASTM standard E 1050 \_86 (ASTM (1986)) with an internal diameter of 150 mm giving a cut off frequency of 1343 Hz. Figure 7.1 and plate 7.1 show the equipment used.

Fig. 7.1 Absorption Coefficient Measurement Equipment.



A: Impedance Tube

B: Microphones With Power Supplies

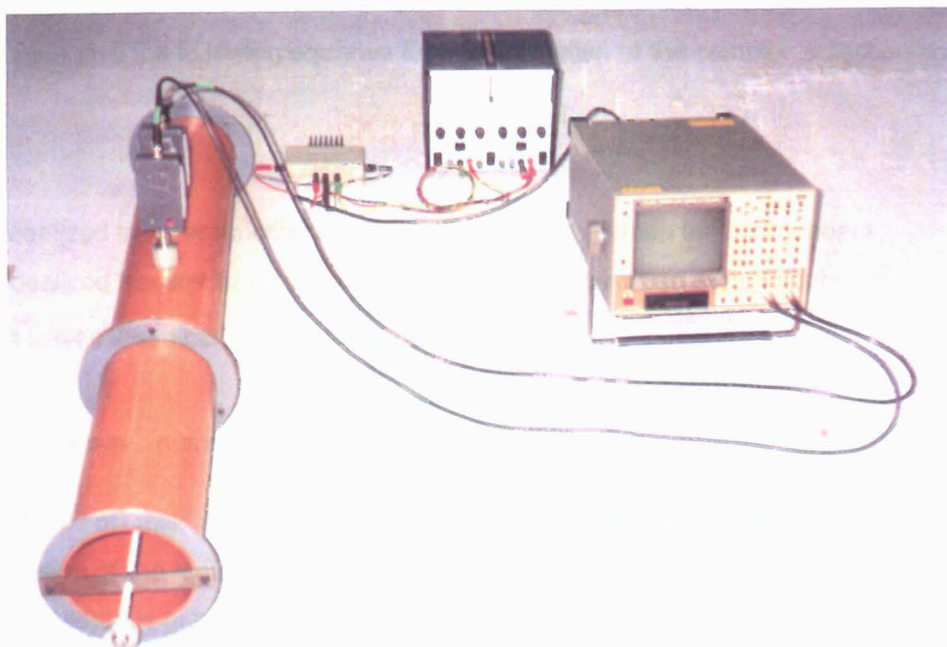
C: Ono-Sokki CF350 FFT Analyser

With Swept Sine signal to Speaker  
GPIB Bus To D (Data Transfer)

D: REM 486 Personal Computer With Excel Spreadsheet Software

Plate 7.1 Impedance Tube and FFT Analyser.

Original In Colour



There are several formulations available for determining the absorption coefficient of materials using a twin microphone impedance tube. The formulation given by Højberg (1991) was used in conjunction with the calibration of the microphone pair by the sensor switching technique described by Chung & Blaser (1980). The effects of propagation losses within the tube were corrected by dividing the calculated reflection coefficient for the sample by the calculated reflection coefficient of the bare tube as proposed by Powell & Van Houten (1970). The method used is summarized below:

1) A transfer function was measured between the microphones for a frequency range of 0 to 200 Hz at a sound level of 70 dB(C) (measured with a sound level meter). This was carried out with the microphones in their nominal locations and interchanged. The transfer function data was transferred to and stored on a personal computer using the ICATS modal acquisition software (Modacq - ICATS (1993)).

2) The processing of the transfer functions was done with the Excel spreadsheet (Microsoft (1992)) on a personal computer. The main stages in the calculation of the absorption coefficient are:

#### Calibration of the system by the sensor switching technique.

This involves calculating the geometric mean of the two transfer functions to give a result that is independent of the microphone gain and phase factors for further processing. This is given by Chung and Blaser (1980) as

$$H_c = \sqrt{H_{\text{original configuration}} \times H_{\text{swapped}}}$$

Where  $H_c$  is the calibrated transfer function between the two microphones

(7.1)

Calculation of the uncorrected reflection coefficient.

From the measured transfer function,  $H_c$ , the reflection coefficient can be determined. Chung & Blaser (1980) give the following equation for the calculation of the complex reflection coefficient

$$R = \frac{H_c - H_i}{H_r - H_c} \quad (7.2)$$

Where

$H_i$  is an idealized transfer function for the incident wave between the microphones.

$H_r$  is an idealized transfer function for the reflected wave between the microphones.

For plane waves these can be expressed as

$$H_i = e^{-jks} \quad \text{and} \quad H_r = e^{+jks}$$

Where  $k$  is the wave number and  $s$  is the microphone spacing (7.3)

As derivation of this relationship is somewhat involved and not directly relevant to the implementation of the method for this work it has not been included. A full discussion of the theory behind the method is given in the paper referenced above.

Correction of the reflection coefficient for tube losses.

Powell & Van Houten (1970) give the following equation for the correction of propagation losses in the tube

$$\frac{R_s}{R_a} = \frac{R_o}{R_t} \quad (7.4)$$

where

$R_s$  is the measured reflection coefficient of the sample.

$R_a$  is the actual reflection coefficient of the sample.

$R_o$  is the measured reflection coefficient of the rigid tube termination.

$R_t$  is the actual reflection coefficient of the rigid tube termination.

Assuming a reflection coefficient of unity for the actual tube termination,  $R_t$ , and rearranging 7.4 gives

$$R_a = \frac{R_s}{R_o} \quad (7.5)$$

Calculation of the absorption coefficient.

This can now be calculated using equation 3.60 and the corrected reflection coefficient.

$$\alpha = 1 - |R_a|^2 \quad (7.6)$$

where  $\alpha$  is the absorption coefficient

The absorption coefficient was calculated at 133 frequencies over the frequency range 1.5 to 199.5 Hz, these being the frequencies of interest for the finite element model of the forced response of the Metro passenger compartment as described in the next chapter.

The following materials were tested and the results are shown in the next section.

Seat foam  
Carpet with foam underlay  
Carpet with felt underlay  
Rear seat back covering

## 7.2 Results.

The absorption coefficient of the bare tube and the above materials are plotted against frequency.

Fig. 7.2 Absorption Coefficient for the Bare Tube.

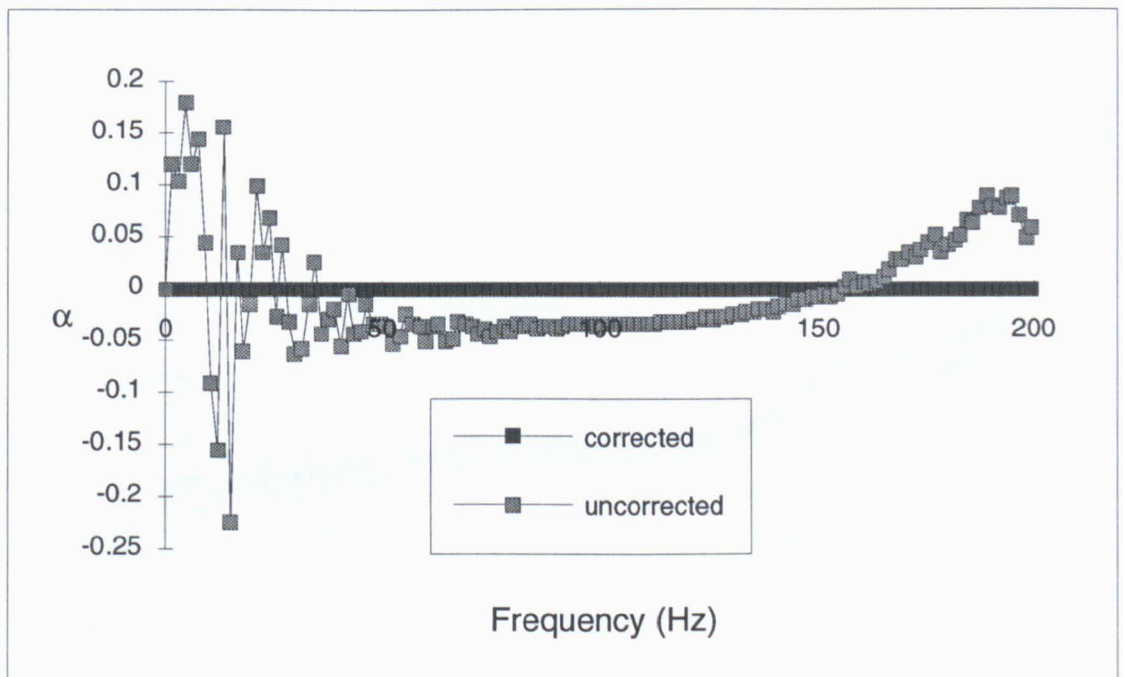


Fig. 7.3 Absorption Coefficient for Seat Foam.

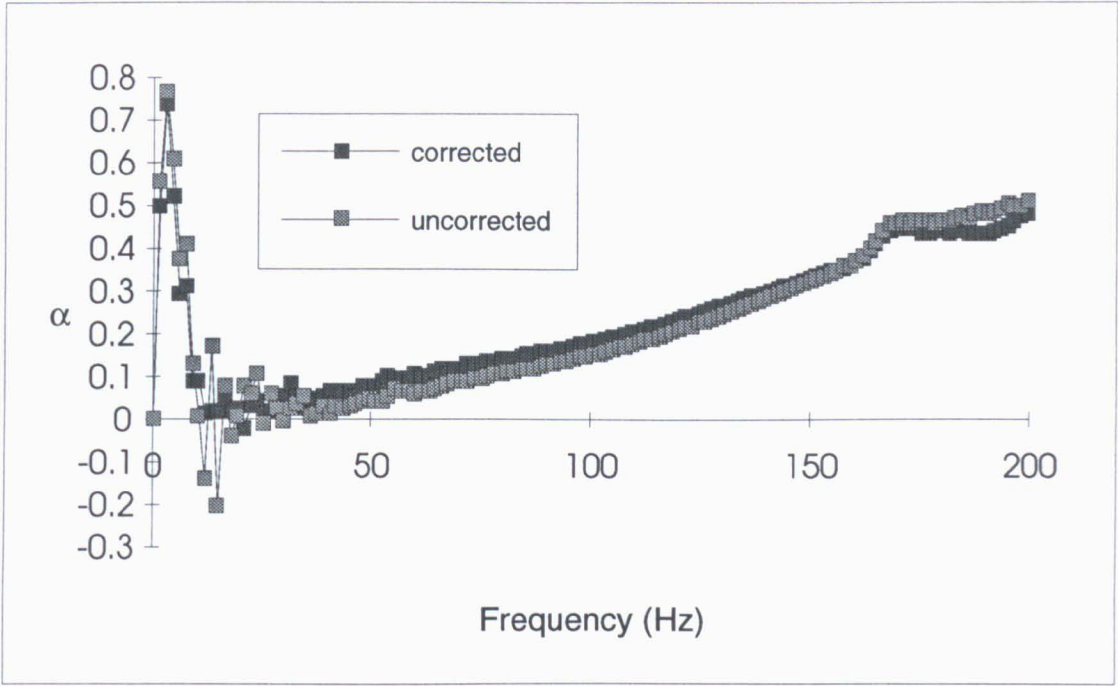


Fig. 7.4 Absorption Coefficient for Carpet with Foam Underlay.

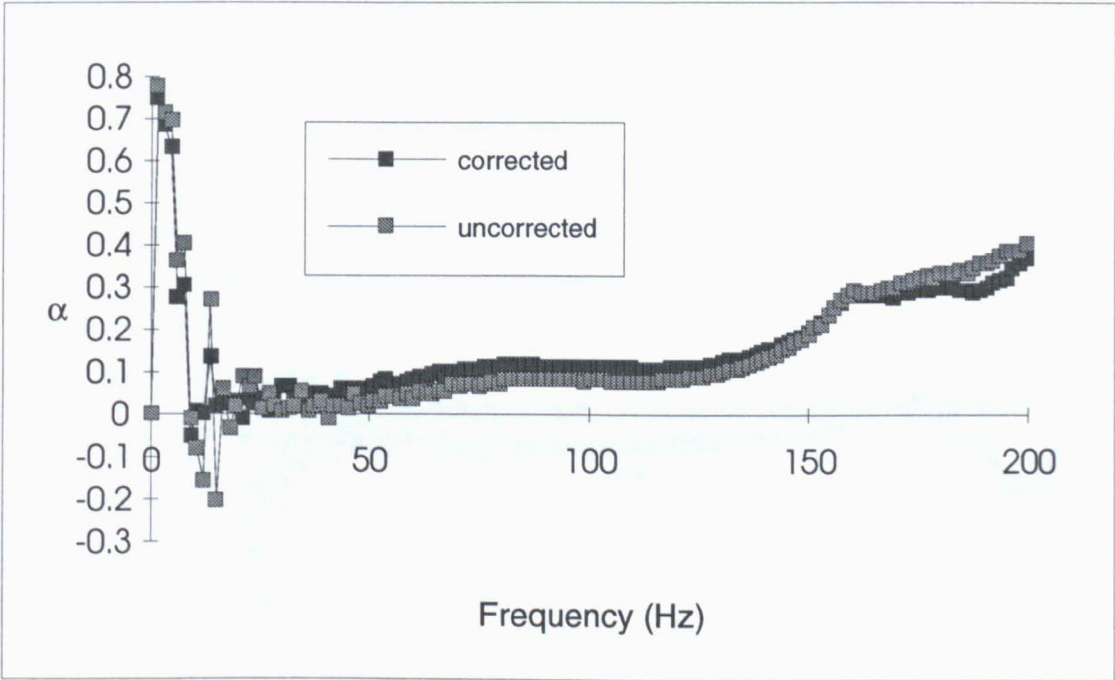




Fig. 7.5 Absorption Coefficient for Carpet with Felt Underlay.

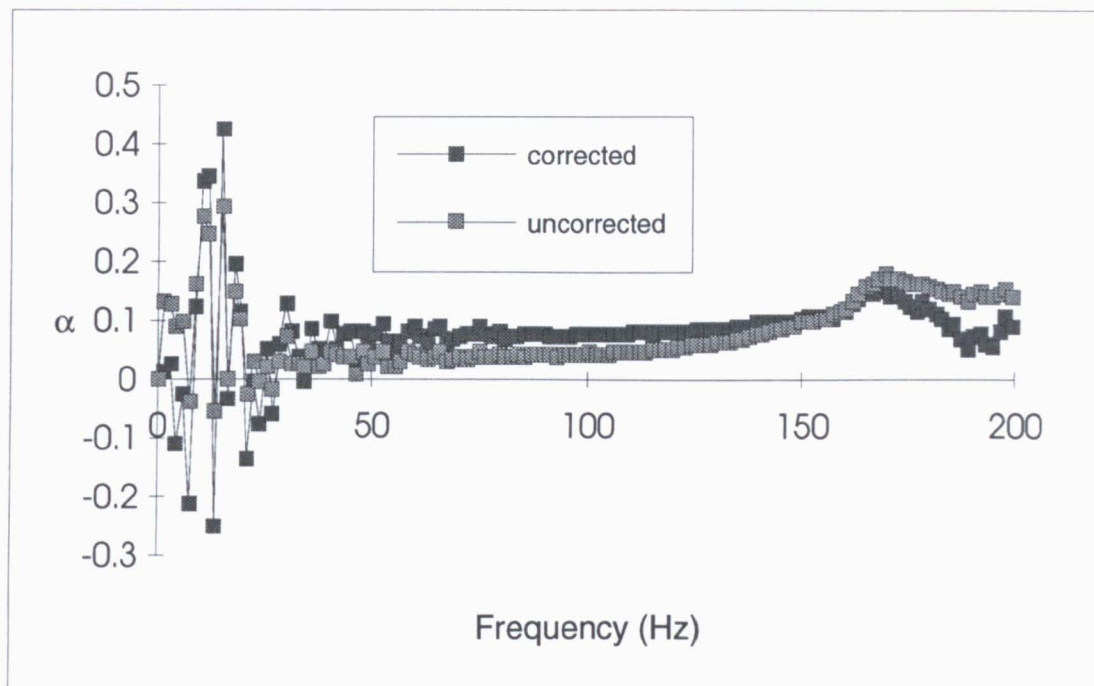
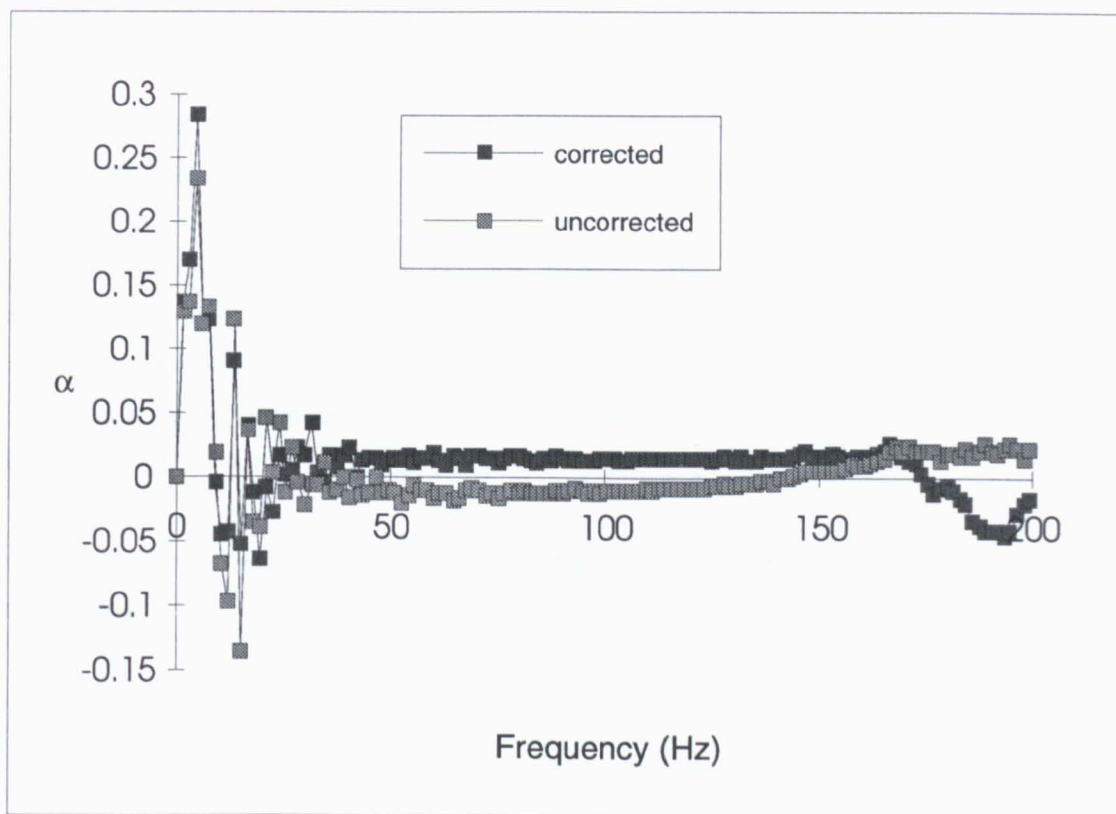


Fig. 7.6 Absorption Coefficient for Rear Seat Back Covering.



### 7.3 Discussion.

In general the materials show the characteristic of increasing absorption with increasing frequency expected of porous materials. The exception to this was the rear seat backing material which in practice is backed by steel sheet acoustically isolating the rear of the seat from the absorbent foam that forms the seat body. It should be noted that the microphones used had a lower operating frequency of 20 Hz. Thus the low frequency scatter shown in the absorption plots (Figures 7.2 - 7.6) represents a low frequency characteristic of the microphones rather than the acoustic behaviour of the material under test.

The absorption coefficients can be used in the finite element model of the acoustic cavity to represent the effects of lining materials and seats. The absorption coefficients at the frequencies of interest were stored in a text file for direct entry into the ANSYS database.

The main difficulty in the design and construction of the impedance tube was the very general nature of the specifications set out in the relevant ASTM standard (ASTM (1986)). The tube was designed for low frequency measurements and could be greatly improved with some development work. The main aspects of the tube design that would benefit from further development are:

A) Optimization of the spacing of the microphones. The low frequency performance could be improved with a greater pitch between the microphone pair (A spacing of 100 mm was used).

B) The acoustic source used was an 150 mm diameter wide range loudspeaker. Højberg (1991) found that the low frequency limit imposed by a 75 mm diameter speaker was 50 Hz. Although the larger speaker used for this work gave a lower low frequency limit It should be possible to improve the low frequency performance of the tube by mounting a tuned volume behind the speaker or replacing it altogether with a piston driven by an electromagnetic shaker.

Unfortunately time constraints did not allow for the construction of a second tube to verify these considerations.



## **8. Modelling Car Cavity Acoustic Response to Structural Excitation.**

This chapter covers the modelling of the acoustic response of the Rover Metro passenger compartment to excitation by the vibration of the body structure. The use of the finite element method for this application is discussed and the modelling process used described in detail. A final section briefly covers the application of the boundary element method, in particular the calculation of the noise contribution of individual panels.

The finite element method and other numerical techniques have previously been applied to modelling the response of an acoustic field to structural excitation and these have been detailed in the previous work described in chapter 2. The most usual solution method applicable to this work is the steady state response of the structural-acoustic system to a sinusoidal excitation at a given frequency (harmonic analysis). The results of this type of analysis can be used to study the acoustic field within the domain of the model or the results of several analyses at different frequencies combined to give noise spectra at individual nodes.

For automotive applications the most usual approach has been to either apply structural modal data (either experimental or finite element results) as a forcing function on the model of the car passenger compartment acoustics or a combined structural-acoustic model to predict the characteristics of either system with the effects of the other included. The former method is presented here with experimental structural vibration data applied as an input to a finite element model of a Rover Metro passenger compartment.

### **8.1 Assumptions and Restrictions.**

The basic assumptions and restrictions discussed in chapter 4.1 apply as well as the considerations applicable to this work in particular which are discussed below.

The ANSYS manual (ANSYS (1993)) specifies a maximum element edge length of  $\lambda/15$  at the highest frequency of interest for acoustic harmonic analyses. Applying this requirement and assuming a speed of sound of  $344 \text{ ms}^{-1}$  gives an element edge length of 0.115 m at 200 Hz. The acquisition of structural vibration data at this measurement pitch would not be practical given the time constraints imposed in a manufacturing environment. A coarse mesh based on the pitch of a previous test carried out on the test body by Rover Group was used with a maximum pitch of approximately 0.3 m. The use of this coarse mesh is valid for the following reasons:

- a) In chapter 7 the major noise generating structural modes at low frequencies were shown to be the major body and ring modes of the structure. These can be adequately described with a relatively coarse mesh.
- b) At higher frequencies the excitation is provided by local panel modes with the acoustic response dominated by three close modes. There is little interaction between the structural and acoustic

mode shapes, therefore, it is only necessary to provide a representative structural input to excite the relevant acoustic mode.

c) Given that the body shell is likely to be subject to later modification the major characteristics of the acoustic field are more important than achieving a model that is accurate in every detail. This argument also applies to the variation in structural response between individual production bodies.

d) This work is only concerned with the structurally induced component of the sound field associated with the engine. In practice different variants of the same model have different engines and suspension systems. Differences in these components can have significant effects on the overall interior sound field, for example, sportier variants have a harder suspension which leads to increased interior road noise. This work does not set out to give a definitive description of the interior sound field but to reduce the likelihood of engine induced cavity boom. Thus excessive detail in modelling at this stage is worthless without a detailed knowledge of the characteristics of all the inputs associated with structurally induced noise.

## **8.2 Construction of the Model.**

The ANSYS revision 5.0 (ANSYS (1993)) finite element software was used on a 486 personal computer utilizing the FLUID30 acoustic element and a full harmonic analysis. The model was run in batch mode and the structure of the batch file for the analysis of the untrimmed body is given in appendix three.

The model itself is based on that used for the prediction of the acoustic modes in chapter 4 having the same dimensions but with approximately half the nodes removed. It was decided to use the FRF data rather than the structural modal data for the following reasons:

- a) There is no need to include out of range modes as any residual effects are included in the FRF data.
- b) Refinement or alteration of the model is simplified as the FRF data for any additional modes or modifications can be read into the finite element database without the need for reprocessing the modal data.
- c) It is not necessary to calculate the amplitude and phase of the displacement at each node defining the behaviour of the structure at the boundary for each load step by modal superposition.

The structural vibration data was measured at points on the car body corresponding to the location of the surface nodes of the model for vertical excitation at the torsion engine mount. This mount was selected as it is attached directly to the body structure and gave particularly coherent transfer functions. The equipment used for these measurements and the directions of the FRF data have already been described in chapter 6.2.1. The measurements were made normal to the panel surfaces except for the front and rear windscreens where measurements were made along the longitudinal and vertical axis.

The structural FRF data was used to describe the displacement of the surface nodes of the model after it had been read into the ANSYS database by dividing the measured inertance data by  $-\omega^2$  to give the receptance (displacement/force) values required by the software.

The car interior acoustic field was determined at 133 frequencies between 1.5 and 199.5 Hz in increments of 1.5 Hz.

### **8.2.1 Modelling the Untrimmed Body.**

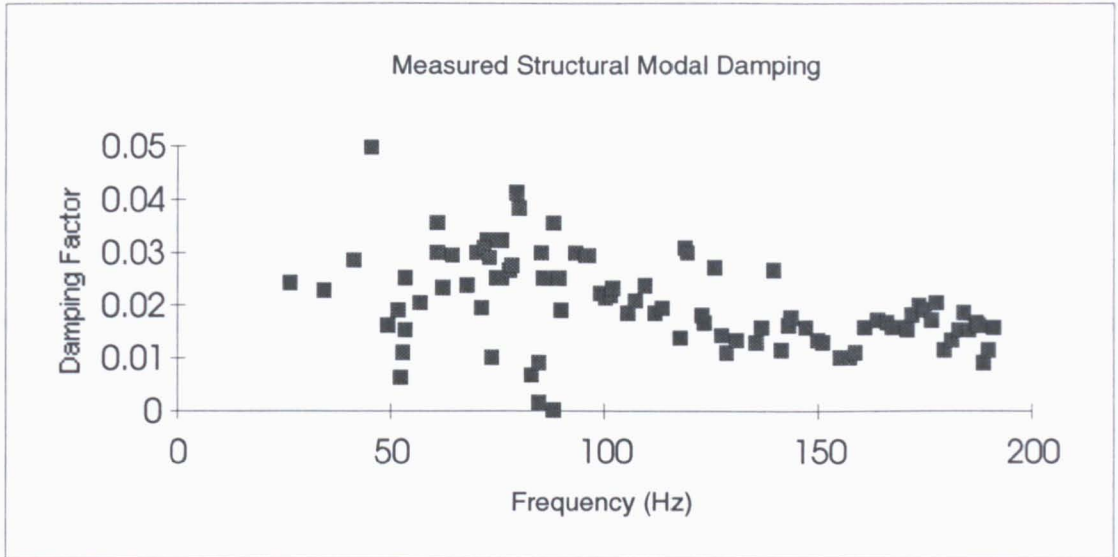
The main difficulty in modelling the forced response of the acoustics of cavities is the correct definition of the losses. The effects of porous trim materials such as seats etc. can be modelled by including their measured acoustic absorption coefficient as a frequency dependent property. However this is more difficult for the untrimmed body. The body panels are not acoustic absorbers, their energy dissipation is caused by internal and radiation losses as they vibrate.

To model the losses in the untrimmed body the following assumptions were made:

- a) The internal losses of the air within the cavity are negligible.
- b) Thus, the only losses are the internal losses within the body and radiation losses of the sound energy from the structure.
- c) Both these losses are included in the modal damping factors of the structure as these describe all energy lost by the panels.

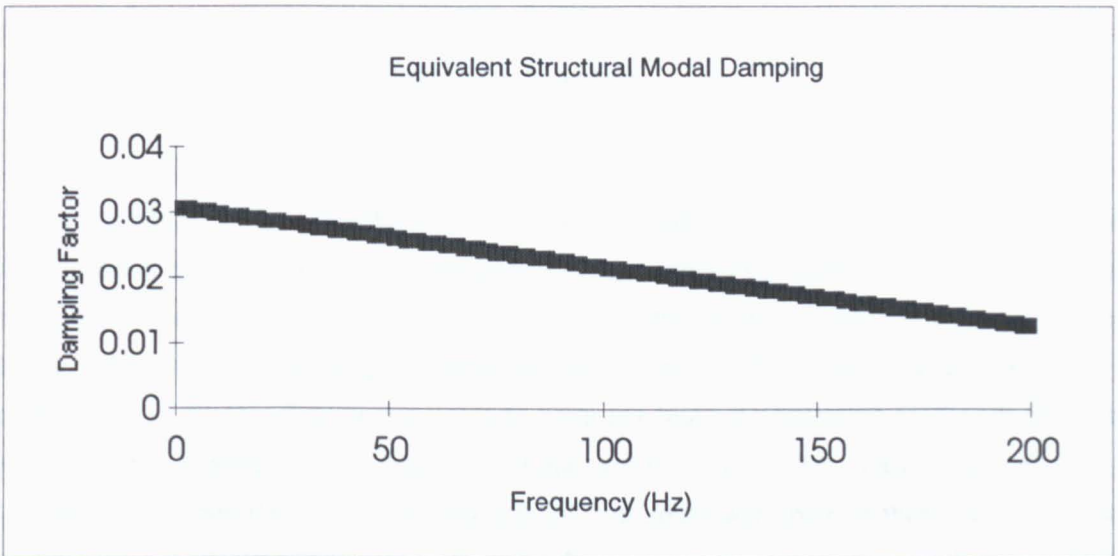
To study the characteristics of the structural loss factors ninety five modes were extracted from the structural modal data. Figure 8.1 shows the variation of damping values with frequency.

Fig. 8.1 Structural Modal Damping.



Despite the scatter a trend of decreasing damping with increasing frequency is apparent. To obtain values for the model a least squares best fit line was calculated and an effective modal damping predicted for each frequency of interest. This is shown in figure 8.2.

Fig. 8.2 Equivalent Structural Modal Damping.



The ANSYS software requires acoustic losses to be described as a boundary absorption coefficient. The structural loss factor,  $\eta$ , and the acoustic absorption coefficient,  $\alpha$ , can be related by considering their basic definitions

$$\eta = \frac{\text{Energy lost to the system}}{\text{Energy stored in the system}}$$

(8.1)

$$\alpha = \frac{\text{Absorbed energy}}{\text{Incident energy}} \quad (8.2)$$

As can be seen equations 8.1 and 8.2 are conceptually similar. The structural loss factor and the acoustic absorption coefficient are both energy ratios describing the loss per cycle. Thus the losses for the untrimmed body were modelled by applying the equivalent structural modal damping values at each frequency shown in figure 8.2 as a boundary acoustic absorption. The values at the frequency of each load step of the model were stored in an ASCII text file and then read into the ANSYS database. These values were then used to define the boundary absorption of the model at each solution.

### 8.2.2 Modelling the Trimmed Body.

It was decided only to model the acoustic effects of the more significant trim items. These were the footwell carpets and seats. The acoustic effect of the trim was added to the existing boundary losses already defined earlier in this chapter.

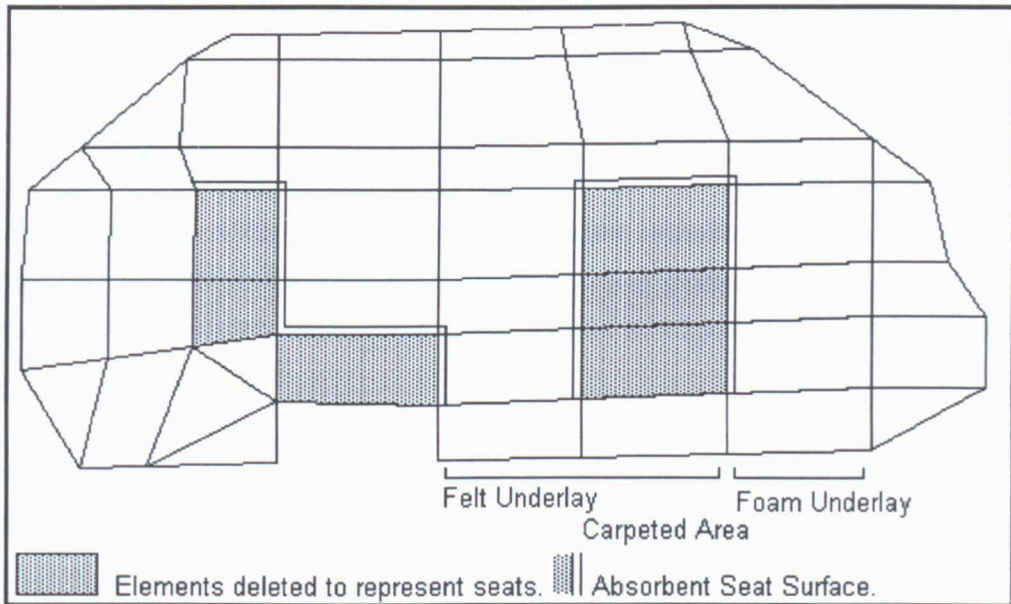
The front and rear footwell carpets had different underlay materials which caused a significant variation in the measured absorption coefficient of the backed carpet (see figures 7.4 and 7.5). The carpeted areas of the floor were modelled by using the relevant measured absorption coefficient in the appropriate region of the model boundary (figure 8.3). As the absorption coefficient of the carpet materials is significantly greater than the untrimmed boundary losses the structural losses were not included in the carpeted areas of the boundary.

Whilst the absorption coefficient of the trim items describes their dissipative effects it does not allow for the effect of the seat volume on the cavity acoustics. A detailed model of the seats was not produced as there are variations between models of different specifications and the front seats are movable along the longitudinal axis. Because of these factors the modelling of the seat volumes was limited to removing elements across the car as shown in figure 8.3. However the results shown in chapter 7 show the seats to have the highest absorption coefficient of the trim items over the frequency range of interest. The acoustic response of the cavity is dominated by the first three axial modes ( $\frac{1}{2}$  0 0, 1 0 0 and 2 0 0). The seats with their relatively high absorption coefficient are ideally placed to attenuate these first modes. Thus the seat absorption coefficient needs to be defined using the measured values obtained in chapter 7 (figure 7.3) at the seat surfaces to give the correct attenuation of the acoustic response at low frequencies. The back of the rear seat was defined as a reflective surface because of the low absorption coefficient of its covering (figure 7.6).

The various absorption coefficients were calculated on a spreadsheet at each frequency of interest and read into the ANSYS database.

Three models of the forced acoustic response of the car cavity were run for various states of trim. These were for carpets only, seats only and both carpets and seats.

Fig. 8.3 Trimmed Cavity Acoustic Model.



### 8.2.3 Application Of The Boundary Element Method.

Part of the transfer of this work has involved the running the untrimmed model of the Metro passenger compartment at Rover Group's Cowley works to demonstrate the method of modelling vehicle interior noise using structural FRF data. Rover Group use the Sysnoise revision 5.0 acoustics software and the LMS structural modal test system in their noise, vibration and harshness work. The Sysnoise package is capable of both finite element analysis (FEA) and boundary element method (BEM) analyses of acoustic behaviour. The BEM was used for the model as it has three distinct advantages for this type of work:

- a) There is no internal meshing of the model reducing solution times and facilitating the use of detailed models of trim items.
- b) The collocation (uncoupled interior) variant of the BEM has the capability to output the complex contributions of individual panels to the total acoustic pressure at a given point at a given frequency. This is within the capabilities of the finite element method (Shippen & Dunn (1988)) but is not included in the ANSYS package.
- c) The nodal pitch required for a harmonic analysis is  $\lambda/6$  at the maximum frequency of interest as opposed to  $\lambda/15$  for the FEM.



A BEM model was constructed using the surface nodes and FRF data used on the finite element model described earlier in this section. Because of the present limitations of the software no damping was included in the model. Thus the results presented are limited to polar panel contribution plots at several pertinent frequencies.

8.3 Results.

The results are presented in three sections.

- a) The finite element prediction of the structurally induced acoustic field within the untrimmed car passenger compartment at the frequencies of the acoustic modes shown in chapter 4 and the studies of structural acoustic interaction given in chapter 6 in figures 6.18 to 6.23 (figures 8.4 to 8.14).
- b) Experimental and modelled (FEA) NTF data is shown for the drivers head location for the untrimmed body and each of the trim conditions described in 8.2.2 (figures 8.15 to 8.18).
- c) The results of the BEM analysis are given as polar panel contribution diagrams at the frequencies of the finite element prediction of the passenger compartment acoustic field shown in figures 8.4 to 8.14 (figures 8.19 to 8.29).

Fig. 8.4 Structurally Induced Acoustic Field at 33 Hz.

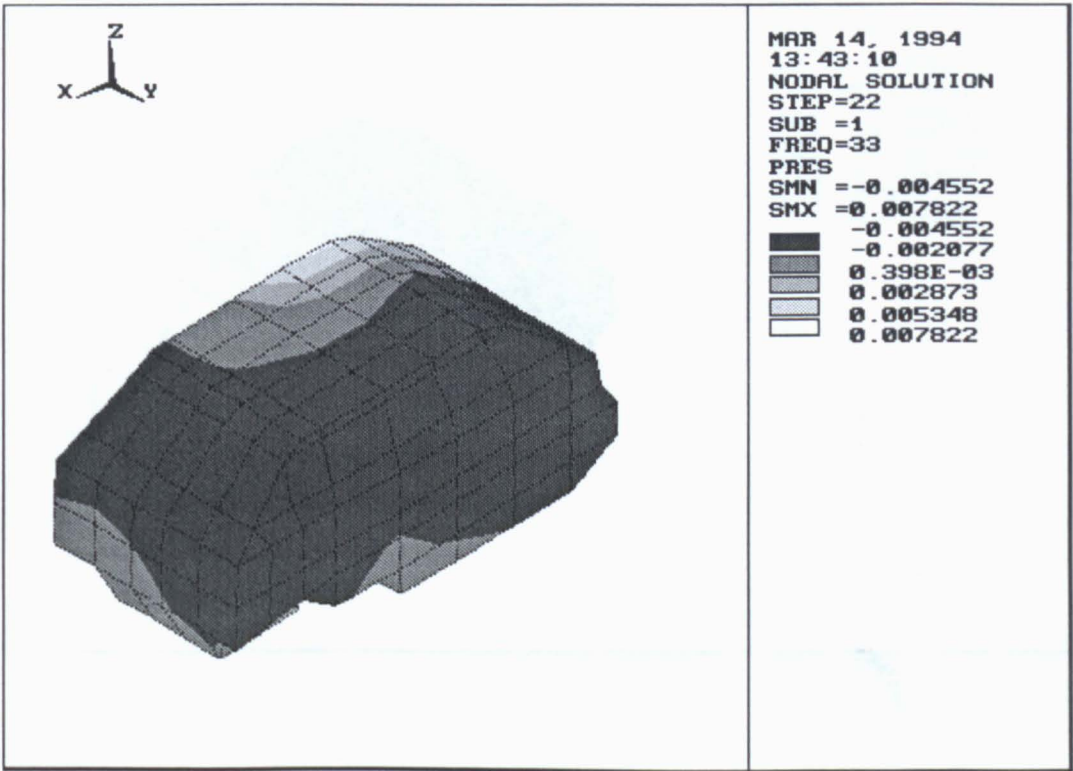


Fig. 8.5 Structurally Induced Acoustic Field at 48 Hz

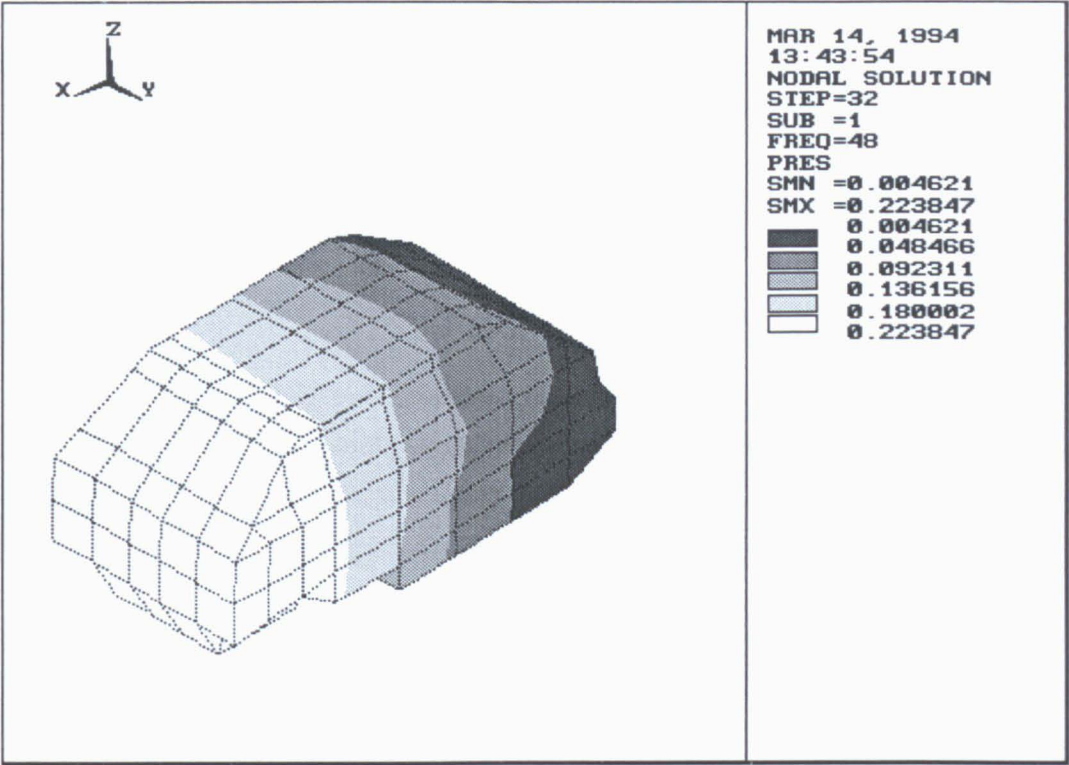


Fig. 8.6 Structurally Induced Acoustic Field at 73.5 Hz.

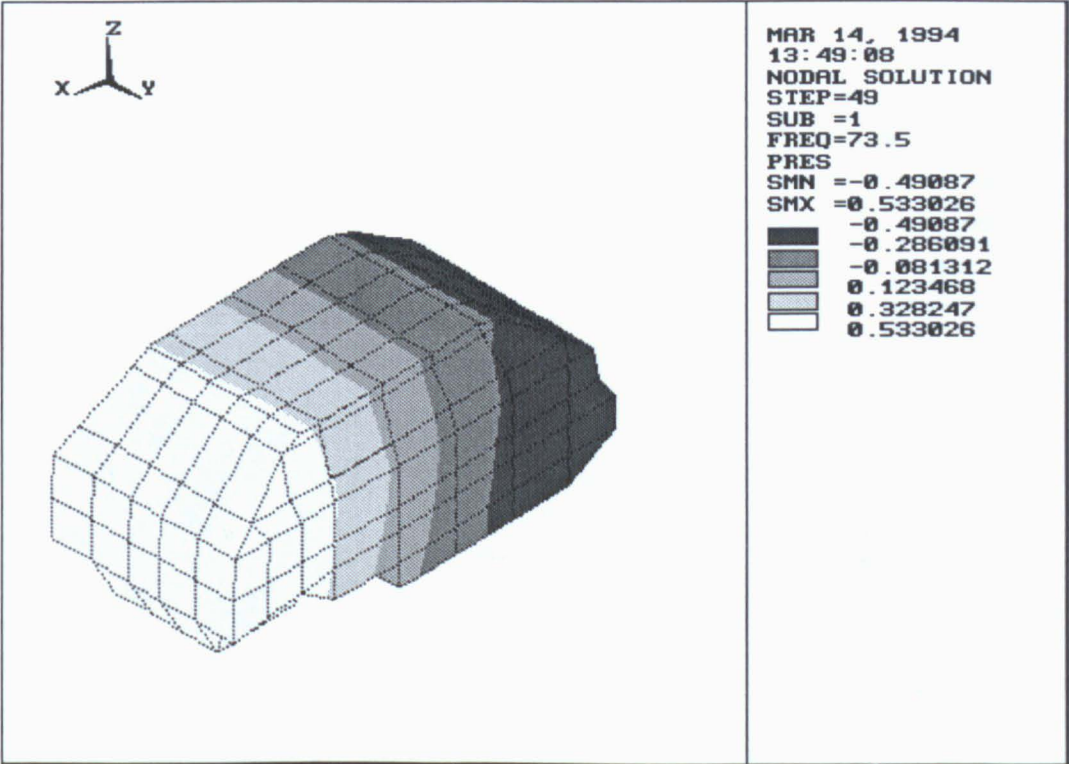




Fig. 8.7 Structurally Induced Acoustic Field at 84 Hz.

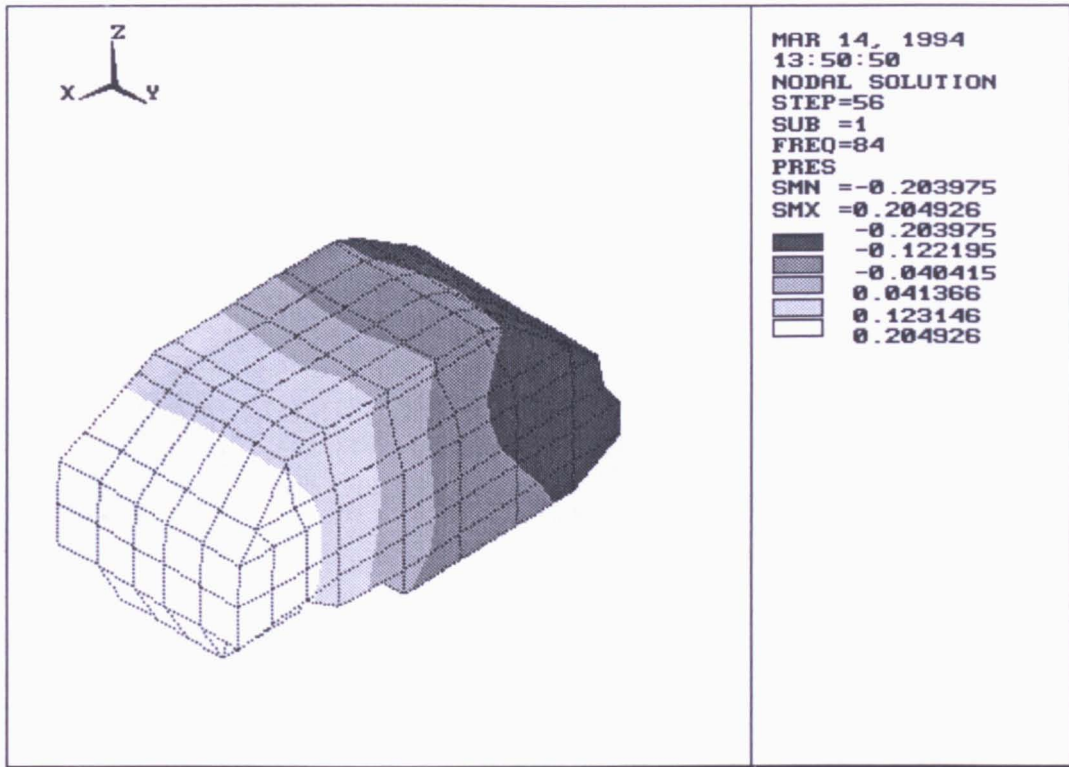


Fig. 8.8 Structurally Induced Acoustic Field at 138 Hz.

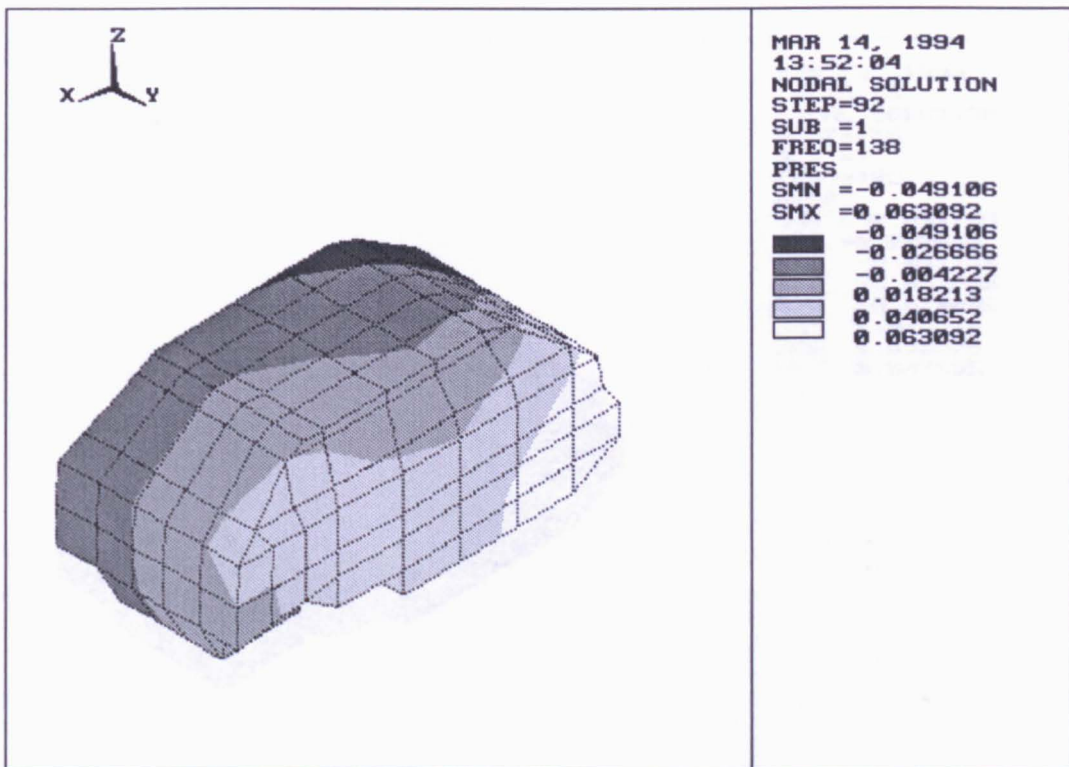


Fig. 8.9 Structurally Induced Acoustic Field at 141 Hz.

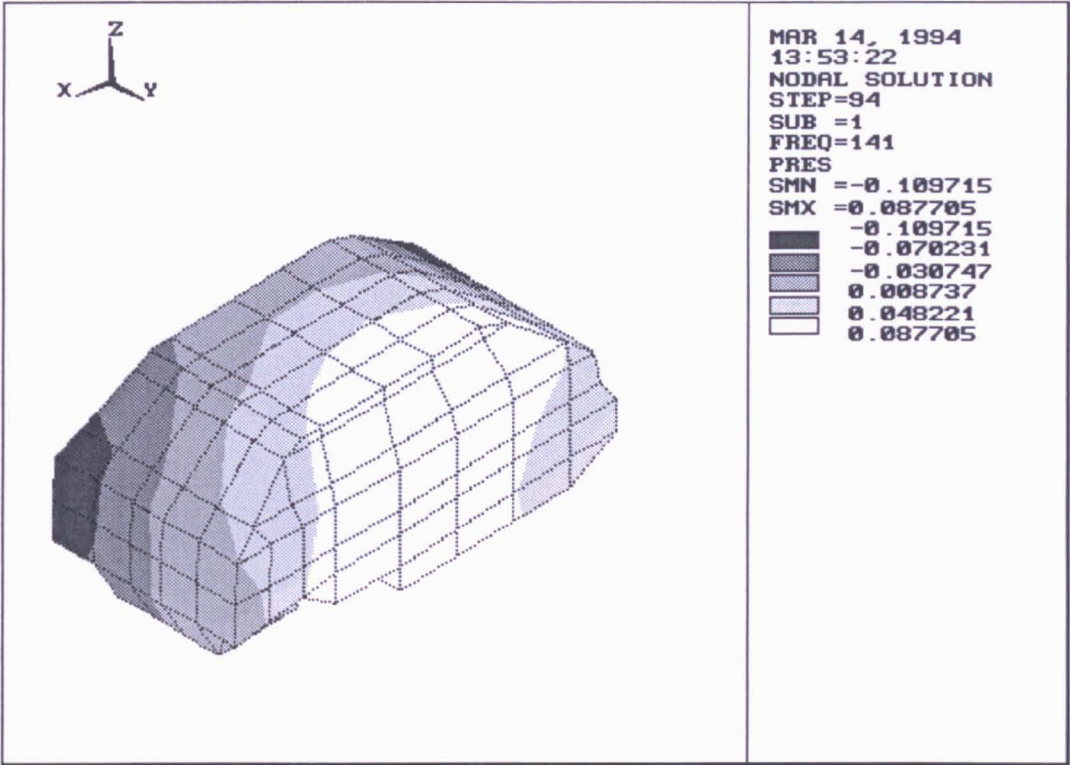


Fig. 8.10 Structurally Induced Acoustic Field at 162 Hz.

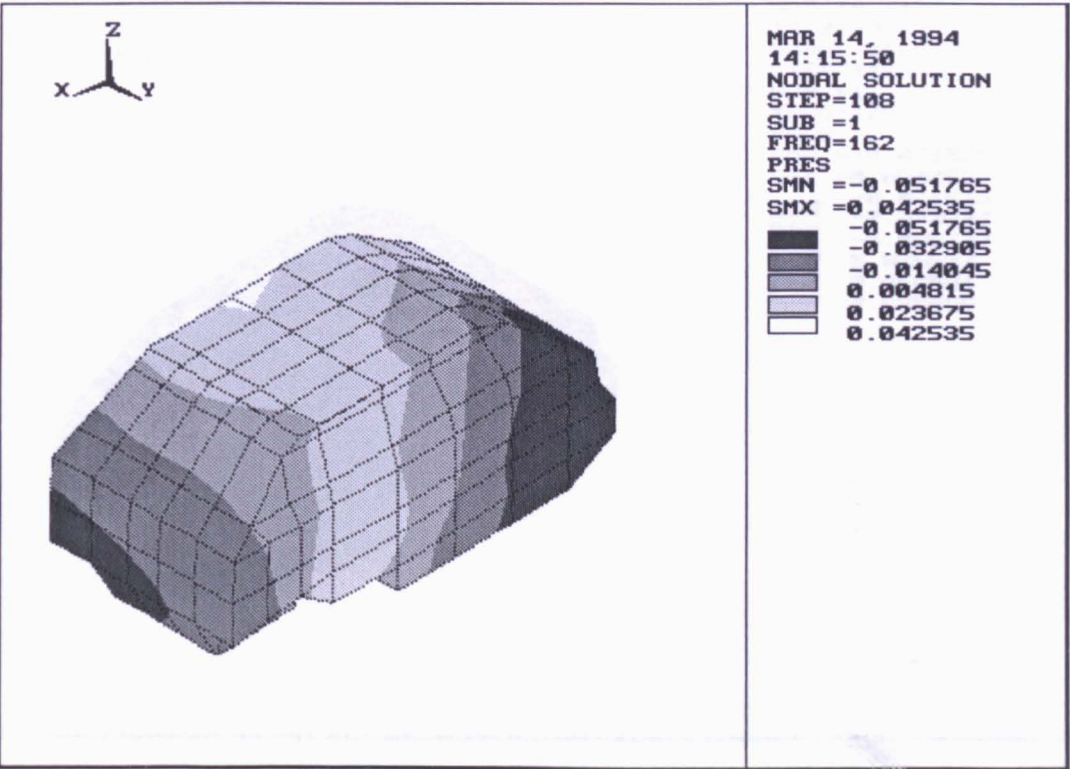


Fig. 8.11 Structurally Induced Acoustic Field at 166.5 Hz.

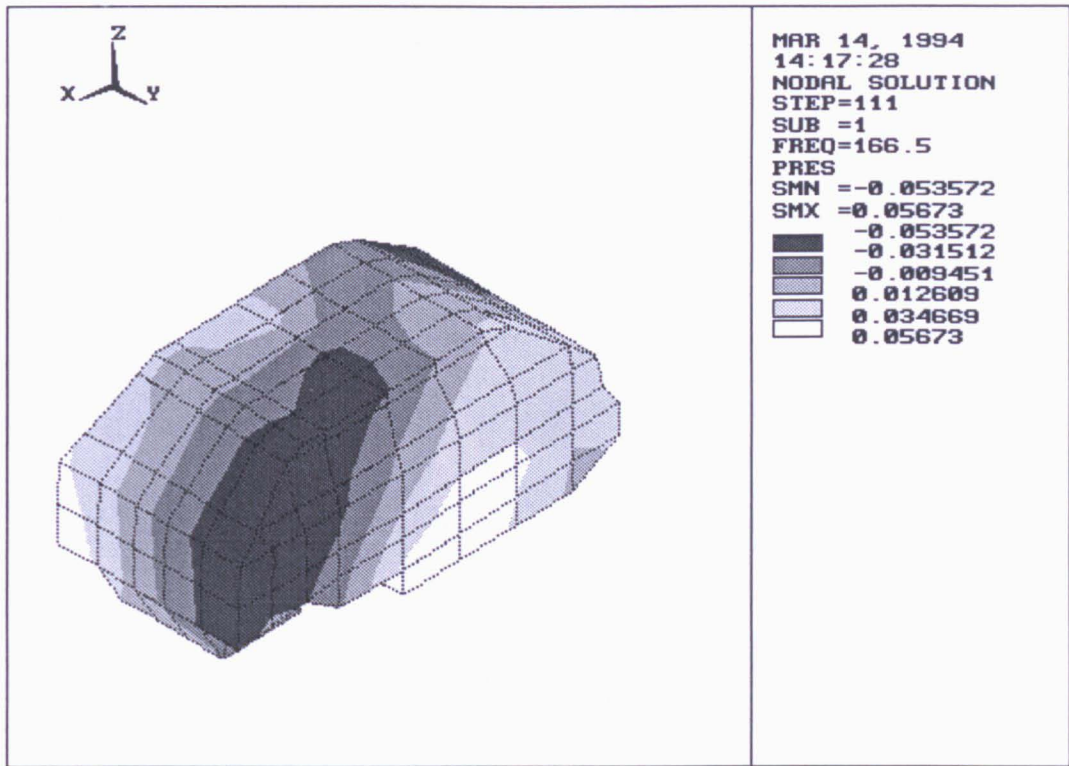


Fig. 8.12 Structurally Induced Acoustic Field at 175.5 Hz

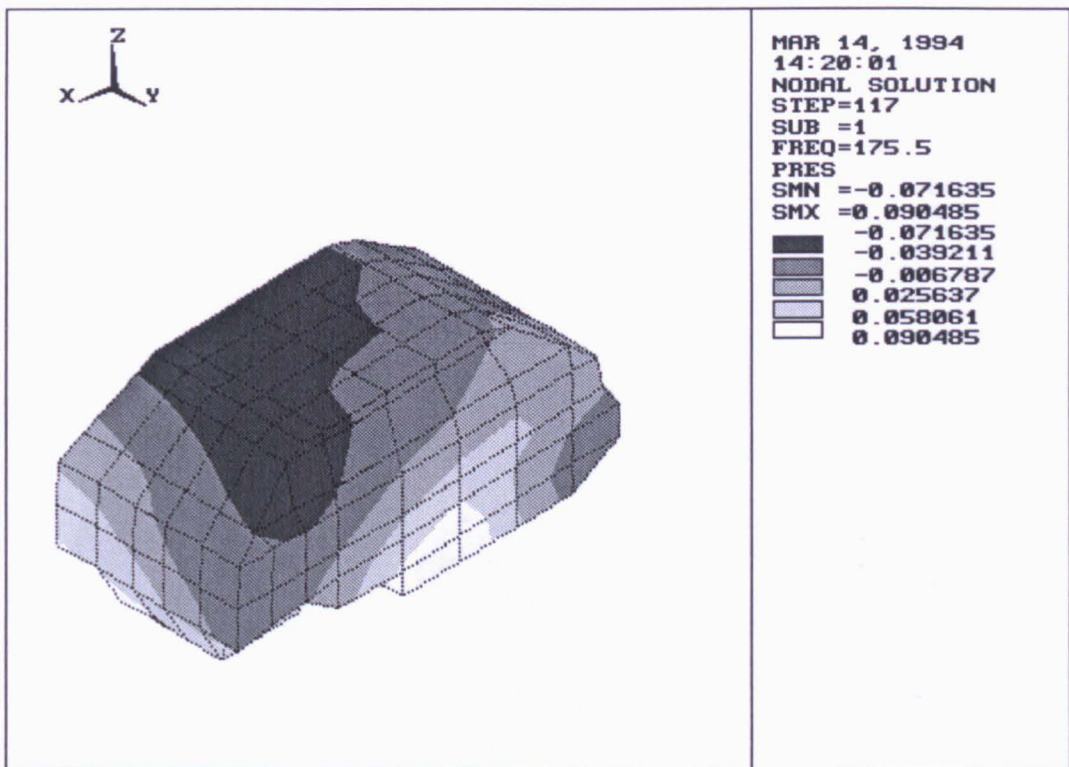




Fig. 8.13 Structurally Induced Acoustic Field at 189 Hz.

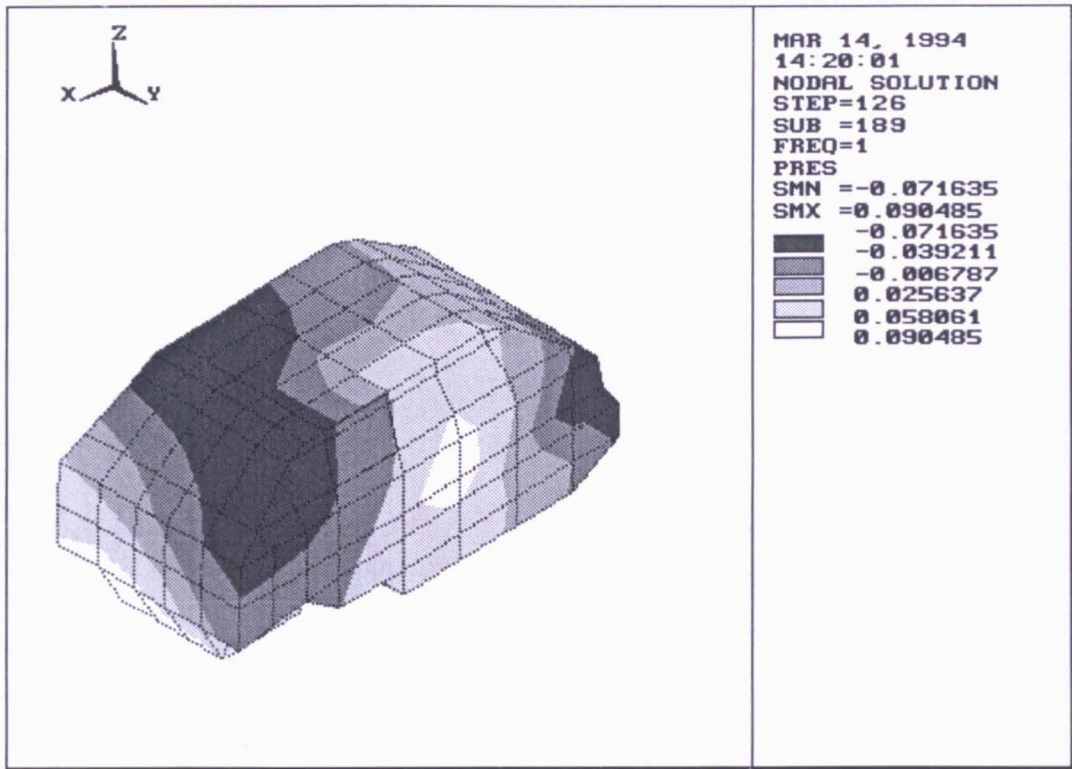
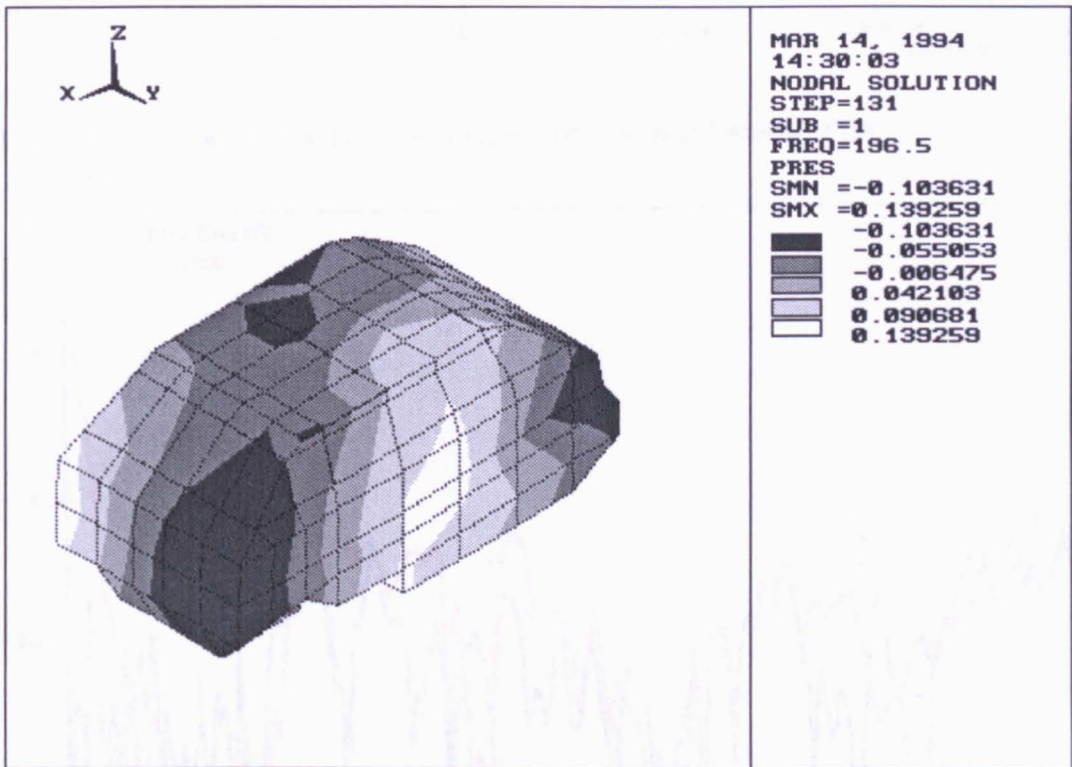


Fig. 8.14 Structurally Induced Acoustic Field at 196.5 Hz.



The following figures compare the experimental and modelled (ANSYS FEA) acoustic response of the cavity to structural excitation at the drivers head location for various states of trim.

Fig. 8.15 Acoustic Response at the Drivers Head Location, Untrimmed -FEA.

Original In Colour

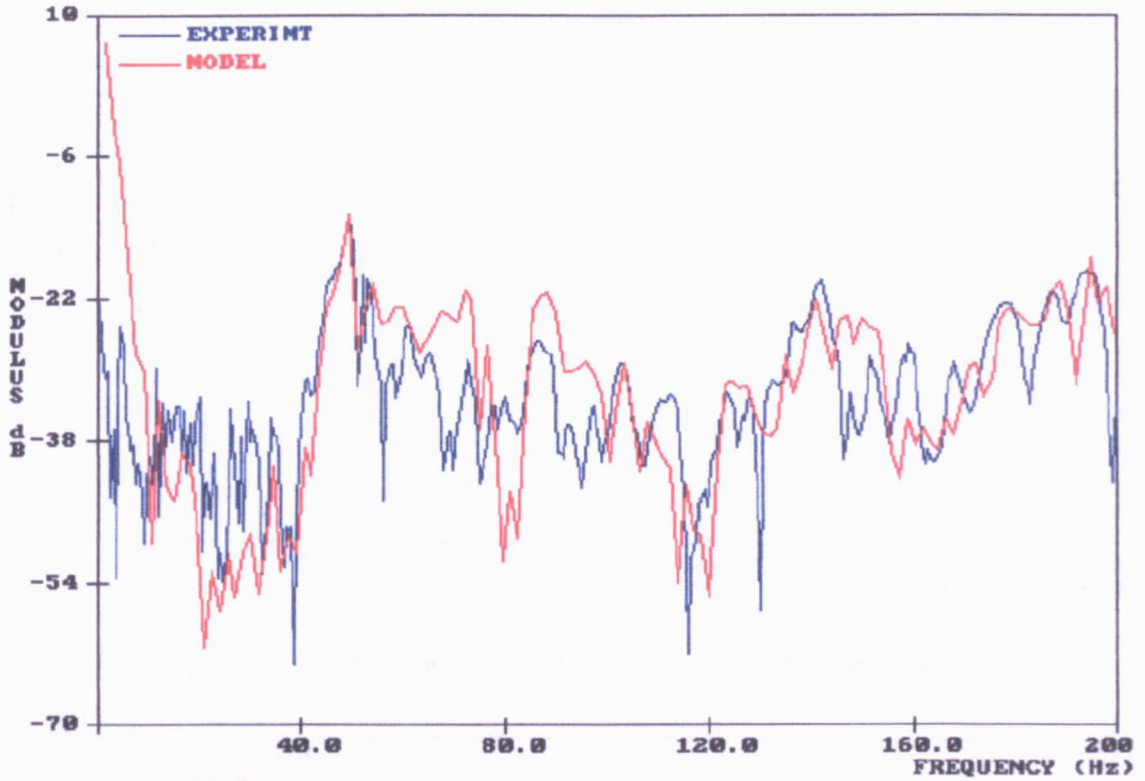


Fig. 8.16 Acoustic Response at the Drivers Head Location with Carpets - FEA.

Original In Colour

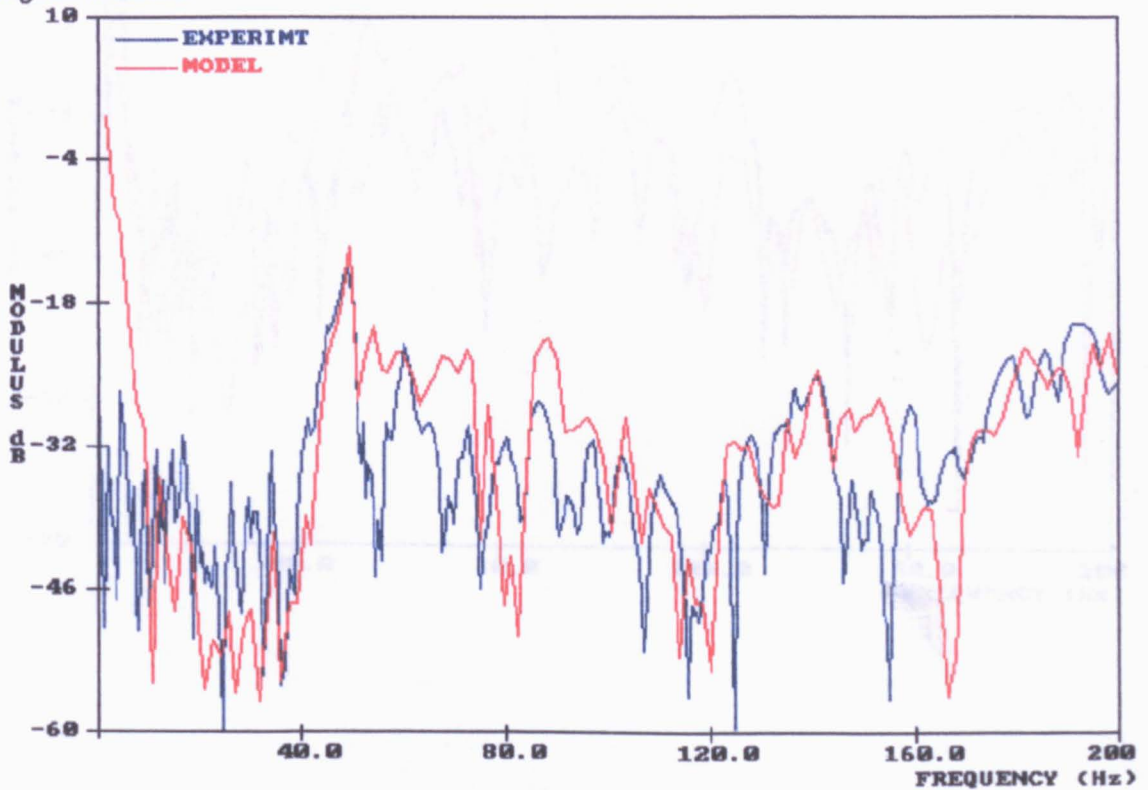


Fig. 8.17 Acoustic Response at the Drivers Head Location with Seats - FEA.

Original In Colour

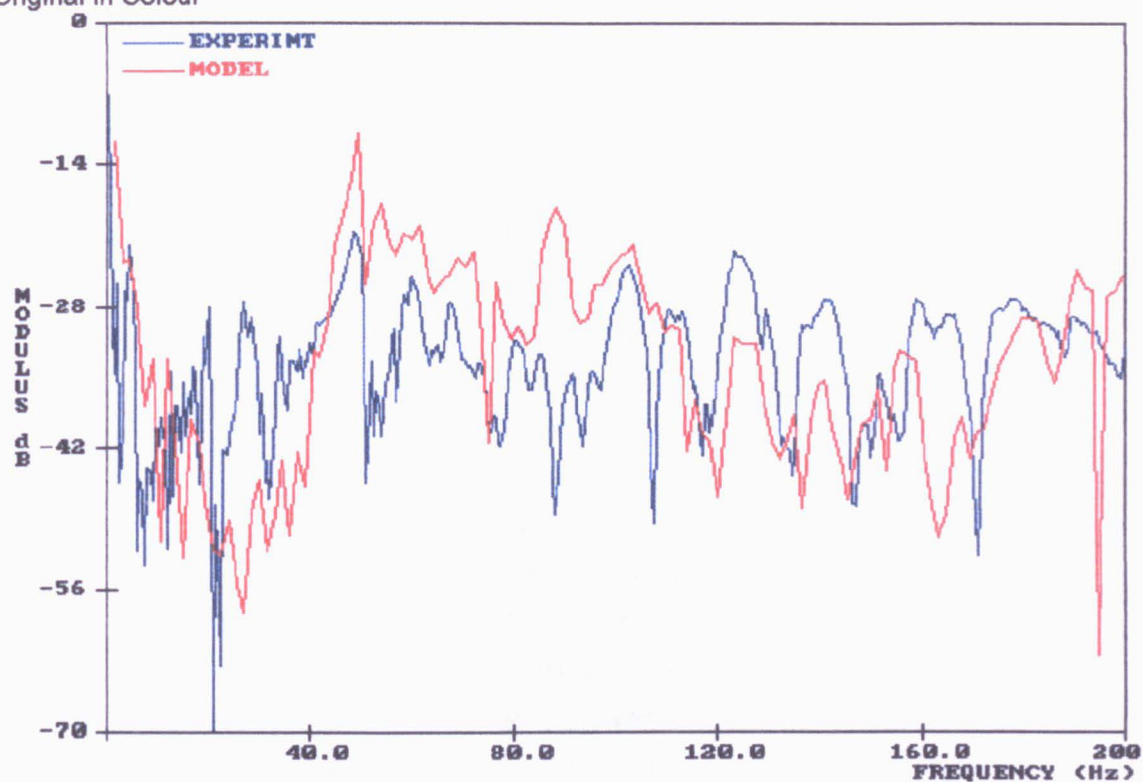
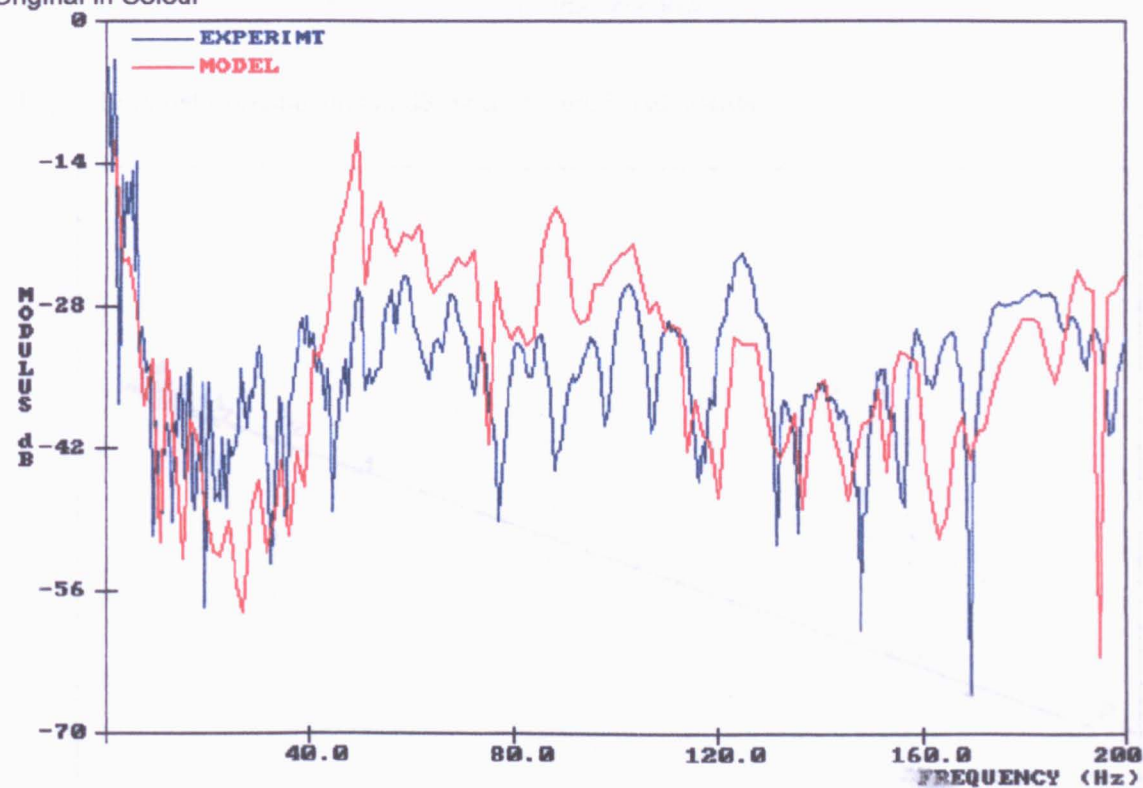


Fig. 8.18 Acoustic Response at the Drivers Head Location with Carpets and Seats - FEA.

Original In Colour



The following figures show polar plots of the individual panel contributions to the total acoustic response, P, at the drivers head location at three frequencies of interest. A key is given below to identify the individual panels from the numbers given on the diagrams.

P	Combined Acoustic Response
1	Roof
2	Front Windscreen
3	Rear Windscreen
4	Back Panel
5	Tyre Well
6	Rear Seat Mount
7	Floor
8	Fire Wall
9	Rh Door Panel
10	Rh Door Window
11	Rh Rear Panel
12	Rh Rear Window
13	Lh Door Panel
14	Lh Door Window
15	Lh Rear Panel
16	Lh Rear Window

Fig. 8.19 Panel Contributions at 33 Hz at Drivers Head Location.

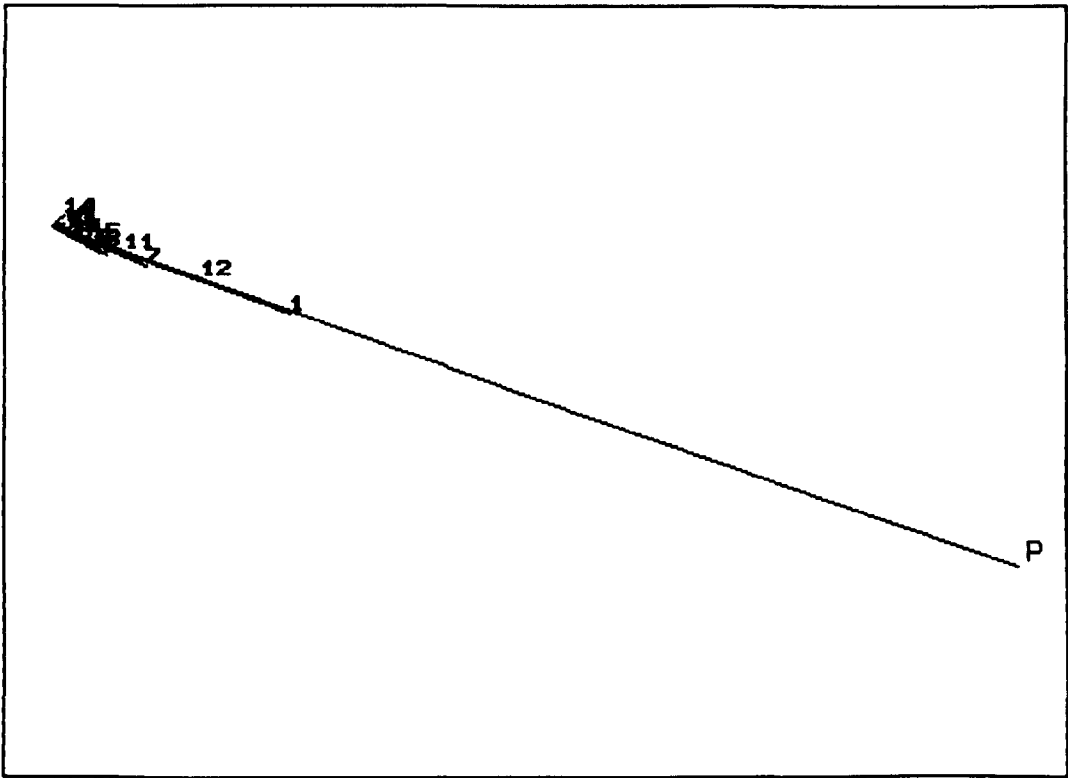


Fig. 8.20 Panel Contributions at 48 Hz at Drivers Head Location.

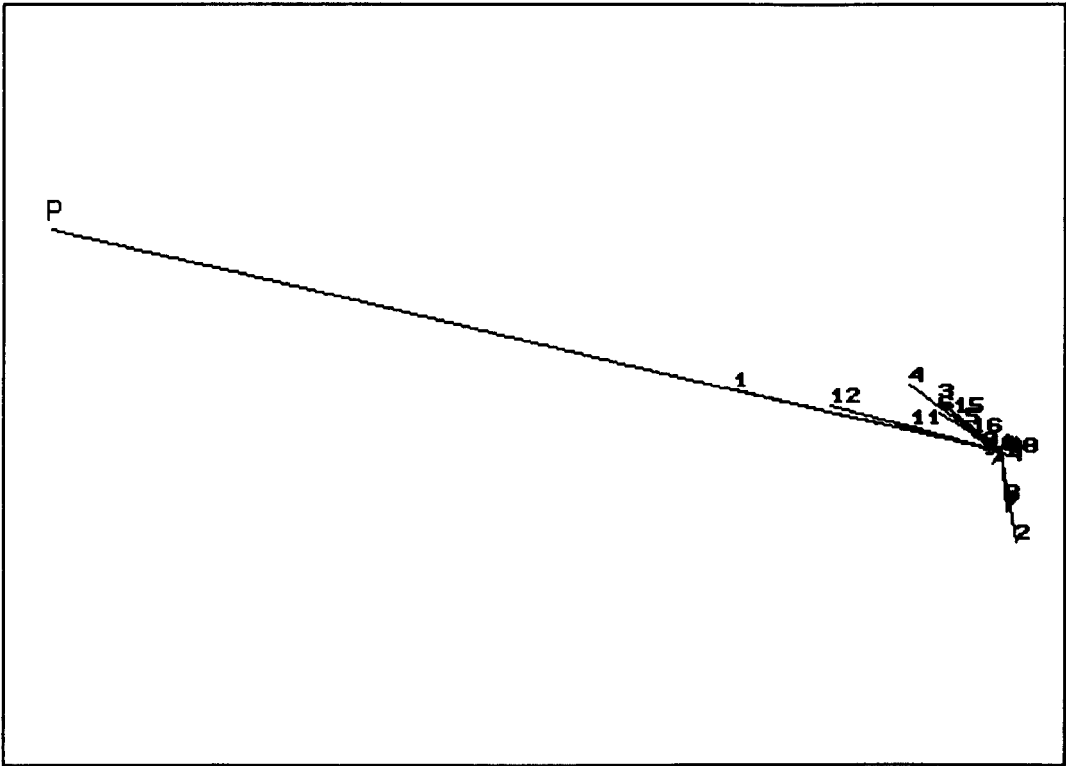


Fig. 8.21 Panel Contributions at 73.5 Hz at Drivers Head Location.

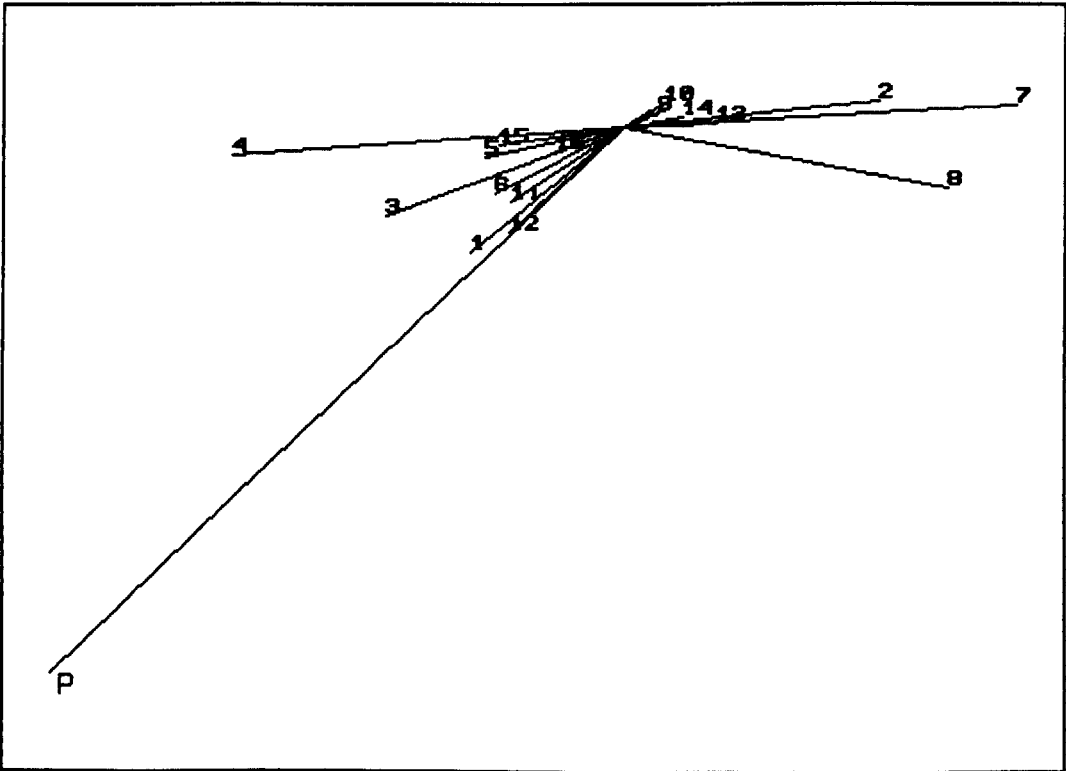




Fig. 8.22 Panel Contributions at 84 Hz at Drivers Head Location.

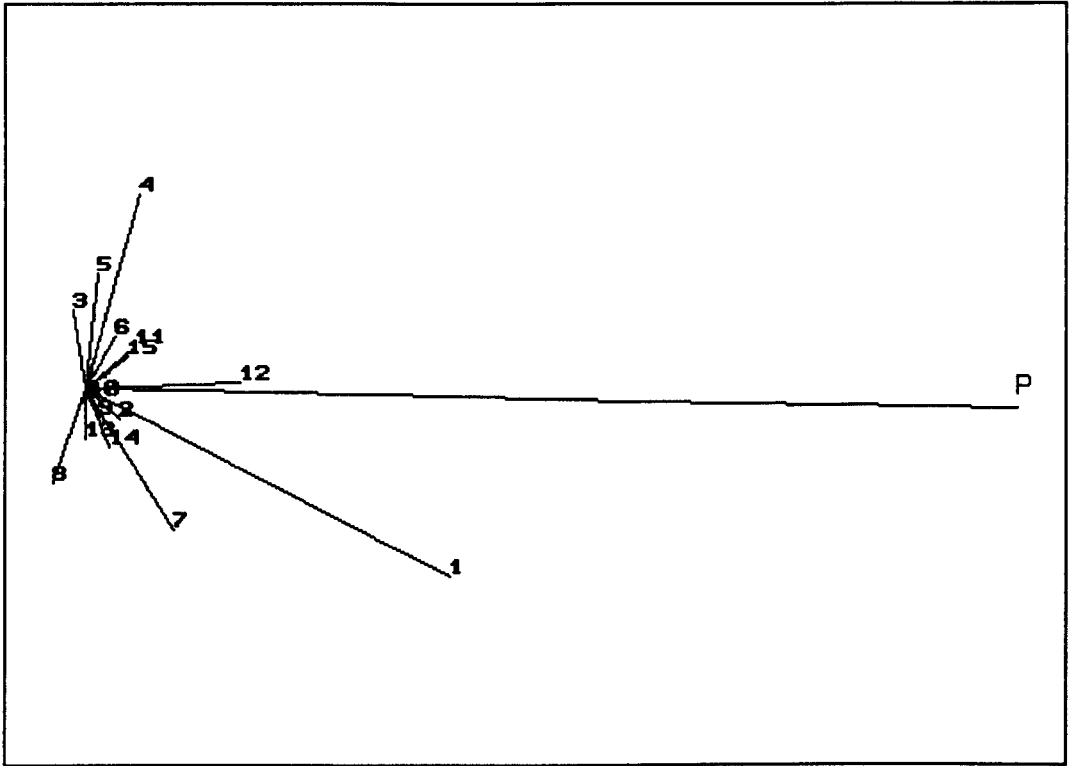


Fig. 8.23 Panel Contributions at 138 Hz at Drivers Head Location.

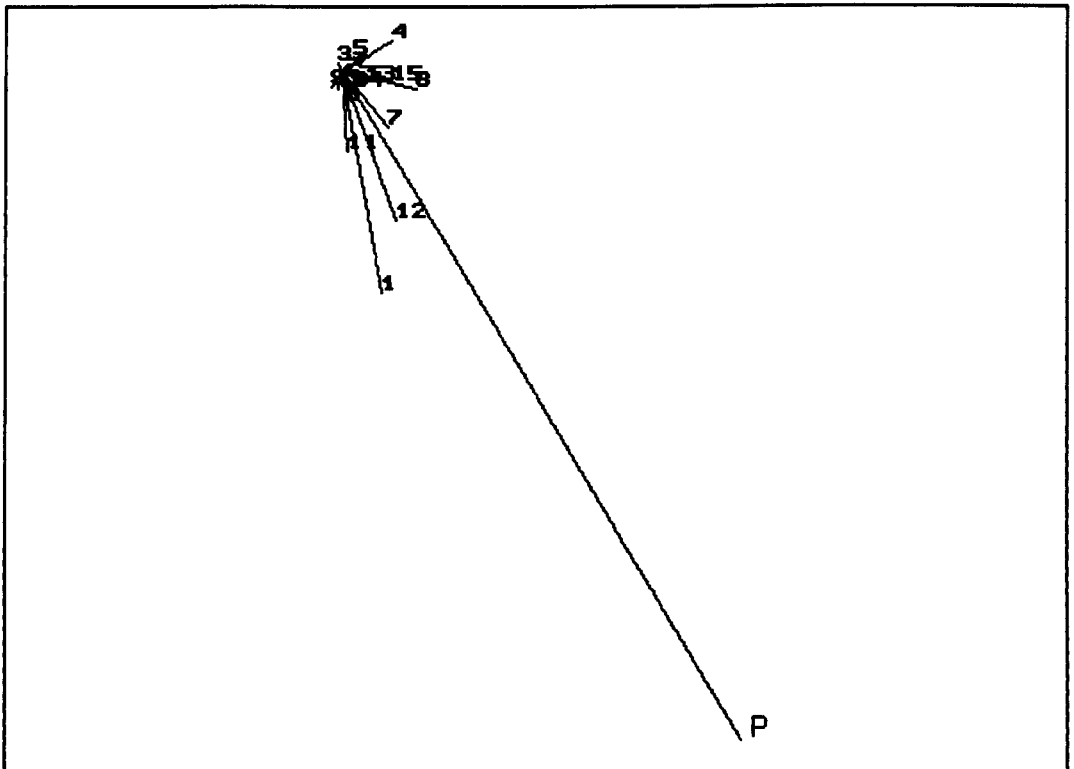


Fig. 8.24 Panel Contributions at 141 Hz at Drivers Head Location.

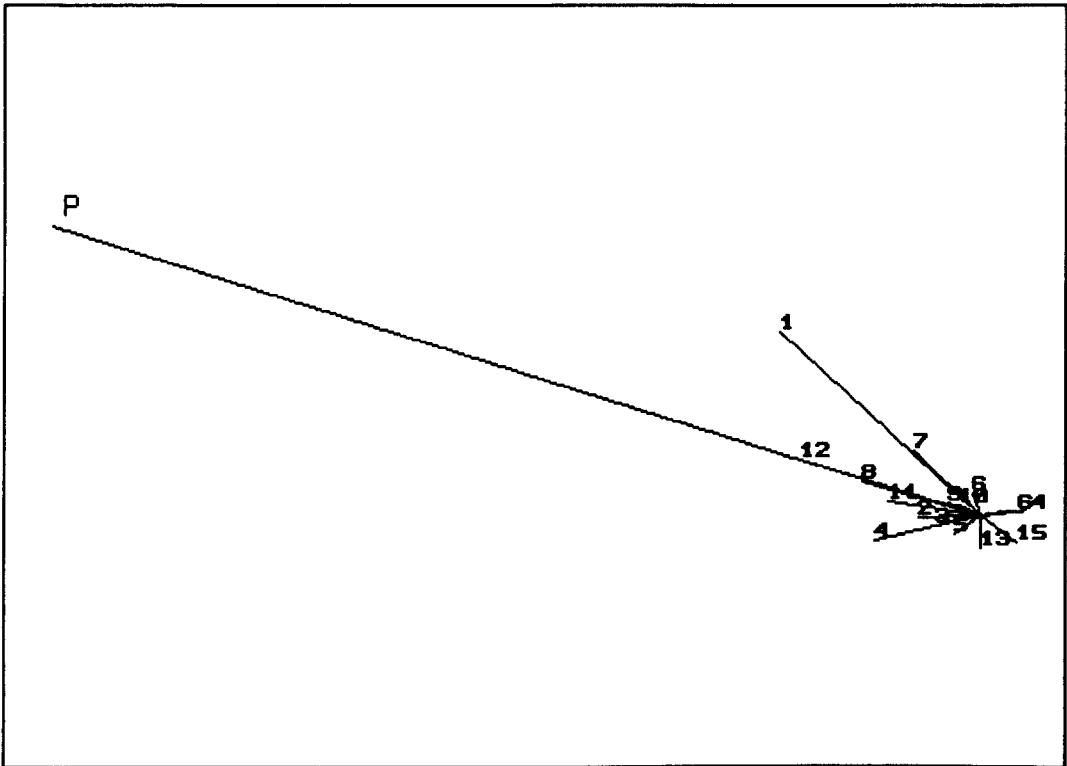


Fig. 8.25 Panel Contributions at 162 Hz at Drivers Head Location.

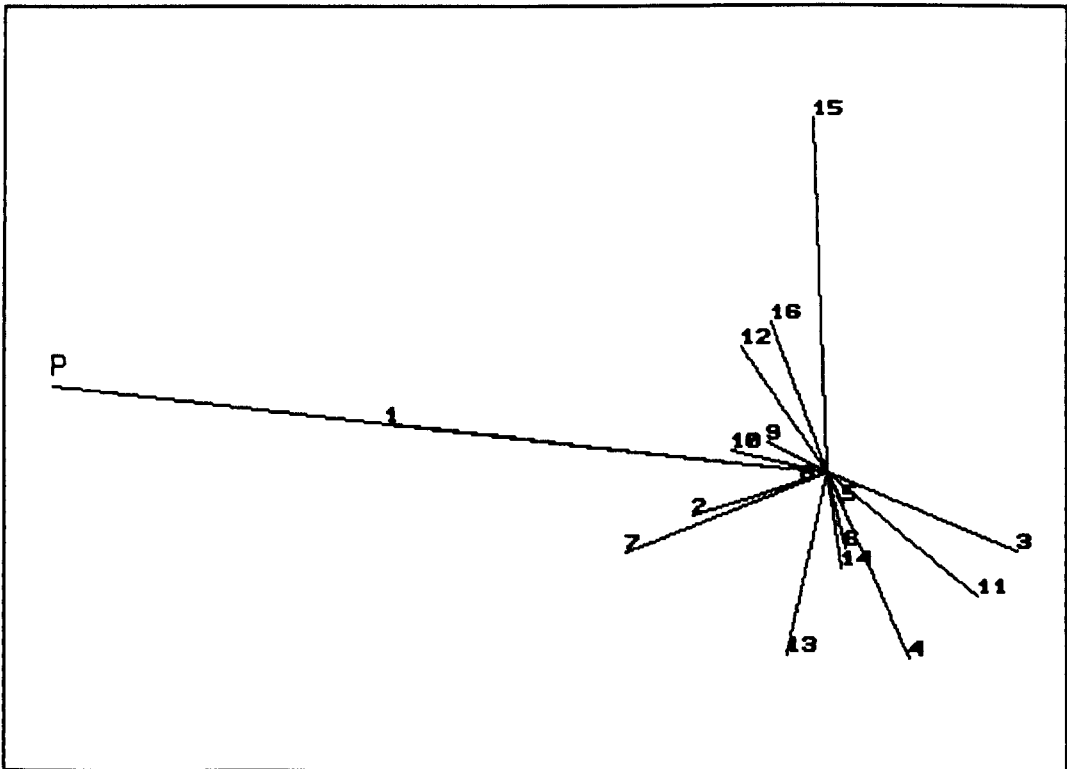


Fig. 8.26 Panel Contributions at 166.5 Hz at Drivers Head Location.

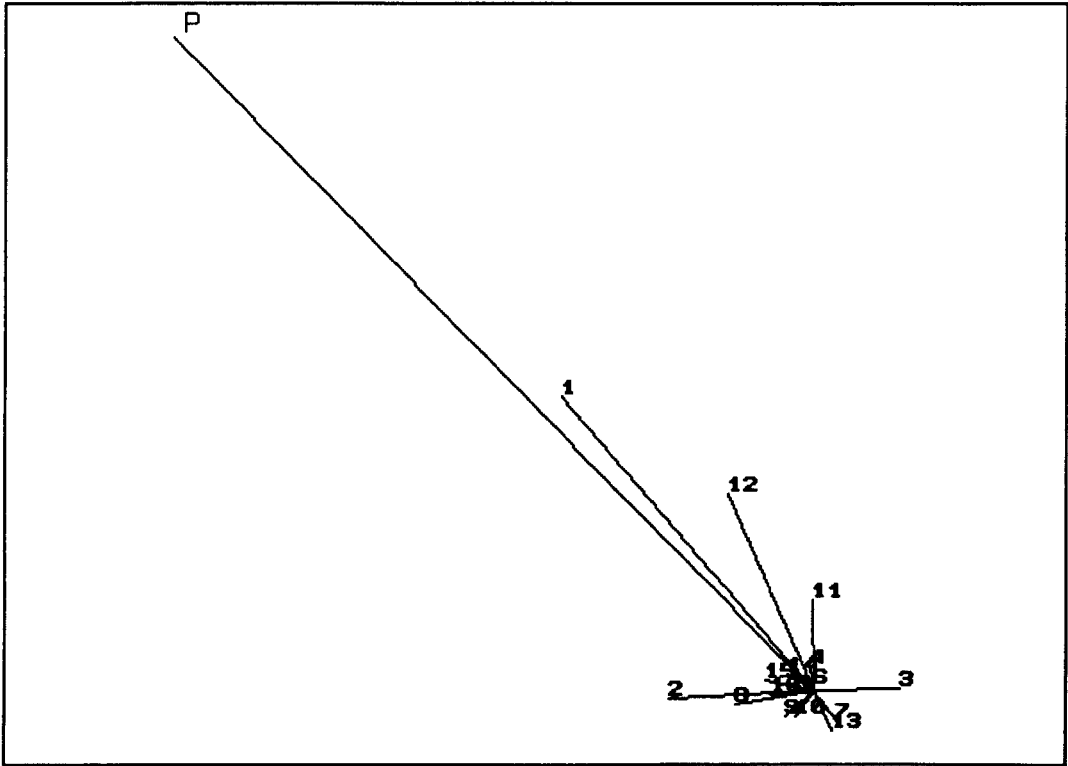
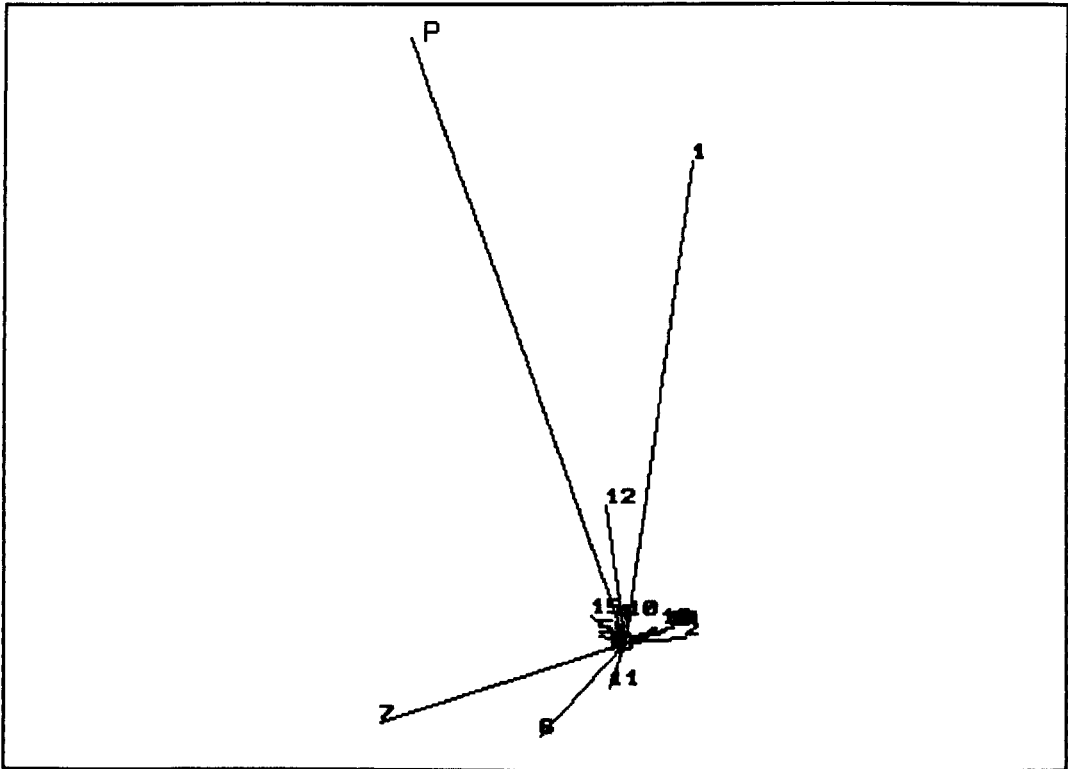
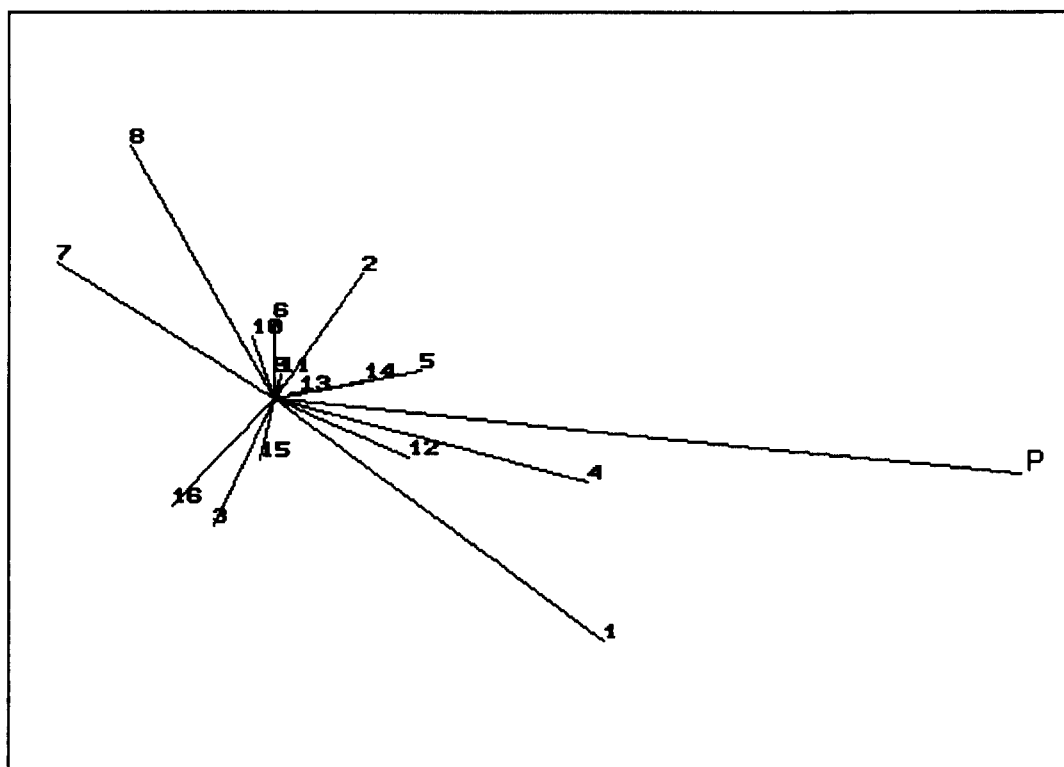


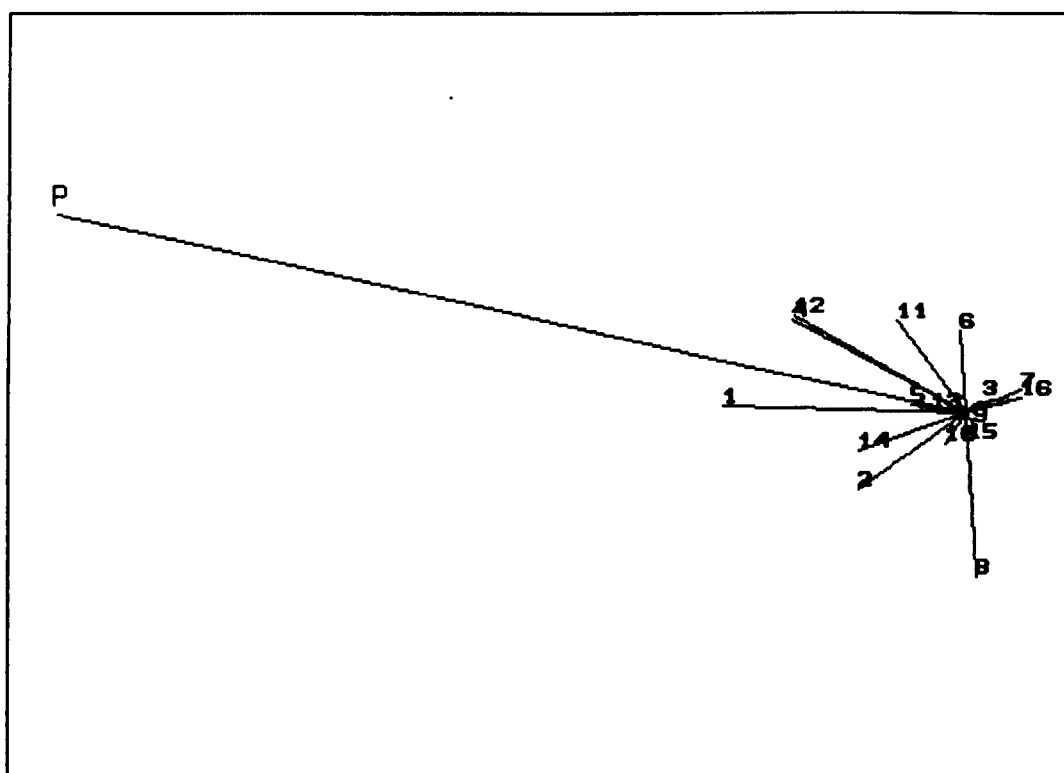
Fig. 8.27 Panel Contributions at 175.5 Hz at Drivers Head Location.



**Fig. 8.28 Panel Contributions at 189 Hz at Drivers Head Location.**



**Fig. 8.29 Panel Contributions at 196.5 Hz at Drivers Head Location.**



#### 8.4 Discussion.

The acoustic field at 33 Hz (figure 8.4) shows the same trend as the experimental results shown in chapter 6 figure 6.18 associated with low frequency structural body modes. The acoustic response at the boundary is small and any acoustic effects are localized.

At 48 Hz (figure 8.5) the modelled acoustic field shows the effect of the front panels acting as a pressure release surface causing an effective first mode similar to that experienced by a pipe with an open end as shown experimentally in figure 6.19 and the panel contribution diagram (figure 8.20).

The results at 73.5 and 84 Hz (figures 8.6 and 8.7) show the effect of the first mode extending over a wide range of frequencies. Again these agree well with the experimental results given in chapter 6 (figures 6.20 and 6.21).

At higher frequencies the effects of modal superposition of closely coupled modes becomes apparent. This is particularly noticeable in the region of the two close modes at 138 Hz (2 0 0 - modelled) and 141 Hz (0 1 0 - modelled). The asymmetry of the acoustic field at 141 Hz causes the one side of the car to be louder than the other at the occupants head locations. The results at higher frequencies also show the influence of close modes but not to the same extent as the previous example.

The four sets of experimental FRFs (figures 8.15 to 8.18) demonstrate the importance of the seats in suppressing noise below 200 Hz. The effect is particularly pronounced in the region from 40 to 100 Hz where the dominant modes ( $\frac{1}{2}$  0 0 and 1 0 0) are the axial modes along the longitudinal axis of the cavity. Thus each mode has a seat near its node (where the particle velocity, hence absorption, is highest) with the backs of the seats normal to the axis of the mode for effective absorption. The mesh density used proved adequate for predicting the major trends of the noise spectra for the untrimmed body but lacked sufficient refinement to adequately predict the effects of the trim items in suppressing low frequency structurally induced noise (below 100 Hz). The main aim of these results has been to show the frequency dependent characteristics of structurally induced interior noise and identify the significant noise generators at each frequency. The degree of refinement used was sufficient to show this. However the results could be improved by using a finer mesh and the study of the relationship between mesh density and accuracy of the results requires further investigation.

The polar plots of panel contributions from the boundary element analysis are for the untrimmed body with no damping. They are included to show the significance of phase considerations in the suppression of interior noise. Figure 8.20 shows the panel contributions at 72.5 Hz (in the region of the first acoustic mode). Panels 2,7 and 8 corresponding to the front windscreen, floor and fire wall respectively act as acoustic sinks at this frequency and any reduction in their amplitude or phase of

vibration will increase the interior noise level. The main contributions come from panels 1, 3, 4, 5, 6, 11 and 12 (see key) associated with the roof, rear and sides of the car. The panel contribution information at low frequencies (figures 8.19 to 8.21) shows the global nature of noise generation in this range with no panel contribution with an amplitude of more than half the interior noise at the drivers head location at any of the three frequencies shown. Also if the panel contribution information is compared to the structural modal data given in figures 6.19 to 6.21 for these frequencies then it is clear than the noise contribution from an individual panel does not relate directly to the amplitude of its vibration.

Time constraints limited the modelling of trim items to the carpets and seats. The other main items to include in any future work are the dashboard, head liner, trim casing and parcel shelf. Of these only the head liner is suitable for modelling as an absorption coefficient. The dashboard is usually a plastic moulding and its main effect is to shift the some of the acoustic natural frequencies of the cavity as it is located at the antinode of the longitudinal axial modes. The parcel shelf and trim casing pose more of a problem as these are panels in their own right. As they are made of fairly reflective materials (trim casing is made from hardboard sheet) their acoustic effects could either be modelled as a measured transmission loss for the whole panel or as an absorption coefficient derived from their structural modal loss factors similar to that used to describe the losses of the untrimmed body.

## **8.5 Conclusion.**

These results show that a relatively coarse mesh can be used for modelling the interior sound field of an untrimmed body and determining the contributions individual panels make to the noise levels experienced by the occupants of the vehicle using experimental structural data. To model the effects of trim items on the acoustic field a more refined model must be used to effectively represent the damping and volumetric effect of trim items. This work is intended for use at the body in white stage of vehicle development and establishes a procedure for the effective analysis of the noise generated by the vibrations of the structure.

## 9 Discussion.

The results of individual sections of work undertaken have been discussed at the end of the relevant chapters. This section is therefore an overall discussion of the project and an attempt to summarise earlier findings.

The work set out in this thesis is not intended to be a definitive discussion of the methods available for the study (and hence control) of structurally induced interior vehicle noise. The aim of the project has been to prove a technique which could be used in this application, and which the Rover Group can therefore develop their own procedures from. One problem is that the requirements of the body refinement process change from model to model, due to variations in funding and time constraints. It was felt that a better understanding of the nature of low frequency structurally induced interior noise, and techniques for its analysis, would be more useful than a highly developed and restrictive procedure.

In general the modelling results shown in chapter 8 would benefit from refinement of the meshes used for both the modal testing and the numerical analyses. Certainly at low frequencies, where the structural ring modes dominate, a two dimensional model such as that used by Richards (1982) could be used to achieve more accurate results without excessive increases in the model size. However at higher frequencies where the sound field becomes asymmetric (130 Hz and above in the Rover Metro), a three dimensional model is required for a full acoustic analysis.

It has been shown that some items of trim are very significant in the reduction of low frequency interior noise. It would be desirable to extend the modelling undertaken to include the remaining major trim items (head liner, dashboard, trim casing and parcel shelf) in order to reduce the likelihood of unnecessary structural modifications. The seats, in particular, play a significant role in the reduction of noise below 120 Hz where the acoustic response is dominated by the longitudinal axial modes.

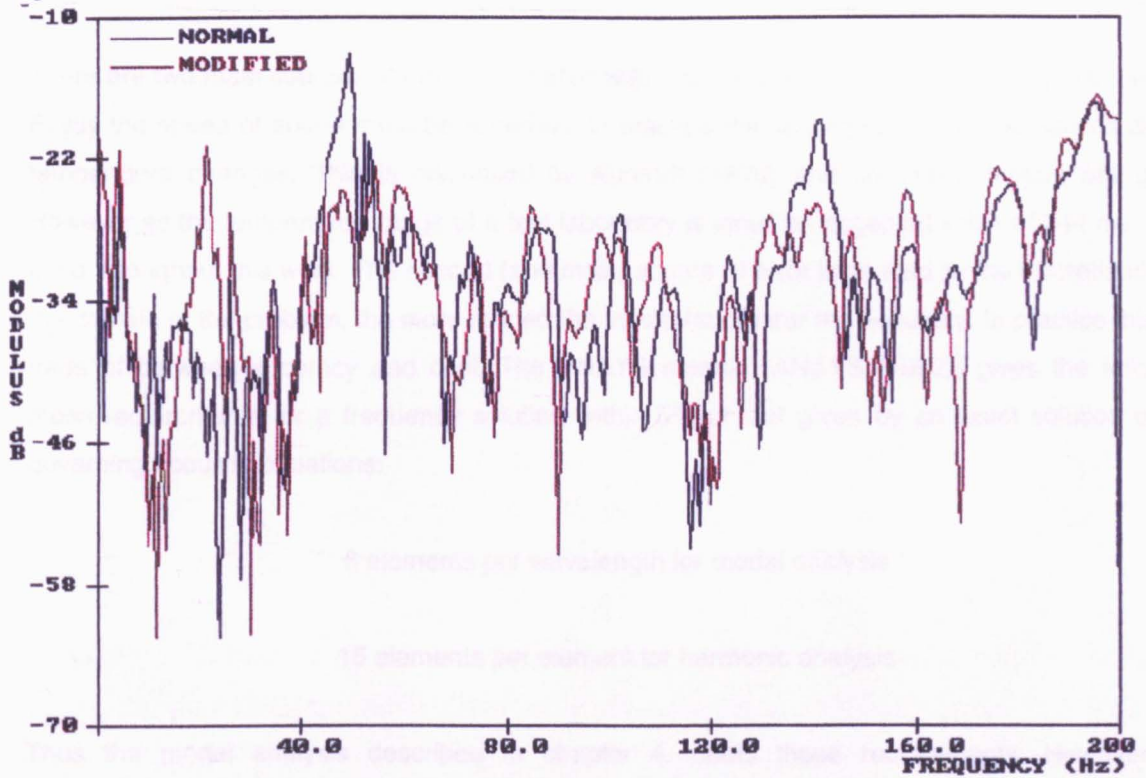
The generation of low frequency interior noise has previously been shown to be due to the ring modes of the structure as identified by Jha (1976), and the major panel modes (Jennequin (1971)), and this has been further verified by the work undertaken here. Thus the reduction of interior noise requires a global rather than local attenuation of the structural vibration in the region of the major ring modes, and localized attenuation of panel vibration above these frequencies.

This work has been limited to the consideration of a single Rover Metro-R6 body. What is not known at present is whether the any of the characteristics described are particular to this model or a characteristic of cars in general. Examples of this debate are the asymmetrical effects where the close 2 0 0 and 0 1 0 modes interact. This characteristic is a feature of the vehicle cavity geometry and is likely to be a feature of most small hatchback cars. However the generation of the  $\frac{1}{2}$  0 0 mode is dependent on the structural modes forming a pressure release surface at the correct frequency. This type of characteristic is more likely to be model dependent and the reduction of the

boom at this frequency can be achieved by structural modification. This is illustrated by considering the pressure transfer functions of the response at the drivers head for an unmodified body, compared with the response for a body with the floor pan weighted with five 10 Kg masses in order to reduce the frequency of the first bending mode of the structure at 49.5 Hz. These response measurements are shown in Fig. 9.1.

Fig. 9.1 Acoustic Response For The Unmodified And Modified Structure.

Original In Colour



The peaks of the acoustic response at 49 and 140 Hz have been significantly reduced by the shift in the natural frequency of the first bending mode of the structure. At higher frequencies, where the response is dominated by acoustic modes which are excited solely by the local panel modes of the structure, there is little change.

Many of the characteristics determined in this work such as the measured absorption coefficients and the equivalent structural modal damping are unlikely to vary much from model to model. If general trends can be established for these factors for particular sizes and styles of body the modelling aspects of this work could be extended. These could be applied to the results of finite element analyses, or to data of dynamic characteristics of the structure at low frequencies, in order to identify problem frequencies and optimize the location of measurement positions before the testing of the actual body has begun.



## 9.1 Errors and Experimental Accuracy

To compare experimental and analytical results it is necessary to understand the sources and magnitude of the errors associated with each. These are discussed below for the finite element and experimental methods.

### 9.1.1 Finite Element

There are two main sources of error associated with analytical work undertaken using this method. Firstly the speed of sound must be specified. In practice this is subject to small variations due to temperature changes. This is discussed by Kuntruff (1979) and correction factors are given. However as the temperature range of a test laboratory is small an accepted value of  $344 \text{ ms}^{-1}$  was used throughout this work. The second (and main) source of error is caused by the discretization of the domain of the problem, the more refined the mesh the greater the accuracy. In practice this is a trade off between accuracy and cost. The ANSYS manual (ANSYS (1992)) gives the following mesh requirements for a frequency solution within 5% of that given by an exact solution of the governing acoustic equations:

6 elements per wavelength for modal analysis

15 elements per element for harmonic analysis

Thus the modal analysis described in chapter 4 meets these requirements. However the requirements for the harmonic analysis described in chapter 8 were considered excessive for a commercial environment. Given that the boundary conditions for the model were described by the measured structural data which in turn defined the solution frequencies the main errors inherent in the finite element aspects of this model would be magnitude dominated. These could be quantified by comparing the results with experimental data of known accuracy.

### 9.1.2 Experimental

All the equipment used in this work was calibrated and as such considered to be of an acceptable accuracy. Analogue devices (such as accelerometers, force transducers and charge amplifiers) used in measuring structural dynamics have minimal errors compared with those encountered in the post processing. The microphones used for the acoustic transfer function measurements are frequency calibrated at the factory. The gain factor was calibrated using a pistophone for single microphone measurements before and after every test session, and the procedure described in chapter five was used for acoustic modal tests. For these tests the frequency difference between the channels of the differential amplifier were found to be less than one degree and the gain was set to give a transfer function of  $1 \pm 0.05$  between any two channels over the frequency range of interest.

The post processing of the time history data involved the calculation of the transfer function and the extraction of the modal properties. The Ono-Sokki analyser produces a 400 line transfer function giving a resolution of 0.25 Hz for a frequency range of 0 to 100 Hz (office) and 0.5 Hz for a frequency range of 0 to 200 Hz (car). The frequency accuracy of the analyser is given as  $\pm 0.01\%$  of its full scale in the manufacturers specification. Thus the frequency accuracy for the two test is 0.01 and 0.02 Hz respectively for the cases mentioned. Thus the main error involved in the determination of the transfer function data can be defined by the resolution of the spectrum. The modal extraction routines overcome this by interpolation between the points on the spectrum. To quantify the accuracy of this procedure the first accoustic mode of the office was extracted using the ICATS software with the method used in the rest of the work. Five runs produced the following natural frequencies of the first mode:

54.21 Hz

54.20 Hz

54.20 Hz

54.22 Hz

54.22 Hz

Mean	54.21 Hz
------	----------

Standard Deviation	8.94E-3 Hz
--------------------	------------

Assuming a Gaussian distribution for these results the range of frequencies can be defined as three times the standard deviation. Thus the modal extraction method has a spread of  $\pm 0.027$  Hz. However it must be borne in mind that this process must be repeated for every mode analysed due to variations in the quality of the FRF data for extraction purposes.

## 10 Conclusion.

The conclusions of individual sections of work undertaken have been given at the ends of most of the relevant chapters. This section is therefore an overall conclusion of the project by considering the four major sections of work outlined in the Introduction.

A finite element model of the car passenger compartment was developed. This predicted the first axial mode to be at 73.4 Hz, with the second axial mode at 138.2 Hz. All other modes including the transverse and the more complex modes occurred above this frequency.

A new experimental technique for the acoustic modal analysis of three dimensional cavities was developed. This involved measuring the pressure response associated with the particle motion along a particular axis, by using a three microphone probe. A finite difference calculation was used to obtain the second derivative of the pressure function, giving an output which exhibited the same nodes and antinodes as the original pressure distribution, and hence information about the directional nature of the pressure mode shapes. The technique was verified by carrying out the acoustic modal analysis of a bare office.

The technique was also shown to be suitable for studying the forced response of a car passenger compartment to structural excitation. From this the nature of the structural excitation of the interior cavity of a car has been shown to match that demonstrated by previous researchers in this field. Notably structural ring modes which are excited by the main structural modes (Jha (1976)), and the higher frequency modes excited by the major panel modes (Jennequin (1971)). In addition, this phase of the work also demonstrated significant acoustic behaviour at frequencies other than those of the acoustic natural frequencies. The most significant of these is at a frequency much lower than that of the first axial mode i.e.49 Hz, where the experimental results clearly show the generation of an acoustic mode. This is due to the structural modes of the car acting as a pressure release surface. This makes the car acoustically analogous to a pipe with one open and one closed end.

Experimental equipment was developed for the measurement of the acoustic absorption coefficient of trim materials. This used an impedance tube, two microphones and a dual channel FFT analyser. Measurements were taken for seat foam, carpet with foam underlay, carpet with felt underlay, and for rear seat back covering.

A finite element model was developed to model the response of the car acoustic cavity to structural excitation. The vibration of the surface of the acoustic boundary was obtained by taking experimental frequency response functions over the surface of the vehicle when being driven by structural excitation. These functions were then applied to the boundary of the finite element model of the cavity as a forcing function. Both an untrimmed and a trimmed body were modelled. The losses for the untrimmed body were modelled by using the measured structural modal loss factors to define the boundary absorption coefficient as a frequency dependent property. The resulting

FRFs were compared with those obtained experimentally, and these gave reasonable agreement. The results also showed the important effects of the seats in suppressing noise below 200 Hz. This demonstrated the usefulness of this technique in modelling the effects of trim items on the acoustic response of the passenger compartment, and it shows the feasibility of using structural vibration data to predict the need for noise control measures in the early stages of body development.

In addition some work was carried out using the boundary element method with the modelled data which had been obtained. This allowed the significance of individual panels in the generation of a cavity boom to be assessed. From this the most effective areas for structural modification for control of low frequency interior noise could be decided upon.

In conclusion, the work has developed an experimental method for determining the three dimensional acoustic mode shapes of cavities. This was used in order to verify the effects of structural-acoustic interaction in the car passenger compartment which had already been demonstrated by other researchers. In addition, acoustic behaviour at frequencies other than those of the acoustic modes was investigated. An experimental set-up using an impedance tube was developed for the measurement of the acoustic absorption coefficients of trim materials. These values were then used within a finite element model of the cavity which was forced using experimental FRFs obtained using structural excitation. The experimental and modelling methods presented in the work are complimentary but require only structural and acoustic FRF data and measured absorption coefficients to carry out all the procedures described in this thesis.

## **11 References.**

**Allard J.F. Sieben B. (1985)**

**'Measurements of Acoustic Impedance in a Free Field with Two Microphones and a Spectrum Analyser.'**

**Journal of the Acoustical Society of America 77(4) April 1985 pp 1617-1618**

**ANSYS (1992)**

**'The ANSYS Users Manual for Revision 5.0.'**

**Swanson analysis Systems (SASI)**

**P.O. Box 65**

**Johnson Road**

**Houston**

**Pa 15342-0065**

**ASTM (1986)**

**'Standard Test Method for Impedance and Absorption of Acoustical Materials Using a Tube, Two Microphones, and a Digital Frequency Analysis System.'**

**E 1050 - 86**

**ASTM (1990)**

**'Standard Test Method for Impedance and Absorption of Acoustical Materials by the Impedance Tube Method.'**

**C 384 - 90a**

**Biering H.B. (1)**

**'Measurement of Loud Speaker Performance Using Dual Channel FFT Analysis.'**

**Bruel & Kjør Application Notes**

**2850 Nørum**

**Denmark**

**Bruel & Kjør (1986)**

**'Sound Intensity.'**

**2850 Nørum**

**Denmark**

**Bryne K.P. (1985)**

**'The Use of Acoustic Pressure Measurements to Determine the Particle Motions Associated with the Low Order Acoustic Modes in Enclosures.'**

**Journal of the Acoustical Society of America 77(2) February 1985 pp 739-746**

Chung J.Y. Blaser D.A. (1980)

'Transfer Function Method of Measuring In-duct Acoustic Properties.

I. Theory

II. Experiment

Journal of the Acoustical Society of America 68(3) Sept 1980 pp 907-921

Craggs A. (1972)

'The use of Simple Three-Dimensional Acoustic Finite Elements for Determining the Natural Modes and Frequencies of Complex Shaped Enclosures.'

Journal of Sound and Vibration (1972) 23 (3) pp 331-339

Craggs A. Burna C.J. (1989)

'The Effect of an Absorbent Lining on the Natural Frequencies and Modal Damping Factors of a Small Room.'

Applied Acoustics. 28 (1989) pp 229-239

Craggs (1986)

'A Finite Element Model for Acoustically Lined Small Rooms.'

Journal of Sound and Vibration (1986) 108(2) 327-337

Elliott S.J. (1981)

'A Simple Two Microphone Method of Measuring Absorption Coefficient.'

Acoustics Letters Vol. 5 No. 2 1981 pp39-44

Ewins D.J. (1986)

'Modal Testing: Theory and Practice.'

Research Studies Press Ltd, Somerset

Fahy F.J. (1984)

'Rapid Method for the Measurement of Sample Acoustic Impedance in a Standing Wave Tube.'

Journal of Sound and Vibration (1984) 97(1) pp 168-170

Fillod R. Lallement G. Piranda J. Raynaud J.L. (1985)

'Global Method of Identification.'

Proceedings of the 3<sup>rd</sup> Modal Analysis Conference (IMAC) Orlando Florida 1985

Vol 2 pp 1145-1151

Franco L. (1991)

'Low Frequency Noise Control in Car Cabin by Means of the Luggage Compartment Resonator.'

Applied Acoustics 32 (1991) pp 23-34

Højberg K. (1991)

'A New Two-Microphone Impedance Tube with Improved Microphone Design for Materials Testing.'  
SAE Paper 911091

ICATS (1993)

'ICATS Reference Manual (ver 3.8D)'

Imperial College, Analysis, Testing And Software.'

Imperial College Of Science, Technology And Medicine

Mechanical Engineering Department

Exhibition Road

London SW7 2BX

Jennequin G. (1971)

'Is the Computation of Noise Level Inside a Car Feasible.'

Proceedings of the Institute of Mechanical Engineers: Symposium on Vibration and Noise in Motor Vehicles.

London, July 1971

Paper No. C108/71 pp 132-137

Jha S.K. (1976)

'Characteristics and Sources of Noise and Vibration and Their Control in Motor Cars.'

Journal of Sound and Vibration. (1976) 47(4) pp 543-558

Jha S.K. Cheilas N. (1977)

'Acoustic Characteristics of a Car Cavity and Estimation of Interior Sound Field Produced by Vibrating Panel.'

ASME Publications. October 1977

Kojic M. Petronijevic Z. Manojlovic V. (1984)

'Influence of Car Body Constructive Parameters on Acoustic Characteristics of Car Cavity.'

International Journal of Vehicle Design Vol. 5 No 6 1984 pp 704-720

Knittel J.D. Oswald L.J. (1987)

'An Experimental Technique for Acoustic Modal Analysis in Three Dimensional Cavities.'

SAE Paper 870974

Kung C. Singh R. (1985)

'Experimental Modal Analysis Technique for Three Dimensional Acoustic Cavities.'

Journal Of The Acoustical Society Of America. 77(2) February 1985 pp 731-738

Kuntruff H. (1979)

'Room Acoustics 2<sup>nd</sup> edition.'

pp 227-231

Applied Science Publishers

Microsoft (1992)

'Excel Spreadsheet Manual'

Microsoft Corporation

One Microsoft Way

Redmond

WA 98052-6399

USA

Nefske D.J. Howell L.J. (1978)

'Automobile Interior Noise Reduction Using Finite Elements.'

SAE Paper 780365

Nefske D.J. Wolf J.A. Howell L.J. (1982)

'Structural-Acoustic Finite Element Analysis of the automobile Passenger Compartment a Review of Current Practice.'

Journal of Sound and Vibration. (1982) 80(2) pp 247-266

Nefske D.J. Sung S.H. (1985)

'Vehicle Interior Acoustic Design Using Finite Element Methods.'

International Journal of Vehicle Design. Vol 6 No 1 pp 24-31

Nieter J.J Singh R. (1982)

'Acoustic Modal Analysis Experiment.'

Journal of the Acoustical Society of America. 72(2) August 1982 pp 319-326

Petyt M. Lea J. Koopman G.H. (1976)

'A Finite Element Method for Determining the acoustic Modes of Irregular Shaped Cavities.'

Journal of Sound and Vibration. (1976) 45(4) pp 495-502

Powell J.G. Van Houten J.J. (1970)

'A Tone Burst Technique of Sound-Absorption Measurement.'

Journal of the Acoustical Society of America Vol 48 No. Pt. 1 pp1299-1303

Powers W.R. Rudinoff C.D. (1975)

'The Noise Box Test: A Novel Method for Evaluating Sound Absorbers.'

SAE Paper 750777



Richards T.L. (1982)

'The Reduction of Structural Acoustic Coupling in Car Bodies.'

Ph.D Thesis

Cranfield Institute of Technology, School of Automotive Engineering, April 1982

Richards T.L. Jha S.K. (1979)

'A Simplified Finite Element Method for Studying Acoustic Characteristics Inside a Car Cavity.'

Journal of Sound and Vibration. (1979) 63(1) pp 61-72

Saha P. Davis C.W. (1982)

'Developing a Small Sample Facility for Testing Automotive Acoustical Materials at Low Frequencies.'

SAE Paper 820755

Shippen J.M. Dunn J.W. (1988)

'A Finite Element Technique for Acoustic Analysis of Car Body Structures at the Conceptual Design Stage.'

Proceedings ISATA '88 Vol 1 Paper 88043

Shippen J.M. Dunn J.W. (1991)

'Selective Elasto-Acoustic Modal Synthesis by Orthogonality Criteria Applied to Vehicle Structures.'

International Journal of Vehicle Design. Vol 12 No 2 1991 pp 208-216

Shuku T. Ishihara K. (1973)

'The Analysis of The Acoustic Field in Irregularly Shaped Rooms by the Finite Element Method.'

Journal of Sound and Vibration. (1973) 29(1) pp 67-76

Smiley R.G. Wey Y.S. Hogg K.D. (1984)

'A Simplified Frequency Domain MDOF Curve-Fitting Process.'

Proceedings Of the 2<sup>nd</sup> Modal Analysis Conference (IMAC) Orlando Florida 1984  
vol. 1 pp 432-436

Smith D.L. (1976)

'Experimental Techniques for the Acoustic Modal Analysis of Cavities.'

Internoise 76. Washington D.C. April 1976 pp 129-132

Succi G.P. (1987)

'The Interior Field of an Automobile Cabin.'

Journal of the Acoustical Society of America. 81(6) June 87 pp 1688-1694

- Sung M.H. Kang Y.J. Lee J.M. Kim S.H. Kim J.H. Jung S.G. (1991)  
 'A Study on the Interior Noise-Reduction of a Passenger Car.'  
 Proceedings of the International Modal Analysis Conference IMAC vol 2 pp 956-961  
 Florence Italy April 1991
- Sung S.H. Nefske D.J. (1984)  
 'A Coupled Structural-Acoustic Finite Element Model for Vehicle Interior Noise analysis.'  
 Transactions of the ASME. Vol 106, April 1984 pp 314-318
- Suzuki S. Maruyama S. Ido H. (1989)  
 'Boundary Element Analysis of Cavity Noise Problems with Complicated Boundary Conditions.'  
 Journal of Sound and Vibration (1989) 130(1) pp 79-91
- Swenson G.W. (1993)  
 'A Standing Wave Facility for Low-Frequency Impedance/Absorption Measurement.'  
 Applied Acoustics 40 (1993) pp 355-362
- Synnoise (1993)  
 'Synnoise Users Manual.'  
 Numerical Integration Technologies N.V. (NIT)  
 Ambachtenlaan 29,b-3001  
 Leuven  
 Belgium
- Wood L.A. Joachim C.A. (1984)  
 'Variability of Interior Noise Levels in Passenger Cars.'  
 Proceedings of The Conference on Vehicle Noise and Vibration  
 The Institution of Mechanical Engineers, London, 1984 pp 197-206
- Wood L.A. Joachim C.A. (1986)  
 'Scatter of Structure Borne Noise in Four Cylinder Motor Vehicles.'  
 SAE Paper 860431
- Yashiro H. Suzuki K. Kajio Y. Hagiwara I. Arai A. (1985)  
 'An Application of Structural-Acoustic Analysis to Car Body Structure.'  
 SAE Paper 850961
- Yuzawa M. (1975)  
 'A Method of Obtaining the Oblique Incident Sound Absorption Coefficient Through an on-the-Spot Measurement.'  
 Applied Acoustics (8) 1975 pp 27-41

Zienkiewicz O.C. And Newton R.E. (1969)

'Coupled Vibrations of a Structure Submerged in a Compressible Fluid.'

International Symposium on Finite Element Techniques.

Stuttgart 1969

Zienkiewicz & Taylor (1989)

The Finite Element Method 4<sup>th</sup> edition.

McGraw-Hill (1989)

## **12 Bibliography.**

**Acoustics for Engineers.**

**Turner and Pretlow**

**Macmillan (1991)**

**Applied Mechanical Vibrations.**

**D.V. Hutton**

**McGraw-Hill (1981)**

**Elements of Vibration Analysis.**

**L. Meirovitch**

**McGraw-Hill (1975)**

**Introduction to Acoustics.**

**R.D. Ford**

**Elsevier (1970)**

**Noise Control Engineering.**

**Bies and Hansen**

**Unwin Hyman (1988)**

**Sound Intensity.**

**F.J. Fahy**

**Elsevier Applied Science (1989)**

**The Finite Element Method 4<sup>th</sup> edition.**

**Zienkiewicz and Taylor**

**Mcgraw-Hill (1989)**

**The Finite Element Method: Principles and Applications.**

**Lewis and Ward**

**Addison-Wesley Publishing Company (1991)**

**Vibration and Sound 2<sup>nd</sup> edition.**

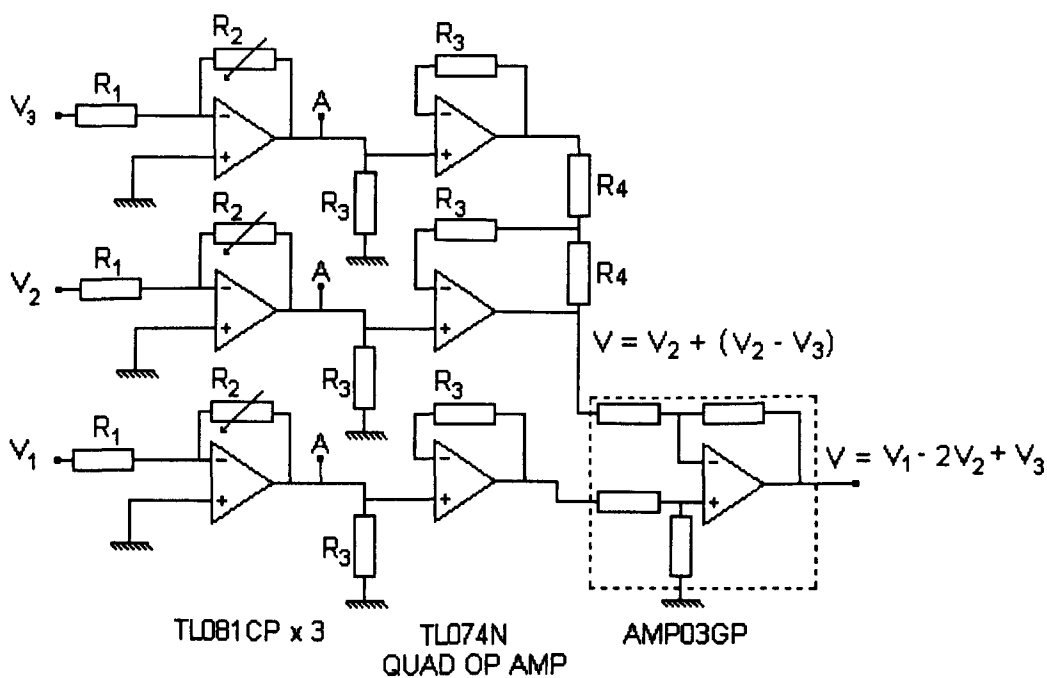
**P.M. Morse**

**Mcgraw-Hill (1948)**

## **Appendix 1: ANSYS Batch For Extracting The Acoustic Modes Of A Rover Metro.**

```
/BATCH
/COM ANSYS BATCH FILE FOR BUILDING MODEL FOR MODAL ANALYSIS
/COM OF ROVER METRO PASSENGER COMPARTMENT ACOUSTICS
/COM DEFINE TITLE
    /TITLE,METRO-R6 ACOUSTIC MODES
/COM ENTER PREPROCESSOR
    /PREP7
/COM DEFINE ELEMENT TYPE AND MATERIAL PROPERTIES
    ET,1,30,,1
    MP,DENS,1,1.2
    MP,SONC,1,344
/COM DEFINE NODES DIRECTLY
    N,1,1.5467,0.1,-2.33E-02
    N,2,0.1986,0.1,3.48E-02
    N,3,1.3541,0.1,-1.50E-02
    .
    .
/COM DEFINE ELEMENTS DIRECTLY
    E,751,800,801,759,694,802,803,703
    E,694,802,803,703,719,805,807,727
    .
    .
/COM SAVE DATABASE
    SAVE
/COM EXIT PREPROCESSOR
    FINISH
/COM EXTRACT AND EXPAND FIRST 8 MODES
/COM ENTER SOLUTION PHASE
    /SOLU
/COM SPECIFY MODAL ANALYSIS
    ANTYPE,MODA
/COM SUBSPACE SOLVER EXTRACT 8 MODES
    MODOPT,SUBSP,8,,,,ON
/COM DEFINE PRESSURE MASTERS AT ALL NODES
    M,ALL,PRES
    SOLVE
/COM EXIT SOLVER
    FINISH
/COM EXPANSION PASS ENTER SOLVER
    /SOLU
/COM DEFINE EXPANSION PASS
    EXPASS,ON
/COM EXPAND 8 MODES
    MXPAND,8
    SOLVE
/COM EXIT SOLVER
    FINISH
/COM EXIT ANSYS
    /EXIT
```

**Appendix 2: Analogue Differential Amplifier Circuit.**



**Key:**

- R<sub>1</sub> - 0.4 MΩ Resistor
- R<sub>2</sub> - 0-1 MΩ Variable Resistor
- R<sub>3</sub> - 1 MΩ Resistor
- R<sub>4</sub> - 10 KΩ (1%) Resistor
- A - Probe connection point for channel calibration.

### Appendix 3: ANSYS Batch File For A Harmonic Analysis Of A Rover Metro.

The structure of the ANSYS batch file for the harmonic analysis of the bare Metro acoustics is given below followed by the structure of RDT1.MAC the FRF data reading macro. RDT2.MAC has a similar structure and is used to fill table 2.

```
/BATCH
/COM ANSY SBATCH FILE FOR HARMONIC ANALYSIS OF ROVER METRO ACOUSTICS
/COM RECEPTANCE FRF DATA USED AS ABOUNDARY CONDITION
/COM INERTANCE FRF DATA REQUIRED IN ICATS FORMAT CONVERTED TO
/COM RECEPTANCE BY ANSYS
/COM USED IN CONJUNCTION WITH RDT1.MAC AND RDT2.MAC
/COM USE JOB NAME MET
/COM ANSYS 5.0 VERSION
/COM UNTRIMMED BODY ONLY
/COM
      /TITLE,METRO-R6
/COM ENTER PREPROCESSOR
      /PREP7
/COM DEFINE ELEMENT TYPE AND MATERIAL PROPERTIES
/COM TYPE 1 EXTERIOR, 2 INTERIOR
      ET,1,FLUID30
      ET,2,FLUID30,,1
      MP,DENS,1,1.2
      MP,SONC,1,344
      MP,MU,1,0
/COM DEFINE NODES DIRECTLY
      N,9,1.5467,0.1,3.54E-02,
      N,12,1.1615,0.1,5.20E-02,
      N,14,0.77636,0.1,6.86E-02,
      .
      .
/COM DEFINE ELEMEMENTS DIRECTLY
      E,603,636,638,605,597,631,633,599
      E,605,638,569,557,599,633,567,555
      .
      .
      TYPE,2
      E,.....
      .
      .
/COM SAVE DATA BASE
      SAVE
/COM EXIT PREP7
      FINISH
/COM ENTER SOLUTION PHASE
      /SOLU
/COM SETUP ANALYSIS TYPE
/COM FULL HARMONIC,STEPPED LOADS, REAL IMAGINARY RESULTS
      ANTYPE,HARM
      HROPT,FULL
      HROUT,ON
      KBC,1
/COM SET ALL DISP DOF TO 0
      D,ALL,UX,0
      D,ALL,UY,0
      D,ALL,UZ,0
/COM DIMENSION THREE DATA ARRAYS FORCOMPLEX FRFDATA STOREDAS
/COM RECEPTANCE ANDMATERIAL PROPERTIES
/COM DEFINE ARRAYS
      *DIM,T1,,133,254
      *DIM,T2,,133,254
      *DIM,T3,,133,1
/COM FILL FIRST COLUMN OF EACH WITH FREQUENCY DATA
```

```

/COM AND CALCULATE W SQUARED
  *VFILL,T1(1,1),RAMP,1.5,1.5
  *VFILL,T2(1,1),RAMP,1.5,1.5
/COM FILL COLUMN 254 WITH 2PI
  *VFILL,T1(1,254),RAMP,6.28318
  *VFILL,T2(1,254),RAMP,6.28318
/COM W=2*PI*F
  *VOPER,T1(1,254),T1(1,1),MULT,T1(1,254)
  *VOPER,T2(1,254),T2(1,1),MULT,T2(1,254)
/COM W SQUARED = W*W
  *VOPER,T1(1,254),T1(1,254),MULT,T1(1,254)
  *VOPER,T2(1,254),T2(1,254),MULT,T2(1,254)
/COM READ IN MATERIAL PROPERTIES
  *VREAD,T3(1,1),STRDAMP,TXT
  (E9.2)
/COM DEFINE FLUID STRUCTURE INTERACTION AT BOUNDARY AND ABSORBENT
/COM BOUNDARY
/COM FRONT LOWER
  NSEL,S,LOC,X,0.08
  SF,ALL,FSI
  SF,ALL,IMPD,1
  D,ALL,ALL,0
/COM FRONT MIDDLE LOWER
  NSEL,S,LOC,X,0.08,0.185
  SF,ALL,FSI
  SF,ALL,IMPD,1
  D,ALL,ALL,0
.
.
/COM RESELECT FULL SET
  ALLSEL,ALL,ALL
/COM READ IN BOUNDARY INERTANCE DATA USE RDT1.MAC MACRO
/COM COPIES FRF AS MET40.DAT THEN USES RDT1.MACTO READ DATA
/COM TABLE COLUMN NUMBERS PASSED TO MACRO
/COM INERTANCE DATA CONVERTED TO RECEPTANCE IN MACRO
  /SYS,COPY9Z.FRFMET40.DAT
  *USE,RDT1.MAC,2,3
  /SYS,COPY34Z.FRFMET40.DAT
  *USE,RDT1.MAC,4,5
.
.
/COM SAVE DATABASE
  SAVE
/COM ALL DATA COPIED
/COM DEFINE DO LOOP 133 SOLUTIONS 1.5 TO 200Hz
  *DO,I,1,133,1
/COM DEFINE TABLES MEANING
/COM SET FREQUENCY FROM COLUMN 1 TABLE 1
  HARFRQ,T1(I,1),T1(I,1)
/COM CHANGE ABSORPTION COEFFICIENT
  MP,MU,2,T3(I,1)
/COM DEFINE COMPLEX DISPLACEMENTS AT BOUNDARY NODES
  D,9,UZ,T1(I,2),T1(I,3)
  D,34,UZ,T1(I,4),T1(I,5)
  D,35,UZ,T1(I,6),T1(I,7)
.
.
/COM SOLVE FOR EACH LOADSTEP
  SOLVE
  *ENDDO
/COM LEAVE SOLVER
  FINISH
/COM EXIT ANSYS
/EXIT

```

RDT1.mac follows.



```

/COM DATA READING MACRO THAT READS ICATS FORMAT FRF FILE MET40.DAT
/COM READS INTO TABLES NUMBERED AS ARGUMENTS IN THE CALL STATEMENTS
/COM CONVERTS INERTANCE DATA INTO RECEPTANCE DATA
/COM READS 1 RECORD PER LINE ONLY
/COM FIRST LINE OF DATA AT 0 Hz IGNORED
/COM JOBNAME MET
/COM READ REAL PART OF FRF DATA
I=1
*VLEN,1
*VREAD,T1(I,ARG1),MET40,DAT
(8(/),E13.7)
I=I+1
.
.
*VLEN,1
*VREAD,T1(I,ARG1),MET40,DAT
(140(/),E13.7)
/COM END OF READ REAL, READ IMAGINARY
I=1
*VLEN,1
*VREAD,T1(I,ARG2),MET40,DAT
(8(/),13X,E13.7)
I=I+1
.
.
*VLEN,1
*VREAD,T1(I,ARG2),MET40,DAT
(140(/),13X,E13.7)
/COM END OF READ IMAG
/COM SET DATA HANDLING FOR FULL COLUMNS
*VLEN,133
/COM DELETE FILE 40
/SYS,DEL MET40.DAT
/COM CONVERT TO RECEPTANCE DIVIDE EACH CELL BY W SQUARED
*VOPER,T1(1,ARG1),T1(1,ARG1),DIV,T1(1,254)
*VOPER,T1(1,ARG2),T1(1,ARG2),DIV,T1(1,254)

```

#### **Appendix 4: Accepted Papers.**

Two papers have been accepted for the 'Vibration and Noise '95' conference in Venice. The abstracts of these papers are given below.

##### **An Experimental Technique for Acoustic Modal Analysis**

by Roland Whear and Denise Morrey, School of Engineering, Oxford Brookes University

Increased commercial pressure to reduce development lead times and find quicker solutions to noise and vibration problems has resulted in the need for an improved experimental method for determining the modal properties of three-dimensional acoustic cavities.

The technique described here has been designed to overcome the problems inherent in acoustic modal analysis. The first of these is the fact that directional information, which is necessary for the determination and plotting of mode shapes, is not available for pressure measurements. The second is related to the fact that the measurement of the associated transfer function requires the measurement of volume velocity as an input variable.

The method uses a finite difference calculation performed with three in-line microphones to determine the second spatial derivative of pressure in a particular direction. This function is  $180^\circ$  out of phase with the pressure and therefore exhibits the same zeroes and stationary points as the original distribution.

The implementation is carried out using a dual channel FFT analyser and commercially available software for structural modal analysis.

The technique is used to determine the acoustic modes of a bare office, and these results compare well with predictions from a finite element model and calculations based on the wave equation.

##### **An analysis of the noise and vibration generated in vehicle structures using experimental techniques**

by Denise Morrey and Roland Whear, School of Engineering, Oxford Brookes University

Noise, vibration and harshness testing during the development of a new motor car has tended to concentrate on the use of structural modal surveys at the body-in-white stage, and the measurement of sound pressure levels in a fully trimmed vehicle. The technique described here uses an experimental method for acoustic modal analysis developed by Whear and Morrey to obtain noise transfer functions and hence determine the acoustic mode shapes for the bare body shell of a Rover Metro-R6.

This information, when analysed in conjunction with the results from an experimental structural modal analysis of the body, the experimental mode shapes of the major panels within the structure, and the acoustic mode shapes of the passenger compartment obtained from a finite element model, enables a greater understanding of the contribution which each of these factors make to the resulting experimental acoustic mode shapes. This allows possible problems such as the generation of cavity boom, or the identification of panels where palliative treatments or stiffening needs to be applied to be identified more at this early stage in the development process.

Results from an experimental and numerical investigation of the Rover Metro-R6 body shell are presented.